

TECHNISCHE UNIVERSITÄT MÜNCHEN

Lehrstuhl für Entwicklungsgenetik

Development and regeneration of the peripheral and central axons in the zebrafish lateral-line afferent neurons

Yan Xiao

Vollständiger Abdruck der von der Fakultät TUM School of Life Sciences der Technischen
Universität München zur Erlangung des akademischen Grades eines

Doktors der Naturwissenschaften

genehmigten Dissertation.

Vorsitzender: Prof. Dr. Martin Hrabě de Angelis

Prüfer der Dissertation:

1. Prof. Dr. Wolfgang Wurst

2. Prof. Dr. Ilona Grunwald Kadow

Die Dissertation wurde am 16.12.2019 bei der Technischen Universität München eingereicht
und durch die Fakultät TUM School of Life Sciences am 09.07.2020 angenommen.

| | |
|---------------------------------------------------------------------------------------|----|
| Table of contents | I |
| Abbreviations | IX |
| Summary/Zusammenfassung | XI |
| 1. Introduction | 1 |
| 1.1 The zebrafish as a model for the development and regeneration..... | 2 |
| 1.2 The development of lateral-line sensory system..... | 3 |
| 1.2.1 The lateral-line sensory organs..... | 4 |
| 1.2.2 The lateral-line sensory afferent nerves..... | 5 |
| 1.3 Glial cells in zebrafish..... | 7 |
| 1.3.1 Schwann cell development..... | 9 |
| 1.3.2 Regulators of Schwann cell development and function..... | 10 |
| 1.4 Repair of the peripheral nerve..... | 11 |
| 1.4.1 Wallerian degeneration..... | 12 |
| 1.4.2 Initial reaction to axotomy..... | 13 |
| 1.4.3 The relationship between the axon and Schwann cells during regeneration..... | 15 |
| 1.4.4 Target reinnervation..... | 16 |
| 1.5 Regeneration in the central nervous system..... | 17 |
| 1.5.1 The capacity of axonal regeneration..... | 17 |
| 1.5.2 The role of cAMP in the regeneration..... | 18 |
| 1.6 The aims of the thesis..... | 18 |
| 2. Materials and Methods | 20 |
| 2.1 Materials..... | 20 |
| 2.1.1 Zebrafish lines..... | 20 |
| 2.1.2 Plasmids..... | 20 |
| 2.1.3 Primers..... | 20 |
| 2.1.4 Antibody..... | 22 |
| 2.1.5 Equipments..... | 22 |
| 2.1.6 Buffers and Materials..... | 23 |

| | | |
|---------|---------------------------------------------------------------|----|
| 2.2 | Methods..... | 25 |
| 2.2.1 | Molecular methods..... | 25 |
| 2.2.1.1 | Genomic DNA extraction and sequencing..... | 25 |
| 2.2.1.2 | PCR..... | 26 |
| 2.2.1.3 | Gateway cloning and DNA constructs..... | 26 |
| 2.2.1.4 | Transformation of competent cells..... | 27 |
| 2.2.1.5 | Restriction digests..... | 28 |
| 2.2.1.6 | Agarose gel electrophoresis..... | 28 |
| 2.2.1.7 | RNA <i>in vitro</i> transcription for sgRNA..... | 28 |
| 2.2.1.8 | sgRNA/Cas9 microinjection and T7 Endonuclease I..... | 29 |
| 2.2.2 | Immunohistochemistry..... | 29 |
| 2.2.2.1 | BrdU immunohistochemistry..... | 29 |
| 2.2.2.2 | General immunohistochemical staining..... | 29 |
| 2.2.3 | Zebrafish embryos injections..... | 30 |
| 2.2.3.1 | Injections for generating transgenic zebrafish | 30 |
| 2.2.3.2 | Injections for mosaic gene expression..... | 30 |
| 2.2.3.3 | Cell transplantation..... | 31 |
| 2.2.4 | Microscopy and imaging..... | 31 |
| 2.2.4.1 | Selection of zebrafish mutants by stereomicroscopy..... | 31 |
| 2.2.4.2 | Laser-mediated axon severing and cell ablation..... | 31 |
| 2.2.4.3 | Photostimulation of bPAC..... | 32 |
| 2.2.4.4 | Live Imaging..... | 32 |
| 2.2.5 | Detection of cell death..... | 33 |
| 2.2.6 | Quantification of Schwann cells..... | 33 |
| 2.2.7 | Determination of cAMP levels..... | 33 |
| 2.2.8 | Quantitative analysis of the defect in the central axons..... | 34 |
| 2.2.9 | Pharmacology..... | 34 |
| 2.2.10 | Zebrafish husbandry and care taking..... | 34 |
| 2.2.11 | Statistics..... | 34 |

| | |
|---------------------------------------------------------------------------------|----|
| 3. Results | 36 |
| 3.1 Axon-glia interactions during the lateral-line peripheral nerve injury..... | 36 |
| 3.1.1 The Tg[gSAGFF202A] transgenic line marking for Schwann cells.... | 36 |
| 3.1.2 The Tg[gSAGFF202A] insertion disrupts the <i>ErbB2</i> gene..... | 38 |
| 3.1.3 Responses of Schwann cells to acute and chronic denervation.... | 40 |
| 3.1.4 Schwann cells facilitate but are dispensable for axonal re-growth..... | 47 |
| 3.1.5 Schwann cells are necessary for the reinnervation of peripheral targets.. | 51 |
| 3.2 The development of central axons in the lateral-line afferent neurons..... | 53 |
| 3.2.1 The defect in central axons of lateral-line afferent neurons..... | 53 |
| 3.2.2 The different effect on other neurons of hindbrain..... | 55 |
| 3.2.3 Cell non-autonomous effect on the central axons growth..... | 59 |
| 3.2.4 The analysis of causative gene by whole genome sequencing..... | 60 |
| 3.2.5 The validation of the causative gene by CRISPR/Cas9..... | 63 |
| 3.3 The regeneration of central axons in the lateral-line afferent neurons... | 64 |
| 3.3.1 The regenerative capacity of central axons..... | 64 |
| 3.3.2 The regeneration of central axons promoted by optogenetic stimulation... | 65 |
| 4. Discussions | 75 |
| 4.1 Axon-glia interactions during peripheral axon injury..... | 75 |
| 4.1.1 The animal model of disease and Schwann cells respond to denervation... | 75 |
| 4.1.2 Schwann cells and neurons are mutually dependent..... | 77 |
| 4.1.3 The identity of the directional cues for axonal re-growth..... | 79 |
| 4.1.4 Different modes of axonal repair..... | 80 |
| 4.1.5 Clinical implications..... | 81 |
| 4.2 The guidance cues of central axons in lateral-line afferent neurons..... | 82 |
| 4.2.1 The central axons pathfinding in lateral-line afferent neurons..... | 82 |
| 4.2.2 The regulation of cell non-autonomous in central axons growth..... | 84 |
| 4.3 Optogenetic stimulation of central axonal regeneration..... | 86 |
| 4.3.1 The limited regenerative capacity of central axons..... | 86 |
| 4.3.2 The enhanced axonal regeneration by increasing neuronal cAMP level... | 87 |

| | |
|-----------------------------------------------|------------|
| 5. Conclusions and Outlook..... | 91 |
| References..... | 94 |
| Acknowledgements | 117 |
| Affirmation..... | 119 |
| Publications based on this thesis..... | 120 |
| Curriculum Vitae..... | 121 |

Abbreviations

| Abbreviations | Definition |
|----------------------|-----------------------------------------------------------|
| AAD | acute axonal degeneration |
| ALL | anterior lateral line |
| ALLG | anterior lateral line ganglion |
| ALLN | anterior lateral line nerve |
| cAMP | cyclic adenosine monophosphate |
| cls | colorless |
| CNS | central nervous system |
| CRISPR | clustered regularly interspaced short palindromic repeats |
| db-cAMP | dibutyryl cyclic adenosine monophosphate |
| dpf | days post-fertilization |
| dpi | days post-injury |
| DRG | dorsal root ganglion |
| ERKs | extracellular signal-regulated protein kinases |
| fss | fused somites |
| GFP | green fluorescent protein |
| GPI | glycosylphosphatidylinositol |
| HEZ | hindbrain entry zone |
| hpa | hours post-axotomy |
| hpf | hours post-fertilization |
| JNKs | c-Jun N-terminal protein kinases |
| MAPK | mitogen-activated protein kinase family |
| mbp | myelin basic protein |
| NGF | nerve growth factor |
| Ngn1 | neurogenin 1 |
| Nrg1 | neuregulin 1 |
| PFA | paraformaldehyde |

| | |
|-------|---------------------------------------------|
| PLL | posterior lateral line |
| PLLG | posterior lateral line ganglion |
| PLLN | posterior lateral line nerve |
| PNI | peripheral nerve injury |
| PNS | peripheral nervous system |
| PTU | N-phenylthiourea |
| RGC | retina ganglion cell |
| Rgmb | repulsive guidance molecule family member b |
| Robo2 | Roundabout-2 |
| SCI | spinal cord injury |
| SNP | single nucleotide polymorphisms |
| SIFT | sorting intolerant from tolerant analysis |
| WD | Wallerian degeneration |

Summary

Neural damage is a devastating outcome of physical trauma. Regeneration of damaged axons is an essential process that allows animals to restore synaptic connectivity and circuit function. Severed axons of peripheral nervous system (PNS), surrounded by Schwann cells, have a better regenerative capacity than those of the central nervous system (CNS), which could be ensheathed by oligodendrocytes. Schwann cells are an important glial cell type as one of major effectors in the regenerative process of PNS, and the interaction between Schwann cells and neurons is crucial to maintain the integrity and function of neuronal circuits. Although axon regeneration has been studied intensely, many questions remain regarding neuronal-glia interactions, extrinsic and intrinsic mechanisms of axon regeneration. The zebrafish has emerged as a favourable system to study neural development and regeneration in the whole animal at high resolution. Additionally, zebrafish have a superficial and accessible sensory-neural system called the lateral line, where the lateral line afferent nerves (LLN) project along the head and trunk of the zebrafish, and form anterior lateral line nerve (ALLN) and posterior lateral line nerve (PLLN). The bipolar LLN have one central axon that projects along the anteroposterior axis of the hindbrain, and one peripheral axon ensheathed by Schwann cells, which innervates mechanosensory hair cells. In this work, I used the LLNs to investigate the function of Schwann cells during peripheral axons injury, the development and regeneration of their central axons.

To investigate axon-glia interactions during peripheral nerve injury, the transgenic line Tg[gSAGFF202A] with a Gal4FF driver marking Schwann cells was firstly confirmed by P0-like myelin glycoprotein and claudin-k junctional protein marking glial cells. Additionally, the Gal4FF insertion was found to disrupt the *ErbB2* gene and lead to nerve defasciculation and absence of myelination. I found that chronic denervation by neuronal ablation caused progressive loss of Schwann cells by inducing cell apoptosis and reducing cell proliferation, whereas the negative effects of acute denervation by axonal severing were reversible because Schwann-cell re-innervation prevented further

glial destruction. During the initial loss of contact with the axolemma, Schwann cells downregulated the expression of the P0-like myelin glycoprotein and Claudin-k junctional protein and dedifferentiated in a proximal-distal gradient. Additionally, axonal severing induced neuronal death and axons failed to regenerate efficiently in *ErbB2* mutant fish. Neuronal-circuit regeneration began when Schwann cells extended bridging processes to close the injury gap. Regenerating axons grew faster and directionally after the physiological clearing of distal debris by the Schwann cells. Further, in the absence of Schwann cells, regenerating axons were misrouted, impairing the re-innervation of sensory organs.

To identify new genes involved in axonal pathfinding, I studied a spontaneous mutant disrupting the central axons of the lateral line neurons. Using cell transplantation, I found that the causative mutation acted cell non-autonomously in lateral line afferent neurons. By whole-genome sequencing, 334 single nucleotide polymorphisms (SNP) were found on chromosome 5. *Rgmb* and *tmem232* were identified as potential candidate genes. To validate them by CRISPR/Cas9 technique, I performed sgRNA/Cas9 microinjection experiments to induce mutation in zebrafish embryos.

In addition, I found that the regenerative capacity of central axons in the lateral line afferent neurons was very poor. However, it can be enhanced by optogenetically elevating neuronal cAMP level based on the expression of blue-light activatable adenylyl cyclase bPAC. Moreover, regenerated central axons re-targeted the correct area of the brain, and re-formed presynaptic structures for the potential of functional recovery, which supports an evolutionarily conserved mechanism for cAMP elicited axonal regeneration.

In summary, this study provides new insights on the development and regeneration of sensory afferent neurons in a vertebrate.

Zusammenfassung

Nervenschäden sind eine verheerende Folge eines körperlichen Traumas. Die Regeneration geschädigter Axone ist ein wesentlicher Prozess, der es Tieren ermöglicht, die synaptische Konnektivität und die Kreislauffunktion wiederherzustellen. Durchtrennte Axone des peripheren Nervensystems, die von Schwann-Zellen umgeben sind, haben eine bessere Regenerationskapazität als diejenigen des zentralen Nervensystems, die von Oligodendrozyten umhüllt sein können. Schwann-Zellen sind ein wichtiger Gliazelltyp und einer der Hauptfaktoren für den Regenerationsprozess des peripheren Nervensystems, und die Wechselwirkung zwischen Schwann-Zellen und Neuronen ist entscheidend für die Aufrechterhaltung der Integrität und Funktion neuronaler Schaltkreise. Obwohl die Axonregeneration intensiv untersucht wurde, bleiben viele Fragen zu neuro-glialen Wechselwirkungen, extrinsischen und intrinsischen Mechanismen der Axonregeneration offen. Der Zebrafisch hat sich als ideales System erwiesen, um die neuronale Entwicklung und Regeneration des gesamten Tieres in hoher Auflösung zu untersuchen. Zusätzlich haben Zebrafische ein oberflächliches und zugängliches sensorisch-neuronales System, das so genannte Seitenlinienorgan. Die Nerven des Seitenlinienorgans projizieren entlang des Kopfes und des Rumpfs des Fisches und bilden den anterioren lateralen Liniennerv und den posterioren lateralen Liniennerv. Die bipolaren Neuronen des PLLn besitzen ein zentrales Axon, das entlang der anteroposterioren Achse des Hinterhirns verläuft, und ein peripheres Axon, das von Schwann-Zellen umhüllt ist, und die mechanosensorische Haarzellen an dem Stamm des Fisches innerviert. In dieser Arbeit habe ich die lateralen Liniennerven verwendet, um die Funktion von Schwann-Zellen während einer Verletzung der peripheren Axone, als auch die Entwicklung und Regeneration ihrer zentralen Axone zu untersuchen.

Die transgene Linie Tg[gSAGFF202A], die Schwann-Zellen markierte, wurde generiert, um Axon-Glia Wechselwirkungen bei peripheren Nervenverletzungen zu untersuchen, und zunächst durch P0-ähnliche Myelin-Glykoprotein und Claudin-k Junction-Protein

Markierungsgliazellen bestätigt. Zusätzlich wurde festgestellt, dass die Gal4FF-Insertion das *ErbB2*-Gen stört und zu einer Defaszierung der Nerven und zum Fehlen einer Myelinisierung führt. Ich fand heraus, dass eine chronische Denervierung durch neuronale Ablation einen progressiven Verlust von Schwann-Zellen verursachte, indem sie Zellapoptose induzierte und die Zellproliferation reduzierte, während die negativen Auswirkungen einer akuten Denervierung durch axonales Durchtrennen reversibel waren, da eine erneute Schwann-Zell-Innervierung eine weitere Zerstörung der Gliazellen verhinderte. Während des anfänglichen Kontaktverlusts mit dem Axolemma regulierten Schwann-Zellen die Expression des P0-ähnlichen Myelin-Glykoproteins und des Claudin-k Junction-Protein herunter und differenzierten in einem proximal-distalen Gradienten. Darüber hinaus verursachte das Trennen der Axone den neuronalen Tod, und Axone konnten sich in mutierten *ErbB2*-Fischen nicht effizient regenerieren. Die Regeneration des neuronalen Kreislaufs begann, als die Schwann-Zellen die Überbrückungsprozesse verlängerten, um die Verletzungslücke zu schließen. Regenerierende Axone wuchsen nach der physiologischen Beseitigung distaler Trümmer durch die Schwann-Zellen schneller und direktional. Außerdem wurden in Abwesenheit von Schwann-Zellen Regenerationsaxone fehlgeleitet was die Reinnervation von Sinnesorganen beeinträchtigte.

Um Gene zu identifizieren, die an der axonalen Wegfindung beteiligt sind, untersuchte ich eine spontane Mutante, bei der die zentralen Axone der lateralen Linienneuronen eine Missbildung aufweisen. Ich habe durch Zelltransplantationen herausgefunden, dass das ursächliche Gen eine zell-extrinsische Funktion ausübte. Ferner zeigte die Genomsequenzierung von der Mutante 334 Einzelnukleotidpolymorphismen auf Chromosom 5. *Rgmb* und *tmem232* wurden als mögliche Kandidatengene ausgewählt um sie durch CRISPR/Cas9 Technik zu validieren.

Die regenerative Kapazität der zentralen Axone wurde auch im Seitenlinienorgan des Zebrafischs untersucht. Die begrenzte regenerative Kapazität wurde durch eine Licht aktivierbare Adenylyl cyclase, bPAC, die den cAMP-Spiegel erhöht, verbessert.

Darüber hinaus innervierten die regenerierten zentralen Axone die richtigen Bereiche des Gehirns und präsynaptischen Strukturen wurden neu gebildet.

Zusammenfassend liefert diese Studie neue Erkenntnisse über die Entwicklung und Regeneration sensorisch afferenter Neuronen bei einem Wirbeltier.

1. Introduction

1.1 The zebrafish as a model for the development and regeneration

Evolutionary proximity makes mammals the obvious choice as an experimental model system to study human biology and disease. On the other hand, invertebrate models are valuable because they enormously facilitate work that necessitates a large number of animals, such as forward-genetic or high-throughput drug screens, and large-scale transgenesis (Wilson-Sanders, 2011). Because of their small size, they are relatively easy to handle, inexpensive to maintain, and facilitate whole-animal imaging (Yanik et al., 2011). Invertebrates, however, suffer from evolutionary divergence, which sometimes preclude the direct extrapolation of results to vertebrate-specific organs, or to human pathology. Non-mammalian vertebrates, therefore, fill a gap between the mammalian and invertebrate model systems. Aquatic vertebrates, such as the zebrafish, share with mammals many of the cellular and physiological mechanisms that underlie how organs form, function, or develop disease (Santoriello and Zon, 2012). The zebrafish (*Danio rerio*) is a small tropical freshwater fish that senses the environment via a functionally sophisticated but anatomically simpler sensory system, whose structure and physiology are homologous to those found in mammals. The simplicity of the zebrafish, combined with their advantage as a small vertebrate with a powerful genetic toolkit for sophisticated experimental intervention and intravital imaging, offers the following advantages to study properties of neural circuit development, homeostasis, degeneration and regeneration:

- It has functionally equivalent but anatomically simpler versions of most mammalian organs, whose basic biology is well understood.
- The zebrafish is small and not expensive to maintain, compared to mammalian models such as rodents (Dahm and Geisler, 2006).
- It has a rapid sexual development producing thousands of progenies and several generations per year. This permits powerful statistical analyses and facilitates the recovery of mutagenized offspring.
- The generation of stable transgenic zebrafish lines is technically simple. Alternatively,

engineered genes can be transiently expressed by DNA or RNA introduced by injections or electroporation, facilitating functional studies by gain- or loss-of-gene function (Pinto-Teixeira et al., 2013). A trained person can inject up to 500 eggs for constructing three transgenic lines per day (Xu et al., 2008).

- In addition of being a powerful system for genome-wide random mutagenic screens, the zebrafish genome can also be altered by targeted mutagenesis. This has been enormously facilitated by standardized Zinc-finger nucleases or transcription activator-like effector nucleases, and most recently, clustered regularly interspaced short palindromic repeats (CRISPR) for targeted-gene mutagenesis (Chang et al., 2013; Gaj et al., 2013; Shah et al., 2015).
- The zebrafish embryo develops rapidly and externally. Its optical transparency enables easy observation of organs for detailed cellular and physiological analyses (Kemp et al., 2009; Pinto-Teixeira et al., 2013). Moreover, zebrafish larva can maintain optic transparency up to two weeks with the addition of N-phenylthiourea (PTU), which allows in vivo visualization of cell behaviors in real time, especially the neural circuit activity in the central nervous system (CNS).
- Many organs or tissues in the zebrafish regenerate after damage, for example: the fins (Tawk et al., 2002; Wills et al., 2008), skin (Chen et al., 2016), kidney (Diep et al., 2011; McCampbell and Wingert, 2014), blood vessel (Huang et al., 2003), maxillary barbels (LeClair and Topczewski, 2010), heart (Curado and Stainier, 2006; Jopling et al., 2010), hair cells in the inner and lateral line (Jiang et al., 2014; Pinto-Teixeira et al., 2015), olfactory bulb (Paskin et al., 2011), motor axons in spinal cord (Becker et al., 2004; Reimer et al., 2008; Reimer et al., 2013), and retina ganglion cell (RGC) axons (McCurley and Callard, 2010).

1.2 The development of lateral-line sensory system

The lateral line is a mechanosensory system that is present along the head and trunk of fishes and some amphibians. The lateral line mediates a distant-touch sense, because it detects changes in water currents and pressure distribution that occur within short-distances of the animal (Dijkgraaf, 1963). The lateral line system is of importance

for a variety of behaviors, including movement against the water flow (Oteiza et al., 2017), prey detection, predator avoidance, schooling and mating (Coombs and Montgomery, 1999).

1.2.1 The lateral-line sensory organs

The lateral-line system is formed by a collection of discrete sensory organs called neuromasts, which contain mechanoreceptive hair cells, similar to those of the mammalian inner ear (Ghysen and Dambly-Chaudière, 2007). Neuromasts can be found on the skin or within sub-epidermal canals open to the water by pores and distribute in stereotypic patterns on each side of the body. Neuromasts on the head and trunk form, respectively, the anterior lateral line (ALL) and posterior lateral line (PLL) branches. The PLL can be further divided into two subsets located in the lateral and dorsal aspects of the animal. In larval zebrafish, the PLL comprises around 7-8 neuromasts (L7-8) (Fig. 1.1A-D) (Ghysen and Dambly-Chaudière, 2007; Metcalfe et al., 1985). The number of neuromasts increases progressively during development. Finally, the linear arrays of neuromasts, called stitches, are generated in the PLL in juvenile and adult animals. They form by budding from one founding neuromast and up to 20 neuromasts may develop in adult fish. All the neuromasts of one stitch innervated by repeated branching of the same neurons (Ledent, 2002), suggesting that they are all progenies of the founding neuromast.

A mature neuromast is composed of 15 to 20 mechanosensory hair cells surrounded by non-sensory supporting cells and mantle cells (Fig. 1.1E) (Hernández et al., 2007). The supporting cells respond to hair-cell death by proliferating to produce new hair cells. In the neuromast, hair bundles extrude into a cupula which link bundles to the water surrounding the zebrafish. The hair bundle comprises an array of stereocilia arranged in rows of increasing length, like a staircase, and a kinocilium located adjacent to the tallest stereocilia (Fig. 1.1F) (Pujol-Martí and López-Schier, 2013). A neuromast contains two populations of hair cells of opposing hair-bundle polarities. Thus, a water movement bending the cupula in a given direction depolarizes one population of hair

cells, whereas hyperpolarizes the other one, which is then translated into an increase or a decrease of the firing rate of the afferent neuron (Pujol-Martí and López-Schier, 2013).

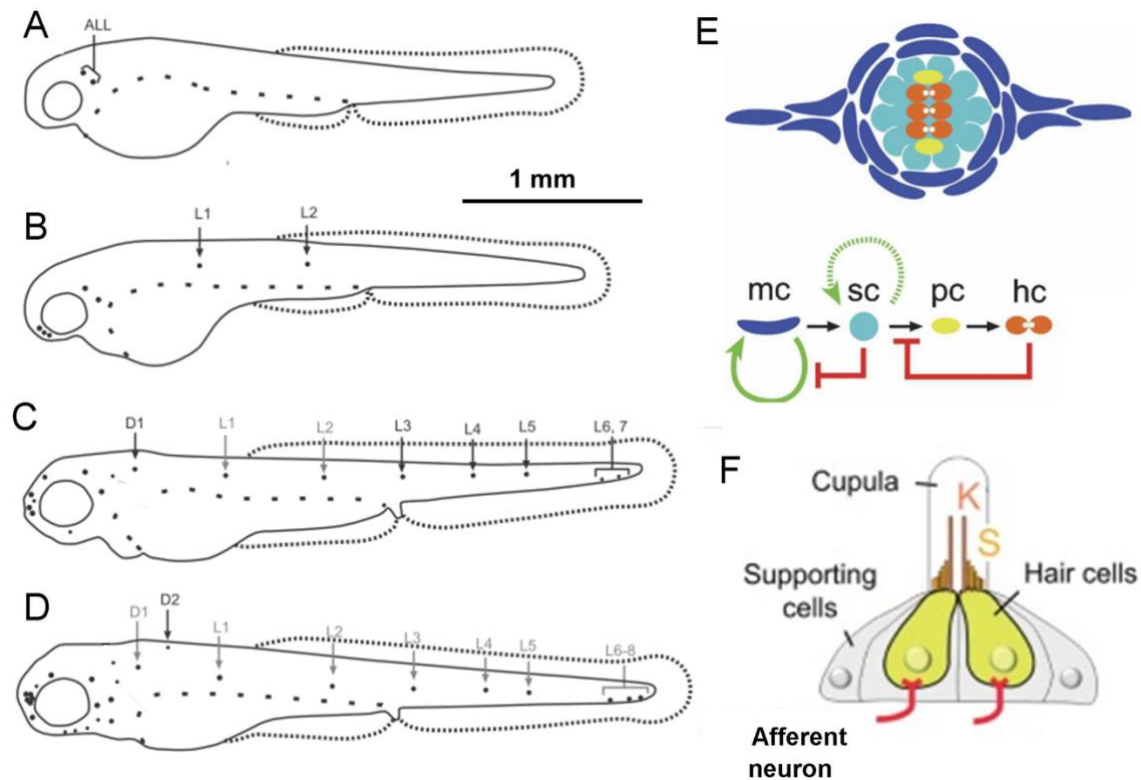


Fig. 1.1 Establishment of the lateral-line system, morphology and renewal of the neuromast

(A) The earliest neuromasts at 48 hours post-fertilization (hpf) belong to the ALL system. The embryonic PLL develops gradually between 55 (B) and 72 hpf (C, D) (adapted from Ghysen and Dambly-Chaudière, 2007). Black arrows point to newly formed neuromasts; neuromasts formed formerly are marked in grey. ALL, anterior lateral line neuromasts; D1-2, dorsal neuromasts; L1-8, lateral neuromasts. Anterior is towards the left and dorsal is upwards. (E) A possible strategy for hair cell renewal (adapted from Hernández et al., 2007). The fates of different cells are linearly arrayed. This demonstrates that each decision comes from a binary choice, either “stay as they are” or “enter into the next step.” Circular arrow indicates self-renewing properties of the peripheral cells. Dotted arrow shows the support cells can also self-renew. Red bars mean inhibitory feedback: new hair cell progenitors form when hair cells die. Mantle cell (mc), support cell (sc), hair cell precursor cell (pc), hair cell (hc). (F) Lateral view of a neuromast innervated by afferent neurons (adapted from Pujol-Martí and López-Schier, 2013). The hair-bundle comprises the kinocilium (K) and the

stereocilia (S), which is contained within a cupula.

1.2.2 The lateral-line sensory afferent nerves

Lateral line nerves project along the head and trunk of zebrafish body to form, respectively, the anterior lateral line nerve (ALLN) and posterior lateral line nerve (PLLN). Much of the research on these nerves was concentrated on the formation, development and structure of peripheral axons (Alexandre and Ghysen, 1999; Andermann et al., 2002; Becker et al., 2001; David et al., 2002; Gilmour et al., 2004; Gompel et al., 2001; Liao, 2010; Metcalfe et al., 1990; Pujol-Martí et al., 2010; Pujol-Martí et al., 2012; Sarrazín et al., 2010; Shoji et al., 1998). However, the development of central axons and the regeneration of lateral line nerve are not well understood.

Mechanical stimulation of the hair cells increases neurotransmitters into the synapses with peripheral-axonal endings of lateral-line afferent neurons, producing an action potential that travels along the axon from the periphery to the neuron's cell body, and then from cell body to the hindbrain along the central axon. The cell bodies of these lateral line afferent neurons form small anterior lateral line ganglia (ALLG) and posterior lateral line ganglia (PLLG) near the otic vesicle (Fig. 1.2A-E) (Alexandre and Ghysen, 1999; Metcalfe, 1985; Faucherre et al., 2009). In the zebrafish larva, central projections from ALLN and PLLN terminate into a neuropil region ventral to the medial octavolateralis nucleus in the hindbrain (Fig. 1.2A). Each central axon of PLLN bifurcates at the level of rhombomere 6 into a rostral and a caudal branch and exhibits terminal buttons along the entire rostrocaudal axis. The rostral branch extends anteriorly to rhombomere 1, whereas the caudal branch extends posteriorly to rhombomere 7/8 (Fig. 1.2F) (Fame et al., 2006).

The PLL system in larval zebrafish is formed in two discrete waves during embryonic development (Ghysen and Dambly-Chaudière, 2007; Metcalfe, 1985; Metcalfe et al., 1985; Sarrazín et al., 2010). It originates from an ectodermal placode located posterior

to the otic vesicle around 18 hpf (Ghysen and Dambly-Chaudière, 2007; Schlosser, 2002). The primary placode gives rise to PLL primordium (primI) and PLLG neurons. The second wave of afferent neurons appears coincidentally with the formation of two additional primordial (primII and primD) at 24 hpf, shortly after the primary placode has given rise to the primI and ganglion (Sarrazín et al., 2010). The lateral-line primordium migrates along the horizontal myoseptum, depositing clusters of pro-neuromast and interneuromast cells along the way (Metcalf et al., 1985; Sarrazín et al., 2010). PLLG neurons project central and peripheral axons simultaneously as soon as they differentiate.

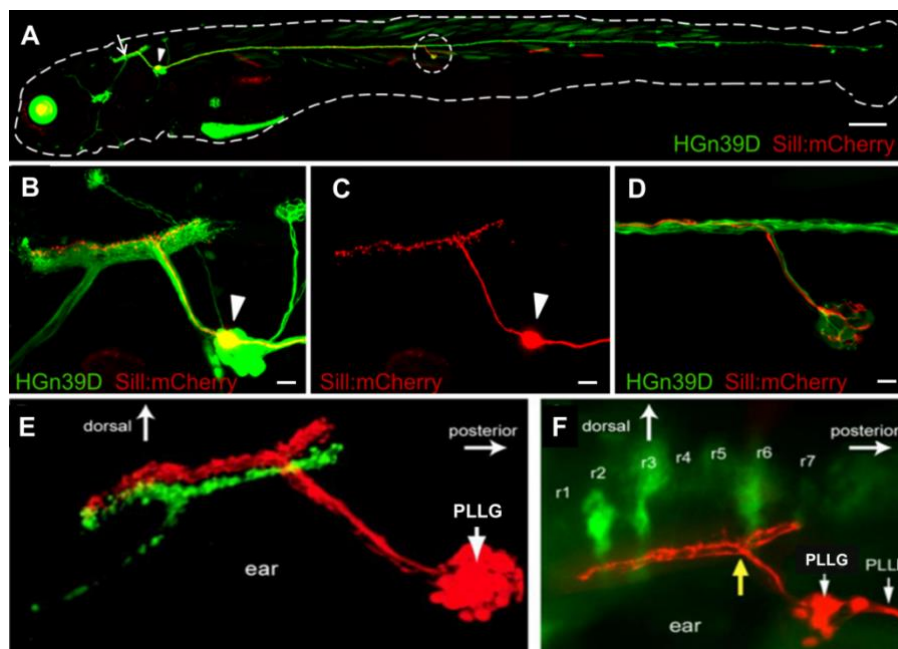


Fig. 1.2. Lateral afferent neurons in the zebrafish larva

(A-D) The Tg[HGn39D] stable transgenic line (green) at 5 days post-fertilization (dpf), with the microinjection of plasmid Sill:mCherry to show the lateral afferent neurons with an individual lateral neuron (red). The arrow points to the central axon projection in the hindbrain. The arrowhead indicates the PLLG. Dotted lines outline the fish body. The circle shows the neuromast innervated by the mCherry-expressing neuron. (E) The central axons of PLLN (red) form a column which lies dorsal to the column formed by the central axons of ALLN (green) (adapted from Alexandre and Ghysen, 1999). (F) Posterior lateral central axons are shown in red and some of the rhombomeres (r) are shown in green. Central axons of PLLN (yellow arrow) split into two branches

at the level of r6. The rostral branch extends anteriorly to the level of r1, whereas the caudal branch extends posteriorly to the level of r7 (adapted from Fame et al., 2006). Scale bars: 150 μ m (A) and 10 μ m (B-D).

The formation of the lateral line ganglion depends on the expression of the transcription factor Neurogenin-1 (Ngn1) (Andermann et al., 2002; Ghysen and Dambly-Chaudière, 2004; López-Schier et al., 2005). Inactivation of the gene encoding Ngn1 prevents the development of the lateral-line afferent neurons, but it does not block the formation and migration of the primordium and the development of neuromasts. Interestingly, inactivation of the transcription factor Ngn1 leads to the development of more than twice the normal number of neuromasts along the PLL of zebrafish larvae (López-Schier et al., 2005; Grant et al., 2005). It seems that, as in the mammalian ear, the expression of Ngn1 determines lateral line neurons (Raft et al., 2007). However, the development of the central axons in lateral line neurons has not been investigated.

1.3 Glial cells in zebrafish

Four major types of glia can be classified in zebrafish based largely on morphology (Table 1.1): astrocytes, star-shaped cells in the brain and spinal cord, were initially described as providing trophic and structural support to neurons in the CNS (Neve et al., 2012); oligodendrocytes enwrap axons of the CNS and form myelin sheaths for saltatory conduction of action potentials (Dutton et al., 2008; Jung et al., 2010; Kirby et al., 2006; Munzel et al., 2012; Schebesta et al., 2009; Shin et al., 2003; Wada et al., 2005; Yoshida et al., 2005); microglia, derived from hematopoietic stem cells, are the resident immune cell of the CNS (Peri and Nüsslein-Volhard, 2008; Rossi et al., 2015; Svahn et al., 2013); Schwann cells, both myelinating and non-myelinating, in the peripheral nervous system (PNS) ensheath and support peripheral nerves (Dutton et al., 2008; Gilmour et al., 2002; Jung et al., 2010; Munzel et al., 2012; Wada et al., 2005).

The Schwann cells are crucial glial cells in the vertebrate PNS (Jessen and Mirsky, 2005; Kidd et al., 2013), and the interaction between neurons and Schwann cells is

essential for the development and function of the nervous system (Arthur-Farraj et al., 2012; Court et al., 2004; Rodrigues et al., 2011; Sharghi-Namini et al., 2006; Shy, 2009). The zebrafish PLL nerve is ensheathed by Schwann cells. Based on an expectation of developmental conservation between flies and vertebrates, it was initially thought that these Schwann cells may play a role in early axonal guidance (Chien et al., 2002). However, experiments demonstrated that the neurites are towed in the wake of the primordium, and Schwann cells do, indeed, migrate along the sensory axons rather than guiding them, as they always slightly lag behind the growth cones of the lateral line axons (Lush and Piotrowski, 2014). In addition to their myelinating function, they also play a role in maintaining the fasciculation of PLL axons (Fig. 1.3A-D) (Freeman and Doherty, 2006; Gilmour et al., 2002).

Table 1.1 Glial subtypes in zebrafish

| Glial type | Primary function | Distribution | Transgenic line |
|------------------|----------------------------------------------------------------|----------------------------------------------------------------|---------------------------------------------------------------------------------------------------|
| Astrocytes | Trophic support of neurons, synapse modulation | Embedded in CNS cell cortex, ensheathing synapses, CNS surface | gfap:GFP |
| Oligodendrocytes | Neuronal ensheathment, trophic support of neurons, myelination | Ensheathing axons in CNS | sox10:GFP mbp:eGFP claudin k:GFP plp:EGFP Olig1:mem-eGFP Olig2:GFP nkx2.2a:mGFP |
| Microglia | Immune surveillance, macrophage function | Throughout CNS | pU1:Gal4-UAS:eGFP pU1:Gal4-UAS:TagRFP ApoE:GFP mpeg1:EGFP/mCherry |
| Schwann cells | Ensheathment and support of peripheral nerves, myelination | Ensheathing PNS nerves | zFoxD3:GFP sox10:GFP mbp:eGFP claudin k:GFP |

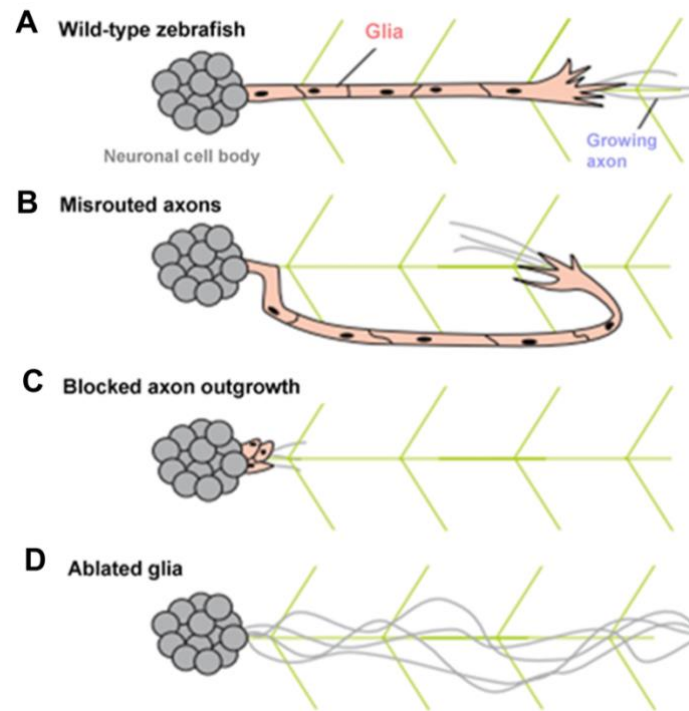


Fig. 1.3. Neuron-glia interactions during lateral-line development in zebrafish

(A) In wild type zebrafish, glial cells follow axons pioneering the lateral line along horizontal myoseptum, never extending beyond axonal substrates. Leading Schwann cells exhibit a ‘pioneering’ phenotype, extending robust processes in the general direction of migration. Axons eventually form a tightly fasciculated nerve ensheathed by glia. (B) When axons are misrouted, as in zebrafish with mutations affecting Sonic hedgehog signaling or *fused somites* (*fss*) gene (Gilmour et al., 2002), Schwann cells always co-localize with mis-localized axons. (C) When axonal outgrowth is blocked by laser ablation of neuronal cell bodies (Gilmour et al., 2002), it leads to a clear arrest of glial migration. *Ngn1* mutant in which the lateral line afferent neurons are genetically ablated lacks the Schwann cells along its trunk (López-Schier et al., 2005). (D) When Schwann cell precursors are genetically prevented from migrating to the lateral line in *Sox10* mutants (also called *colorless* [*cls*]), *ErbB2* mutants and *ErbB3* mutants, axon outgrowth occurs normally, but major defects in nerve fasciculation are observed at later stages (Freeman and Doherty, 2006; Gilmour et al., 2002; Lyons et al., 2005).

1.3.1 Schwann cell development

Before a Schwann cell produces myelin, it must undergo several developmental steps (Jessen et al., 2005). Schwann cell precursors derive from the neural crest, which

delaminate from the neural tube and migrate out to associate with neurons (Jessen et al., 1994; Raphael et al., 2010; Raphael et al., 2011; Sauka-Spengler et al., 2010). These precursors co-migrate with growing axons, when nerves are developing towards their targets. After migration is complete, Schwann cell precursors will differentiate into immature Schwann cells (Jessen et al., 2005; Raphael et al., 2011). Then, the immature Schwann cell is confronted with two distinct choices: to be a myelinating or non-myelinating cell. If a Schwann cell eventually associates with an individual large-diameter axon in the bundle of the developing nerve, it will become a promyelinating cell, which culminates with the formation of a compact myelin sheath covering about 100 micrometers of an axon (Jessen et al., 2005; Lyons et al., 2014; Raphael et al., 2011). The myelin sheath is not continuous and the gaps between adjacent Schwann cells are called nodes of Ranvier. The action potential allows saltatory conduction by jumping from node to node, which can dramatically increase conduction velocity without increasing the axonal diameter. By contrast, if a Schwann cell interacts with several small-diameter axons, it would become a non-myelinating Schwann cell and ensheath the axon in a pocket of its cytoplasm to produce a Remak bundle (Hahn et al., 1987; Jessen et al., 2005; Raphael et al., 2011).

1.3.2 Regulators of Schwann cell development and function

There are several regulators of Schwann cell development, proliferation, survival, specification; including Sox10 and neuregulin 1/ErbB (Nrg1-ErbB) (Finzsch et al., 2010; Gilmour et al., 2002; Jessen et al., 2005; Lyons et al., 2005; Newbern et al., 2010; Raphael et al., 2011; Schreiner et al., 2007). There are at least fifteen neuregulin isoforms, although Nrg1 type III seems likely to be the main isoform active during Schwann cell development (Falls, 2003; Harrison et al., 2006). All of the neuregulin isoforms begin as transmembrane proteins which are then cleaved; Nrg1 type I and II are released as paracrine signaling molecules (Fleck et al., 2013). By contrast, Nrg1 type III has a second cysteine-rich transmembrane domain, and after cleavage of the first transmembrane domain, it remains anchored the plasma to the membrane as a juxtacrine signal (Fricker and Bennett, 2011). The neuregulin can bind to the ErbB

tyrosine kinase receptor family, including epidermal growth factor receptor, ErbB2, ErbB3, and ErbB4 (Citri et al., 2003). ErbB2 and ErbB3 are the receptors primarily expressed in Schwann cells (Birchmeier, 2009; Lyons et al., 2005). ErbB2 cannot bind to the Nrg ligand, but it does have kinase activity (Citri et al., 2003). In contrast, ErbB3 can bind to the Nrg ligand, but lacks kinase activity. Analyses in zebrafish have investigated the functions of Nrg1/ErbB signaling using mutants, small molecule inhibitors, and time-lapse imaging *in vivo*. It was found that mutations in ErbB2 and ErbB3 cause defects in myelin basic protein (*mbp*) expression by a genetic screen (Lyons et al., 2005). Similar to previous studies in mouse models, *ErbB2* and *ErbB3* mutants lack Schwann cells along peripheral axons, although some Schwann cells do exist around the lateral line ganglia in the zebrafish (Lyons et al., 2005; Pogoda et al., 2006; Raphael et al., 2011; Riethmacher et al., 1997; Woldeyesus et al., 1999). Additionally, it is revealed that Schwann cell proliferation is dramatically decreased in *ErbB* mutants, consistent with results that Nrg1 is a Schwann cell mitogen in mammals (Garratt et al., 2000b; Lyons et al., 2005; Morrissey et al., 1995; Newbern and Birchmeier, 2010; Raphael et al., 2011). Time-lapse imaging combined with the ErbB activity inhibitor AG1478 was used to demonstrate that ErbB signaling is required continuously during Schwann-cell migration, in addition to its role in the proliferation of the glia (Lyons et al., 2005; Raphael et al., 2011). When the ErbB inhibitor AG1478 is added after the onset of migration, some Schwann cells can continue to migrate, but in a misdirected fashion or even switching nerves in some cases. These studies support that ErbB signaling is crucial for effective directional migration of Schwann cells, rather than simply promoting their movement (Lyons et al., 2005; Raphael et al., 2011).

1.4 Repair of the peripheral nerve

A traumatic peripheral-nerve injury (PNI) occurs when a nerve is crushed or severed, and proper communication between PNS and CNS is temporarily lost before neuronal repair. Severed axons of PNS, surrounded by Schwann cells, have a better regenerative capacity than those of the CNS, which could be ensheathed by oligodendrocytes (Buckley et al., 2010; Briona et al., 2014; Ceci et al., 2014; Goldshmit et al., 2012;

Graciarena et al., 2014; Lyons et al., 2005; Schuster et al., 2010; Villegas et al., 2012). In the PNS, damaged axons start to regenerate from the proximal stump of the lesion into the distal part, and eventually extend to the target areas.

1.4.1 Wallerian degeneration

When an axon is severed, the part of the axon distal to the injury undergoes Wallerian degeneration (WD) and demyelination (Kerschensteiner et al., 2005). First, immediately after an axon is damaged, both the proximal and distal parts of the axon adjacent to the injury site immediately fragment through a process called acute axonal degeneration (AAD) (Kerschensteiner et al., 2005). Second, the distal axon fragment remains intact during a characteristic lag phase of variable duration. Third, axons with myelin sheaths quickly degenerate into small pieces which are then removed by phagocytic cells. In the PNS, Schwann cells and macrophages play crucial roles in clearance of the debris throughout the process of WD. Schwann cells decrease the synthesis of myelin during the first 12 hours after trauma (Villegas et al., 2012; White et al., 1989) and then stop forming myelin proteins within 48 hours (Trapp et al., 1988; Villegas et al., 2012). In the absence of macrophages, glial cells clear myelin during the earliest stages of axon degeneration (Han et al., 1989; Liu et al., 1995). Glial cells also release cytokines, such as interleukin-1beta, which regulate macrophage recruitment to the site of nerve degeneration in myelin removal (Shamash et al., 2002).

The zebrafish PLLN is an excellent model for studying axon degeneration and regeneration by laser axotomy and time-lapse imaging (O'Brien et al., 2009; Villegas et al., 2012). To do this, researchers inject the HuC:GFP plasmid DNA at one cell stage and obtain embryos expressing GFP in single neurons. After axotomy, a damaged axon experiences three phases of WD: a lag phase, a fragmentation phase and a clearance phase (Fig. 1.4) (Villegas et al., 2012).

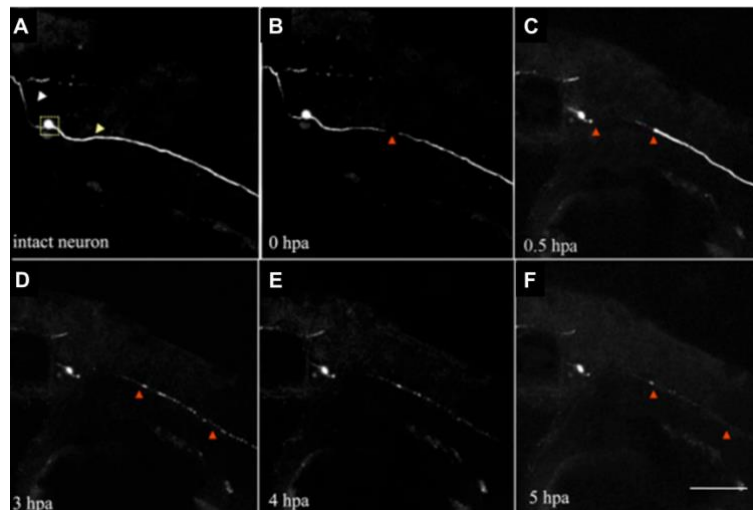


Fig. 1.4. AAD and WD are observed in the zebrafish PLLN after laser axotomy

A 3 dpf larva, injected with plasmid DNA (HuC:GFP) to image and axotomize a single PLLN neuron (adapted from Villegas et al., 2012). (A) Intact neuron with a typical bipolar morphology. White arrowhead shows central projection, yellow arrowhead shows peripheral projection, and square shows cell body. (B) Zero hours post-axotomy (hpa), arrowhead points to position of laser axotomy. (C) Thirty minutes after axotomy. AAD was complete: arrowheads indicate extent of AAD. (D) 3 hours after axotomy, the distal axon began to fragment (arrowheads). (E) 4 hours after axotomy, some fragments remained. (F) 5 hours post-axotomy, clearance of debris was almost complete. Scale bar, 100 μm .

1.4.2 Initial reaction to axotomy

Peripheral nerve injury triggers a cascade of degenerative cellular and molecular changes at the site of injury. Immediately following injury, calcium influx into the Schwann cells is regarded as an initiation mechanism for demyelination, as a result of mechanical insult and interruption of blood and oxygen supply (Smith et al., 1988). The calcium influx also enters into the injured axons, where it activates calpain to promote axonal degeneration (Touma et al., 2007; Vargas et al., 2015). For example, blocking voltage-gated calcium channels (Knöferle et al., 2010), chelating extracellular calcium (Mishra et al., 2013), or inhibiting calcium release from intracellular stores (Villegas et al., 2014) delay axon fragmentation (Vargas et al., 2015). On the other hand, increasing calcium promotes axon degeneration (Knöferle et al., 2010; Mishra et al., 2013).

Importantly, the entrance of calcium into the axon after axotomy is also required for the generation of new growth cones (Chierzi et al., 2005). Indeed, if axotomy occurs in a calcium-free environment, none of the axons will form a new growth cone and nerve regeneration will fail (Bradke et al., 2012; Ghosh-Roy et al., 2010).

Therefore, a well-balanced Ca^{2+} level is essential for nerve regeneration. The calcium changes, in turn, activate many signaling pathways, such as mitogen-activated protein kinase family (MAPK), c-Jun N-terminal protein kinases (JNKs) and extracellular signal-regulated protein kinases (ERKs) (Drerup et al., 2013; Martensson et al., 2007; Munderloh et al., 2009; Napoli et al., 2012). The activation of MAPK induces Schwann cell demyelination and de-differentiation following axon injury, suggesting that the kinase mediating the injury signal triggers distal Schwann cell injury response (Yang et al., 2012). One downstream molecule activated by JNKs, which belong to the MAPK family, is the transcription factor c-Jun. The activation of c-Jun is important for the function of the denervated Schwann cells, the formation of bands of Büngner, Schwann cell proliferation and removal of myelin debris in the distal segment after injury (Arthur-Farraj et al., 2012; Parkinson et al., 2004; Svehlenski et al., 2013; Yang et al., 2012). Without c-Jun activation in Schwann cells, axonal regeneration is impaired, neuronal cell death is increased, and the expression of several neurotrophic factors in dorsal root ganglion (DRG) is decreased (Fontana et al., 2012). The rapid activation of ERK 1/2 is required for nerve injury-induced Schwann-cell proliferation, and the presence of ERK 1/2 is pivotal for axonal outgrowth (Martensson et al., 2007).

The acute inflammatory response also occurs following nerve injury, at the same time the blood-nerve barrier becomes most permeable (Gaudet et al., 2011; Hui et al., 2010; Pope et al., 2014). For example, there is an influx of inflammatory cells, such as neutrophils, monocytes, and macrophages immediately after injury. In zebrafish, macrophages accumulate at the injury site 3 days after spinal cord injury (SCI) and continue to persist in decreasing numbers until 10 days post-injury (dpi). Macrophage activation enhances myelination by playing an important role in removing cellular

debris such as dying neurons, damaged axons and myelin debris, which is normally produced during axon degeneration and demyelination (Hui et al., 2010). During myelin phagocytosis, Schwann cells in the distal part secrete cytokines and chemokines that recruit immune cells to the damaged nerve. The generation of proinflammatory cytokines starts within several hours after the injury, such as interleukin-6, leukocyte inhibitory factor, tumor necrosis factor-alpha, monocyte chemoattractant protein-1, and interleukin-1 α (Boivin et al., 2007; Karanth et al., 2011; Lee et al., 2006; Nelson et al., 2013; Ogai et al., 2014; Svehnigsen et al., 2013). Thus, inflammation is important for successful axon regeneration. The Schwann cells and macrophages involved in the Wallerian degeneration communicate by cytokine signaling pathways, controlling phagocytosis and growth factor release, and therefore preparing for axonal regrowth in the distal part. If a delay occurs in this degenerative or regenerative process, these cells fail to enhance regeneration (Svehnigsen et al., 2013).

1.4.3 The relationship between the axon and the Schwann cells during regeneration

Following damage to peripheral nerves, Schwann cells de-differentiate to a progenitor-like state, proliferate, migrate and align within nerves. The Schwann cells can form unique columnar structures known as bands of Büngner and provide a guidance substrate for the re-growth of axons (Napoli et al., 2012). During axonal regeneration, Schwann cells recover their contact with axons and undergo differentiation once again into myelinating cells (Glenn et al., 2012). Accordingly, when Schwann cells lose the ability to de-differentiate, they become less supportive of axonal regeneration (Arthur-Farraj et al., 2012; Viader et al., 2011). In the PLLN of zebrafish, some evidences indicate that these glia and regrowing axons are mutually dependent during early stages of nerve regeneration (Ceci et al., 2014). Schwann cells provide a preferred substrate for nerve repair and act as a guidance cue for the regenerating nerve to advance along its former path, but axons can regrow in the absence of these glial cells, suggesting that they are not strictly required for regeneration. Yet, in mutants lacking Schwann cells, regenerating growth cones extend at rates comparable with wild type, frequently fail to cross the injury site and instead stray along aberrant trajectories in

motor axons of zebrafish spinal cord (Rosenberg et al., 2014).

The bands of Büngner formed by denervated Schwann cells can synthesize extracellular matrix proteins laminin and fibronectin, and growth factors to guide re-growing axons. Several of these growth factors are neurotrophins, such as nerve growth factor (NGF), brain derived neurotrophic factor and neurotrophic factors-3 (Notterpek, 2003). Schwann cells, resident fibroblasts and growing axons all produce p75 NGF receptor, which may play a role in the advancing of growth cones and downregulate gene expression involved with myelin production (Raivich et al., 1991; Taniuchi et al., 1986; Toy et al., 2013). However, the function of Schwann cells in the degeneration and the regeneration of lateral line peripheral nerves is not well characterized.

1.4.4 Target reinnervation

Although axonal regeneration in the PNS can be robust, accurate reinnervation of the original peripheral targets is essential for functional recovery, otherwise chronic defects can happen (Lago et al., 2006). For example, motor axons formerly innervating muscle are often misdirected to sensory organs, and sensory axons typically innervating skin can be misrouted to muscle (Madison et al., 2009; Svehlenski et al., 2013). The misdirected regeneration of sensory axons is a major problem for the brain, where the somatosensory cortex obtains defective afferent signals from the misdirected nerve (Rosen et al., 2012; Taylor et al., 2009). Yet, axonal regrowth occurs normally, resulting in a highly accurate recovery of function in the PNS.

Considering the effect of Schwann cells on axon regeneration, it is reasonable to assume that Schwann cells are a cellular substrate for regeneration accuracy in the PNS (Ceci et al., 2014; Chen et al., 2007; Graciarena et al., 2014; Hall 2005; Hoke et al., 2006; Painter et al., 2014; Rosenberg et al., 2014). It would be interesting to investigate whether a conserved role played by Schwann cells exists in zebrafish lateral line peripheral nerves.

1.5 Regeneration in the central nervous system

The CNS consists of the brain, the brain stem and the spinal cord. In humans and other mammals, central neurotrauma results in diverse disorders and causes persistent and devastating disability depending on the region affected, because of the poor regenerative capacity of central axons (LaPlaca et al., 2014). By contrast, despite signaling pathways in axonal growth and pathfinding are found to be similar to those in mammals, non-mammalian vertebrates efficiently regenerate axons in the CNS. For instance, larval and adult zebrafish possess an intrinsically high ability for axon regeneration. The injured CNS environment in zebrafish indicates little scarring or expression of inhibitory molecules and regrowing axons use molecular cues in the environment to successfully navigate to their targets (Becker et al., 2014). Therefore, there is a unique opportunity to investigate mechanisms of successful axon regeneration in zebrafish, which can be interpreted to find therapy solutions in non-regenerating animals.

1.5.1 The capacity of axonal regeneration

In zebrafish, retinal ganglion cells (RGC) can survive after injury and their axons regrow and reinnervate termination targets in the brain (Becker et al., 2000; Nagashima et al., 2011; Zou et al., 2005). Additionally, at the level of the brainstem-spinal cord transition zone, 32-51% of neurons in the nucleus of the medial longitudinal fascicle, magnocellular octaval nuclei, and intermediate reticular nuclei regenerate axons across into the distal part of the spinal cord and project up to 4 mm beyond the initial transection site (Becker et al., 1998; Vajn et al., 2013). However, neurons in other brainstem nuclei that project into the spinal cord, such as the red nucleus, nucleus of the lateral lemniscus, and tangential nucleus, as well as Mauthner neurons and ascending axons of DRG neurons, fail to regenerate axons after damage (Bhatt et al., 2004; Vajn et al., 2013). Therefore, not all severed CNS axons in zebrafish regenerate equally well and a number of CNS axons show variable regenerative capacity. Moreover, the regenerative capacity of the central axons in zebrafish lateral line neurons has not been investigated.

1.5.2 The role of cAMP in the regeneration

Several studies have revealed a direct link between cellular cyclic adenosine monophosphate (cAMP) and neurite outgrowth. Increasing intracellular cAMP in neurons after a lesion can promote axonal regeneration in the CNS (Bhatt et al., 2004; Hannila et al., 2008; Martínez et al., 2014; Neumann et al., 2002; Qiu et al., 2002; Spencer et al., 2004). Additionally, cAMP is also partly responsible for overcoming CNS myelin inhibition (Hannila et al., 2008). Furthermore, it has been demonstrated that cAMP-dependent regeneration of DRG neurons is inhibited by treatments with PKA inhibitors. cAMP has been shown to mediate its effect by a series of PKA signaling dependent and independent pathways (Hannila et al., 2008).

The giant reticulospinal Mauthner-cell axons regenerate poorly after a spinal lesion in zebrafish. It was reported that 65% of Mauthner-cell axons cannot regenerate at all, the remaining 35% cannot penetrate the lesion site and grew aberrantly (Bhatt et al., 2004). Pressure injection of membrane-permeable dibutyryl cyclic adenosine monophosphate (db-cAMP) into the soma of injured Mauthner cells induced all the axons to successfully grow through the injury site. Moreover, it was shown that the escape behavior initiated by the Mauthner cell approached normal after the treatment (Bhatt et al., 2004). However, there are still many unknown questions about the molecular mechanisms of axonal regeneration, and efforts on comprehensive understanding of the regeneration process in zebrafish might be helpful for designing effective therapies for CNS regeneration in mammals.

1.6 The aims of the thesis

Functional recovery requires accurate axon guidance during their regrowth across the injured area and a correct reinnervation of the targets. Both extrinsic factors in the environment of the axons as well as intrinsic factors in the neurons themselves play important roles in the regeneration process. Understanding the extrinsic and intrinsic mechanisms involved in the onset and progression of axonal regeneration is therefore of utmost importance to devise effective treatments for axonal injury. Schwann cells

produce the Band of Büngner as important players in axon guidance (Parrinello et al., 2010). However, most of the classical experimental animal models are not amenable to explore the fine details of the dynamic interaction between Schwann cells and neurons during injury and repair, because of the inaccessibility of these cells to direct live imaging at high resolution. Additionally, re-activation of the intrinsic factors can promote axonal regeneration of injured neurons (Park et al., 2008). Studying the mechanisms governing the developmental decline of axon growth competency in the CNS and studying the injury-induced activation of a pro-regenerative programme in the PNS have been widely used to understand the cell-intrinsic mechanisms underlying axon regeneration (Mahar et al., 2018). However, the intrinsic mechanisms involved in axonal regeneration are not completely understood.

In this study, I chose zebrafish lateral-line nerve (LLN) to study axonal development, degeneration and regeneration, because this system has two main advantages over traditional models: it forms and begins to function within a few days after fertilization, and it is located superficially in the animal's body, enabling easy and controllable manipulation and visualization. The lateral-line nerves project along the head and trunk of the fish to form ALLN and PLLN, respectively. The bipolar afferent PLLN have one central axon that projects along the anteroposterior axis of the hindbrain, and one peripheral axon ensheathed by Schwann cells, which innervates mechanosensory hair cells in superficial receptors called neuromasts.

The specific aims are:

1. To investigate the role of the Schwann cells in peripheral axonal degeneration and regeneration of lateral line afferent neurons
2. To investigate genes controlling axon growth during early development for understanding genes need to be reactivated for CNS axon regrowth
3. To search for experimental strategies to enhance central axons regeneration

2. Materials and Methods

2.1 Materials

2.1.1 Zebrafish lines

Tg[UAS:H2A-mTurquoise], Tg[hsp70:bPAC-V2A-mCherry-SILL] (also called SILL:bPAC), Tg[UAS:bPAC-V2A-mCherry], Tg(hsp70:EGFP-Rp110a-SILL) stable transgenic lines were generated in this study. Wild-type zebrafish (*Danio rerio*) of the AB strain were used (Fritz et al., 1996). The Tg[gSAGFF202A] line was generated by random integration of a gene-trap construct from Koichi Kawakami lab (The Graduate University for Advanced Studies, Japan). The Tg[Brn3c:mEGFP], Tg[HGn39D], Tg[hspGFF53A], Tg[Islet:GFP] Tg[SILL:mCherry] and Tg[UAS:EGFP] transgenic lines have been described previously (Faucherre and López-Schier, 2011, 2014; Faucherre et al., 2009; Higashijima et al., 2000; Xiao et al., 2005). The WIK wild type strain was obtained from Herwig Baier lab (Max Planck Institute of Neurobiology, Germany).

2.1.2 Plasmids

The plasmids UAS:H2A-mTurquoise, hsp70:EGFP-SILL (also called SILL:EGFP), UAS:EGFP-UtrCH, hsp70:bPAC-V2A-mCherry-SILL, UAS:bPAC-V2A-mCherry, hsp70:EGFP-Rp110a-SILL were generated in this study. The pEntry vectors containing the UAS sequence, hsp70 minimal promoter, EGFP and polyA were from the Tol2 kit. The pEntry vector containing the SILL enhancer, the hsp70:mCherry-SILL (SILL:mCherry), hsp70:MCS-SILL and hsp70:Gal4-VP16-SILL (SILL:Gal4) have been previously described (Faucherre et al., 2011; Pujol-Martí et al., 2012).

2.1.3 Primers

Lyophilized primers were diluted in double-distilled water and stored as a 100 µM master stock solution at -20°C. 2 µM of each primer was mixed using double-distilled water from the according stock solution. The sequence of the primers used is listed

below:

Genotyping primers for Tg[gSAGFF202A]

forward: 5'- GCTCAAGTGCTCCAAAGAAA-3'

reverse: 5'-ATCAGCAGGCAGCATGTCC-3'

Genotyping primers for Rgmb sgRNA

Rgmb-check-mutForward: 5'-ACGGGGCTAGATTTTCCTTGT-3'

Rgmb-check-mutReverse: 5'-CCAGCACTGCCATAACTCAA-3

Tmem232-check-mutForward: 5'-AAGGCTCCTGGAGAAGCA-3'

Tmem232-check-mutReverse: 5'-CTAAAGAACTTGGTGCAA-3'

H2A-mTurquoise forward: 5'-'GGGGACAAGTTTGTACAAAAAAGCAGGCTGCCA
CCATGGTGAGCAAGGGCGA-3'

H2A-mTurquoise reverse: 5'-GGGGACCACTTTGTACAAGAAAGCTGGGTTTATTT
GCCTTTGGCCTTGTG-3'

EGFP-UtrCH reverse: 5'-GGGGACCACTTTGTACAAGAAAGCTGGGTTTAGTCTA
TGGTGACTTGCTG-3'

V2A-mCherry forward: 5'-CGCGATATCGGGAAGCGGAGCTACTAACTTC-3'

V2A-mCherry reverse: 5'- CGCGATATCCTTACTTGTACAGCTCGTCCAT-3'

bPAC forward: 5'-ACGCGTCGACGCCACCATGATGAAGCGGCTG-3'

bPAC reverse: 5'-CGCGATATCCAGGTCCTCCTCCGAGATCAG-3'

bPAC-V2A-mCherry forward: 5'-GGGGACAAGTTTGTACAAAAAAGCAGGCTGC
CACCATGATGAAGCGGCTG-3'

bPAC-V2A-mCherry reverse: 5'-GGGGACCACTTTGTACAAGAAAGCTGGGTTTA
CTTGTACAGCTCGTCCAT-3'

T7 promoter primer 5'-TAATACGACTCACTATAGG-3'

Rgmb sgRNA primer 5'-AAAAGCACCGACTCGGTGCCACTTTTTCAAGTTGATA
ACGGACTAGCCTTATTTAACTTGCTATTTCTAGCTCTAAAACCGGGGCTGAG
CGCCTCATCCTATAGTGAGTCGTATTACGC-3'

Tmem232 sgRNA primer 5'-AAAAGCACCGACTCGGTGCCACTTTTTCAAGTTGA
TAACGGACTAGCCTTATTTAACTTGCTATTTCTAGCTCTAAAACGTGGTCTGC
AGAACAAGCCCTATAGTGAGTCGTATTACGC-3'

2.1.4 Antibody

| Antibody | Species | Dilution | Company/Reference |
|----------------------------------|---------|----------|------------------------------------|
| Mbp (6D2) | mouse | 1:5 | G. Jeserich, Universität Osnabrück |
| claudin-k | rat | 1:1000 | T. Becker, University of Edinburgh |
| anti-BrdU | rat | 1:100 | Abcam |
| anti-Myc | rabbit | 1:500 | Cell Signaling Technology |
| acetylated-Tubulin | mouse | 1:500 | Sigma-Aldrich |
| 3A10 | mouse | 1:10 | University of Iowa |
| Alexa Fluor 568 goat anti-rat | | 1:300 | Invitrogen |
| Texas Red 647 donkey anti-mouse | | 1:200 | Jackson Labs |
| Texas Red 647 donkey anti-rabbit | | 1:200 | Jackson Labs |
| Texas Red 647 donkey anti-rat | | 1:200 | Jackson Labs |

2.1.5 Equipment

| Equipment | Company |
|--------------------------------------|---------|
| Agarose Gel electrophoresis chambers | Peqlab |
| Microwave | Bosch |

| | |
|--------------------------------------------|----------------------|
| Bacterial culture shaker | ThermoQuest |
| PCR machine T3 Thermocycler | Biorad |
| Benchtop microcentrifuge | Eppendorf |
| Incubator 37 °C | Heraeus |
| Incubator 28.5°C | Binder |
| Thermomixer | Eppendorf |
| Injection needle puller | DMZ universal puller |
| Stereomicroscopy Zeiss Stemi 2000 | Zeiss |
| LSM 510 inverted confocal microscope | Carl Zeiss |
| Spinning-disc inverted confocal microscope | Zeiss |

2.1.6 Buffers and Materials

Buffers

E3 embryo medium

5mM NaCl, 0.17 mM KCl, 0.33 mM CaCl₂, and 0.33 mM MgSO₄ in ddH₂O

25×MS222 (also called MESAB and 3-aminobenzoic acid ethyl ester)

Dissolve 400 mg MS-222 in 97.9 mL of ddH₂O, and adjust the pH to 7 by adding 2.1 mL of 1M Tris (pH9). Store this solution at 4 °C.

Genomic DNA extraction buffer

80mM Tris pH8.5, 200mM NaCl, 0.5% SDS, 5 mM EDTA

10×PBS

80 g NaCl, 2 g KCl, 1.44 g Na₂HPO₄, 0.24 g KH₂PO₄ was dissolved in ddH₂O, then the pH was adjusted to pH 7.3 with HCl. ddH₂O was added to a total volume of 1 L.

0.2% Tween-20 (PBST)

2 mL Tween-20 was added to 998 mL 1× PBS

TE Buffer (pH 8.0)

TE Buffer consisted of 10 mM Tris (pH 8.0) and 1 mM EDTA (pH 8.0) in ddH₂O

4% paraformaldehyde (PFA) for fixation

Samples were fixed using 4% paraformaldehyde diluted in PBST, as described above.

50x TAE Buffer for agarose gel electrophoresis

TAE buffer consisted of 2 M Tris, 57 ml acetic acid, 50 mM Na₂EDTA x 2H₂O pH 8.0, with ddH₂O to a total volume of 1L.

| Materials | Company |
|----------------------------------|-------------------|
| Acetone | Merck |
| 5-bromo-2'-deoxyuridine (BrdU) | Sigma |
| Bovine serum albumins (BSA) | Sigma |
| cAMP ELISA kit | EnzoLife Sciences |
| cAMPS-Sp | Tocris Bioscience |
| Cas9 protein | PNA Bio |
| Cationic styryl pyridinium dyes | Sigma |
| Dimethyl sulfoxide (DMSO) | Merck |
| EDTA | Merck |
| Ethanol | Sigma |
| H89 dihydrochloride | Tocris Bioscience |
| Hydrochloric acid (HCl) | Sigma |
| In Situ Cell Death Detection Kit | Roche |
| isopropyl alcohol | Sigma |
| Low-melting point Agarose | Sigma |
| MEGAscript T7 kit | Ambion |
| Methanol | Sigma |
| NucleoSpin Extract II kit | Qiagen |

| | |
|-------------------------------------------|-------------------|
| Paraformaldehyde | Sigma |
| Phenol:Chloroform:Isoamyl Alcohol 25:24:1 | Sigma |
| Platinum Pfx | Invitrogen |
| proteinase K | Invitrogen |
| Protease inhibitor mix | Sigma |
| 1-phenyl 2-thiourea (PTU) | Sigma |
| RNAse inhibitor | Fermentas |
| RNeasy Mini kit | Qiagen |
| SP6 mMessageMachine Kit | Ambion |
| Taq DNA Polymerase | Roche Diagnostics |
| Tris | Biomol |
| Triton X-100 | Sigma |
| Tween-20 | Sigma |

2.2 Methods

2.2.1 Molecular methods

2.2.1.1 Whole genomic DNA extraction and sequencing

Genomic DNA was extracted from 50 pooled 72 hpf zebrafish embryos or embryos directly stored in 100% methanol at -20°C. If embryos were stored in methanol, the methanol was directly removed and the embryos rehydrated by washing 2 times with 0.5ml extraction buffer (80mM Tris PH8.5, 200mM NaCl, 0.5% SDS, 5 mM EDTA) without proteinase K. Then as much supernatant as possible was removed and 0.5 ml of fresh extraction buffer with proteinase K (1mg/ml) was added. The sample was incubated at 65°C overnight without agitation. The following day, 0.5 ml of phenol/chloroform/IAA (25/24/1) was added and the sample was agitated gently for 10 minutes at room temperature to avoid shearing of genomic DNA. The samples were centrifuged for 10 minutes at 13.000 rpm at room temperature, and then supernatant was transferred into a fresh tube using a 1ml pipette with the tip removed. 1 volume of

(0.5ml) of isopropyl alcohol 100% was added, and the samples mixed gently by inverting several times to avoid shearing of genomic DNA. The samples were centrifuged for 10 minutes at 13.000 rpm at room temperature. Afterwards the pellets were washed with 75% ethanol and resuspended in 0.1ml of water for 10 minutes at 40°C. In order to avoid shearing the genomic DNA, care was taken to avoid pipetting up and down. DNA amounts and purity were determined by measuring absorbance at 260/280 nm in a NanoPhotometer. Genomic DNA was stored at 4°C. Intact genomic DNA was sent to Next Generation Sequencing Core facility (Institute of Toxicology and Genetics, Karlsruhe Institute of Technology, Germany) for sequencing analysis.

2.2.1.2 PCR

The following PCR settings were used during the generation of DNA constructs:

| Temperature | time |
|---------------------------------|----------|
| 95°C | 3 min |
| 95°C | 30 sec |
| 55-65°C (depend on the primers) | 30 sec |
| 72°C | 1 kb/min |
| 72°C | 10 min |
| 4°C | ∞ |

2.2.1.3 Gateway cloning and DNA constructs

Gateway Technology is a commercial cloning system provided by Invitrogen. It uses recombination of particular recombination sites mediated by the clonase enzyme rather than standard restriction digests and ligations. The sequences cloned into pCR®8/GW vector were recombined into the according destination vectors by the LR-recombination reaction.

To generate the middle entry clone containing H2A-mTurquoise cDNA (using pDONR 221), the H2A-mTurquoise forward PCR primer containing an *attB1* site and the H2A-mTurquoise reverse primer containing an *attB2* site were used. To generate the

middle entry clone containing EGFP-UtrCH, the forward primer was the same as that for H2A-mTurquoise, and combined with the EGFP-UtrCH reverse primer.

The UAS:bPAC-V2A-mCherry construct was generated using the Tol2 kit (Kwan et al., 2007). PCRs were performed using primers to add *att* sites onto the end of DNA fragments, using Platinum Pfx (Invitrogen). The pEntry vectors containing the UAS sequence and polyA are from the Tol2 kit. To generate the middle entry clone containing bPAC-V2A-mCherry cDNA (using pDONR 221), the bPAC-V2A-mCherry forward PCR primer containing an *attB1* site and the bPAC-V2A-mCherry reverse primer with an *attB2* site were used.

To generate hsp70:bPAC-V2A-mCherry-SILL (SILL:bPAC), a DNA fragment containing a viral 2A sequence and a fluorescent mCherry was PCR amplified using eGFPCAAX-V2A-mCherry as a template with a forward primer containing a 5' EcoRV site and a reverse primer containing a 5' BamHI site:

forward, 5'-CGCGATATCGGAAGCGGAGCTACTAACTTC-3'

reverse, 5'-CGCGGATCCTTACTTGTACAGCTCGTCCAT-3'

The PCR product was digested with EcoRV and BamHI and cloned into the hsp70:MCS-SILL construct (Pujol-Martí et al., 2012) to generate hsp70:V2A-mCherry-SILL. cDNA encoding Myc-tagged bPAC from bPAC-2A-tdTomato was PCR amplified with a forward primer containing a 5' Sall site and a Kozak sequence GCCACC, a reverse primer containing a 5' EcoRV site:

forward 5'-ACGCGTCGACGCCACCATGATGAAGCGGCTG-3'

reverse 5'-CGCGATATCCAGGTCCTCCTCCGAGATCAG-3'

This amplicon was digested with Sall and EcoRV, and ligated into hsp70:V2A-mCherry-SILL to create hsp70:bPAC-V2A-mCherry-SILL (SILL:bPAC).

2.2.1.4 Transformation of competent cells

Competent cells were thawed on ice, mixed gently with DNA and incubated on ice for 30 min. After a heat shock in a water bath of 42°C for 45 s, cells were immediately

incubated on ice for 5 min. 700 µl LB was added and then was incubated for 40 min at 37°C with shaking. The mixture was centrifuged for 5 minutes at 5000 rpm at room temperature. The pellet was re-suspended in 100µl of LB and then spread on LB agar plates containing the corresponding antibiotics to select positive clones. LB agar plates were incubated at 37°C overnight; single clones were chosen to grow in 5mL LB at 37°C overnight with shaking. After that, DNA was extracted and analyzed by enzyme digest.

2.2.1.5 Restriction digests

Analytical digests contained 0.2-1 µg DNA and 1-5 U restriction enzymes. According to the manufacturer's instructions, respective reaction buffers and temperatures for single or double enzyme digests were chosen, and then incubated for 2-3 h at 37°.

2.2.1.6 Agarose gel electrophoresis

To separate DNA fragments and PCR products, 0.8-1.2% (w/v) agarose gels in 1x TAE buffer were used depending on the size of the DNA fragment. The Fermentas FastRuler DNA ladder was used to define the size of the fragment. 6x loading dye was mixed to the DNA samples, and gels were run at 100 V for 45 min. DNA fragments were cut out with a clean scalpel under reduced UV intensity of the agarose gel and purified with the NucleoSpin Extract II kit according to the manufacturer's instructions.

2.2.1.7 RNA *in vitro* transcription for sgRNA

Single guide RNAs were designed using the online tool (Moreno-Mateos *et al.*, 2015). The sgRNA antisense oligonucleotide sequence (5'-3') was: AAAAGCACCGACTCGGTGCCACTTTTTCAAGTTGATAACGGACTAGCCTTATTTAACTTGC TATTTCTAGCTCTAAAACNNNNNNNNNNNNNNNNNNNNNNNNNNNNNN**CTATAGTGAGTCG TATTACGC**, with the T7 site shown in bold, N20 indicating the targeting sequence (Hruscha *et al.*, 2013).

For direct *in vitro* transcription, the sgRNA antisense oligonucleotide was annealed to the T7 primer (TAATACGACTCACTATAGG) for 5 minutes at 95°C, then cooled at room temperature for 2 hours, followed by *in vitro* transcription using the Ambion MEGAscript T7 kit and RNA cleanup using the RNeasy Mini kit (Qiagen).

2.2.1.8 sgRNA/Cas9 microinjection and T7 Endonuclease I

sgRNAs were microinjected at a final concentration of 250 ng/μl, together with 0.5 μg/μl Cas9 protein (PNA Bio Newbury Park, CA) into fertilized one-cell stage embryos. Embryos at 48-72 hpf were pooled to extract genomic DNA. In the T7 endonuclease I assay (T7E1 is a mismatch-specific DNA endonuclease), the mutated target region is PCR amplified and then the efficiency of mutagenesis was assessed.

2.2.2 Immunohistochemistry

2.2.2.1 BrdU immunohistochemistry

To quantify Schwann-cell proliferation by means of DNA synthesis, transgenic Tg[gSAGFF202A; UAS:EGFP; SILL:mCherry] larvae at 3 dpf were incubated immediately after axonal severing in medium containing BrdU (10 mM) for 24 h. After that, larvae were fixed overnight at 4°C in a solution of 4% paraformaldehyde in phosphate-buffered saline (PBS) solution containing 0.2% Tween-20 (PBST) and subsequently rinsed in PBST and 2 M HCl before being blocked in 10% goat serum. Samples were incubated in rat anti-BrdU primary antibody (1:100; Abcam) followed by goat anti-rat Alexa Fluor 568 secondary antibody (1:300). Images were obtained using a confocal microscope (LSM 510; Carl Zeiss).

2.2.2.2 General immunohistochemical staining

Embryos were fixed using one of the three following protocols:

Protocol 1: Embryos were fixed in a solution of 4% paraformaldehyde in PBS containing 0.2% Tween-20 (PBST) overnight at 4 °C, washed 3 × 10 min in PBST.

Protocol 2: Embryos were fixed in 4% sucrose/4% PFA at room temperature for 1 h

per 24 h of development. Following fixation, embryos were washed in PBS, then dehydrated sequentially in methanol-PBT (PBS + 0.5% Triton X-100) and stored in methanol at -20°C at least overnight. Embryos were rehydrated sequentially, washed in PBST, digested with proteinase K (20-40 µg/ml for 72 hpf for 20 minutes), and post-fixed in 4% sucrose/4% PFA for 20 minutes at room temperature.

Protocol 3: Embryos were fixed in a solution of 4% paraformaldehyde in PBS containing 0.2% Tween-20 (PBST) overnight at 4 °C, washed 3 × 5 min in PBST and incubated for 7 min in acetone at -20°C, then 5 min in dH₂O without shaking and finally 3 x 5 min washes in PBST were performed.

After that, embryos were blocked for 1 h in 2% normal goat serum/2% BSA in PBST, followed by incubation with the appropriate primary antibody diluted in PBST at 4°C overnight. Embryos were washed 3-6 × 1 h in PBST, followed by incubation with the secondary antibody for 3 h at room temperature or overnight at 4 °C.

2.2.3 Zebrafish embryo injections

2.2.3.1 Injections for generating transgenic zebrafish

To generate stable transgenic lines, 20 pg of the Tol2-expression DNA and 20 pg of the transposase synthetic RNA were simultaneously injected into one-cell stage wild-type eggs. The resulting embryos were raised to adulthood and outcrossed for visual inspection for presence of the fluorescent transgene. This experiment was approved by the government of Upper Bavaria (animal protocols Az.:55.2-1-54-2532-202-2014).

2.2.3.2 Injections for mosaic gene expression

To transiently and stochastically express transgenes, 25-30 pg of plasmid DNA was injected into embryos at the one- or two-cell stage. For bPAC expression of individual afferent neurons, either plasmids containing bPAC-V2A-mCherry were injected into eggs from the Tg[HGn39D] stable transgenic line or co-injected with a Synapsin1-GFP construct marking presynaptic boutons into eggs from the Casper transgenic line.

Control animals expressed a mCherry-CAAX fusion instead of bPAC-V2A-mCherry.

2.2.3.3 Cell transplantation

Transplantations were performed using donor embryos obtained from crossing of Tg[HGn39D] wild type fish, and host embryos obtained by incrossing of Tg[SILL:mCherry] mutant carrier fish. About 20 cells were transplanted from a blastula stage donor into the upper-ventral region of a shield stage host.

2.2.4 Microscopy and imaging

2.2.4.1 Selection of zebrafish mutants by stereomicroscopy

Wild-type zebrafish, homozygous and heterozygous mutants for *ErbB2* were incubated in 500 μ M Cationic styryl pyridinium dyes (DiASP) for 3 minutes at room temperature in the dark. Treated larva were washed briefly to remove excess fluorophore and then screened with a stereomicroscope. Homozygous mutants displayed more neuromasts, whereas wild-type and heterozygous larva displayed only seven to nine neuromasts on one side of their trunk. Heterozygous and homozygous Tg[gSAGFF202A; SILL:mCherry] were also screened with a stereomicroscope, as lateral line nerves of heterozygous larva developed along the horizontal myoseptum, whereas those of homozygous mutants were more ventral.

2.2.4.2 Laser-mediated axon severing and cell ablation

Axonal severing or cell ablation was performed using the iLasPulse laser system (Roper Scientific SAS) mounted on a Zeiss Axio Observer inverted microscope equipped with a 63X water objective lens. Zebrafish larvæ were anesthetized, mounted on a glass-bottom dish, and covered with 1% low-melting-point agarose. A train of laser pulses was repeatedly applied to the posterior lateralis ganglion or lateral axons and Schwann cells until all red or green fluorescence disappeared. Samples were assessed again for the presence of mCherry or EGFP in the target region 1 h after axonal severing or cell ablation, total ablation occurred in the target region with no red-fluorescent or green-fluorescent signal. Laser microsurgery was conducted in over

100 animals, resulting in more than 90% survival.

2.2.4.3 Photostimulation of bPAC

To avoid unspecific activation of bPAC prior to the experiments, bPAC-positive (bPAC⁺) and their negative siblings (bPAC⁻) larvae were raised in the dark. Larvae at 5 dpf were anesthetized and mounted onto a glass-bottom small Petri dish (MatTek) with 1% low-melting-point agarose, and then exposed for 180 s to blue-light before laser surgery. Subsequently, the peripheral or central projections were axotomized immediately followed by a repeated exposure to blue-light stimulation for 60 s. For peripheral projections regeneration assays, the nerves were severed close to neuromast L1 and z-image stacks were captured every 2 h for 28 h. For analyses to quantify axon length in three-dimensions, plugins of ImageJ software were used. Specifically, the starting point according to injury site and the following point according to the location of axon were manually selected to trace the axon. For the same axonal branch, tracing from one point to the next point was performed until the axonal tip. After tracing the axon, the length of axon was shown automatically and the distance from cutting site to the position where the proximal tip of the defined axon was located was added by the length of all the tracing paths. The average velocity of axon re-growth is the ratio of the total distance the axon regenerated to the amount of time it took after onset of regeneration. For central projections regeneration assays, neurons were severed at >50 μm from the cell soma. Blue-light stimulation for 180 s at 24 hours post-injury (hpi) and 48 hpi was repeated. The extent of axon regeneration was recorded at 24 hpi, 48 hpi, and 72 hpi. Transected nerves in which axons retracted to soma or did not traverse the lesion site are categorized as *no regeneration*. Nerves that extended through the lesion were categorized as *regeneration*. Control animals for each group were treated identically.

2.2.4.4 Live Imaging

For live imaging, larvae were anesthetized with a 610 μM solution of the anesthetic 3-aminobenzoic acid ethyl ester (MS-222), mounted onto a glass-bottom 3 cm Petri dish (MatTek) and covered with 1% low-melting-point agarose with diluted anesthetic.

Images were acquired with an inverted laser-scanning confocal microscope, or an inverted spinning-disc confocal microscope (Visitron), with a 40X air or 63X water-immersion objective. Z-stacks of Schwann cells and axons consisted of 1- μ m-spaced images.

2.2.5 Detection of cell death

Apoptosis was assessed by the Terminal deoxynucleotidyl transferase dUTP Nick End Labeling (TUNEL) assay. Samples were fixed with 4% paraformaldehyde overnight at 4°C and dehydrated with methanol at -20°C. After gradual rehydration, the larvæ were permeabilized with 20 μ g/ml proteinase K for 20 minutes followed by 4% paraformaldehyde, and then incubated with 90 μ l labeling solution plus 10 μ l enzyme solution (In Situ Cell Death Detection Kit, Fluorescein, Roche) at 37°C for 3 hours in darkness. They were washed three times with PBST for 15 minutes each and the images were examined by confocal microscopy.

2.2.6 Quantification of Schwann cells

To quantify Schwann cells, images of a 1 mm-long segment were taken at the distal part of the injury and followed for 5 days. Schwann-cell nuclei were counted using H2A-mTurquoise expression, EGFP and BrdU staining.

2.2.7 Determination of cAMP levels

50 pg capped bPAC-V2A-mCherry RNA was prepared using a commercial mRNA kit (SP6 mMessageMachine Kit, Ambion) and injected into one-cell-stage wild-type embryos. Embryos were maintained in the dark and subjected to 180 s blue-light stimulation at 2 or 5 dpf. Groups of 30 embryos were collected immediately after the blue-light stimulation and homogenized in 0.1M HCl on ice. The samples were centrifuged at 4 °C and the supernatants were used in subsequent analysis. cAMP level was measured following the acetylation protocol from a cAMP ELISA kit (EnzoLife Sciences). Samples from light-stimulated bPAC-V2A-mCherry-injected embryos were diluted 30 times in order to obtain values within the standard range.

2.2.8 Quantitative analysis of the defect in the central axons

Embryos were mounted in 1% low-melting-point agarose in a glass-bottom small Petri dish (MatTek). Central axons were imaged using a laser-scanning confocal microscope (LSM 510; Carl Zeiss, Inc.). Images were analyzed by maximum-intensity z projections of raw images in ImageJ software (Schneider *et al.*, 2012). Branch tips were counted when $\geq 3.0 \mu\text{m}$ in length. Total branch lengths were measured using the segmentation tool of 3D tracing in simple neurite tracer plugin. Arbor areas were determined by drawing a convex polygon connecting the branch tips using the polygon tool. Arbor order was defined as the mean number of branch points between a terminal branch and the parent axon (Campbell *et al.*, 2007).

2.2.9 Pharmacology

cAMPS-Sp and H89 were dissolved in water before dilution in E3. The working solution of cAMPS-Sp and H89 is 100 μM and 15 μM , respectively. Zebrafish larvae were incubated in the drug solutions for 12 h before axotomy and maintained in the same solutions during the follow-up period after injury.

2.2.10 Zebrafish husbandry and care taking

All animals were kept at 28.5 °C with a 14 h-10 h light-dark cycle in a centralized facility in accordance to guidelines by the Ethical Committee of Animal Experimentation of the Helmholtz Zentrum München, the German Animal Welfare act Tierschutzgesetz §11, Abs. 1, Nr. 1, Haltungserlaubnis (Az.:5.1-5682/Helmholtz München/Erlaubnis G34). All experiments carried out with zebrafish at protected stages have been approved by the government of Upper Bavaria, Germany (animal protocols Az.:55.2-1-54-2532-202-2014 and Az.:55.2-2532.Vet_02-17-187).

2.2.11 Statistics

All the data were analyzed by GraphPad Prism software and shown as mean and standard deviation (SD). Outgrowth was calculated by tracing along all new regenerative processes (including all branches) using ImageJ software. Student's t-tests

(two-tailed) were used for two-group comparisons. Comparison of percentages for regeneration was by Fisher's exact test. A confidence interval of 95% to determine significance was used.

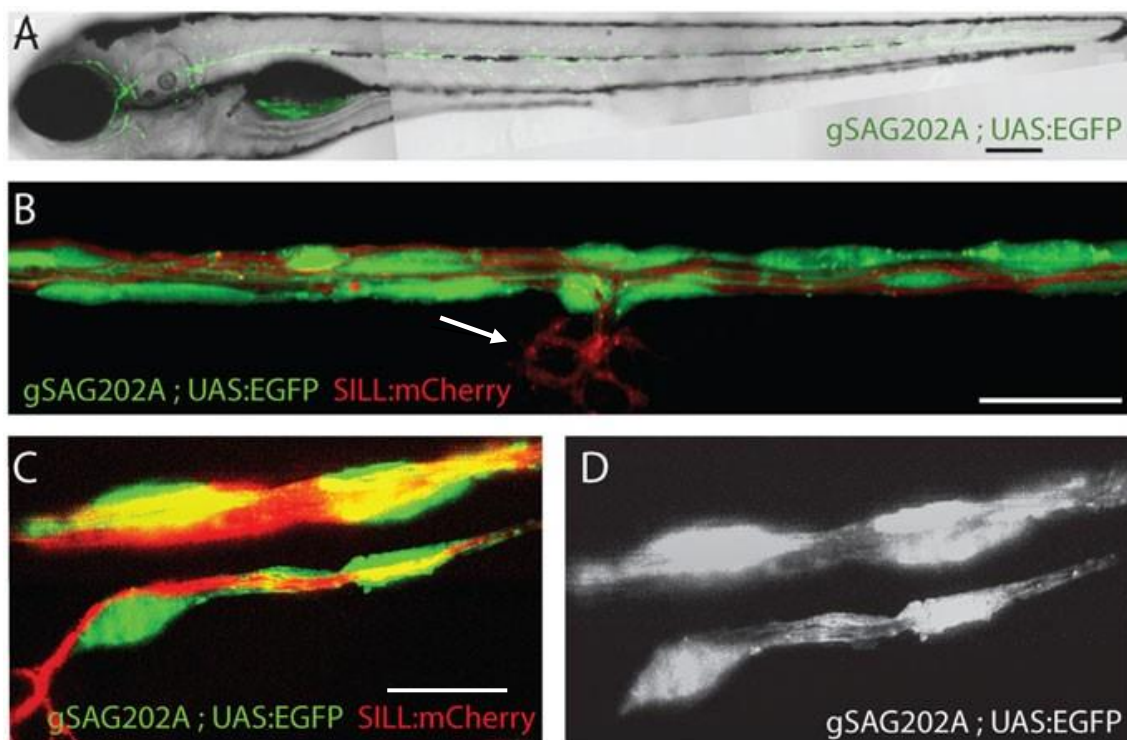
3. Results

3.1 Axon-glia interactions during the lateral-line peripheral nerve injury

3.1.1 The Tg[gSAGFF202A] transgenic line marking for Schwann cells

In the zebrafish, cell-type specific ‘driver’ transgenic lines producing the transcription factor Gal4 can express ‘effector’ genes under the control of an ‘upstream activating sequence’ (UAS). However, no Schwann-cell specific driver line exists in zebrafish. To overcome this deficiency, a large collection of transgenic strains were screened by Adèle Faucherre and Laura Pola-Morell (Dr. Hernán López-Schier lab, Helmholtz Zentrum München) by online database, which were generated in the laboratory group of Prof. Dr. Koichi Kawakami (The Graduate University for Advanced Studies, Japan) by random integration of a gene-trapping construct bearing a Gal4FF driver. One line called Tg[gSAGFF202A] was obtained from Prof. Dr. Koichi Kawakami’s group. By confocal live imaging, I found that this transgenic line activated the expression of UAS-controlled green-fluorescent protein (EGFP) in cells along the anterior and posterior lateral line in larval stages (Fig.3.1A). Initially, it was not possible to clearly identify the cells marked by Tg[gSAGFF202A;UAS:EGFP], because lateralis afferent axons and Schwann cells were in intimate contact. Upon closer examination, I found that neuronal central projections were not evident in the head of these transgenic animals (Fig.3.1A), suggesting that Gal4 expression was not in afferent or efferent neurons. To further test this assumption, I crossed Tg[gSAGFF202A; UAS:EGFP] with the Tg[SILL:mCherry] line, which expresses mCherry in lateral line afferent neurons. Examination of the triple-transgenic larva by laser-scanning confocal microscopy revealed that EGFP and mCherry were not co-expressed (Fig.3.1B). In particular, EGFP was not present in the terminal arborization of the afferent axons below the neuromasts (Fig.3.1B). To visualize the EGFP-expressing cells at higher resolution, lattice light-sheet imaging was taken in collaborative lab (John M. Heddleston, Tsung-Li Liu, Teng-Leong Chew in Janelia Research Campus, USA), which showed that the EGFP(+) cells formed tubes containing the mCherry(+) axons and the Gal4-expressing cells were perineural (Fig.3.1C-D). To better characterize these cells, I generated a new

stable transgenic line expressing the blue-fluorescent protein mTurquoise fused to Histone-2A under the control of UAS, which targets mTurquoise to the nucleus of Gal4-expressing cells. Tg[gSAGFF202A; UAS:H2A-mTurquoise; SILL:mCherry] triple transgenics showed blue-fluorescent nuclei in cells along the entire lateral line. The result showed that lateralis afferent axons were not labeled by mTurquoise (Fig.3.1E). Additionally, I injected the F-actin-binding domain of the calponin-homology domain of Utrophin (Utr-CH) fused to EGFP in single Gal4(+) cells in Tg[gSAGFF202A; SILL:mCherry]. The result showed discrete cells in intimate association with lateralis axons (Fig. 3.1F). To further characterize these cells, I labeled transgenic larva with the monoclonal antibody 6D2, which recognizes a carbohydrate epitope of piscine P0-like myelin glycoprotein in peripheral glial cells. This antibody marked the EGFP-expressing cells but not lateralis neuronal perykaria (Fig.3.1G). To further determine their identity, I did whole mount immunostaining using the Claudin-k antibody, which labels the junctional protein in Schwann cells of zebrafish. This antibody decorated all the Gal4(+) cells (Fig. 3.1H). These data demonstrated that the Tg[gSAGFF202A] transgenic line expressed Gal4 in Schwann cells.



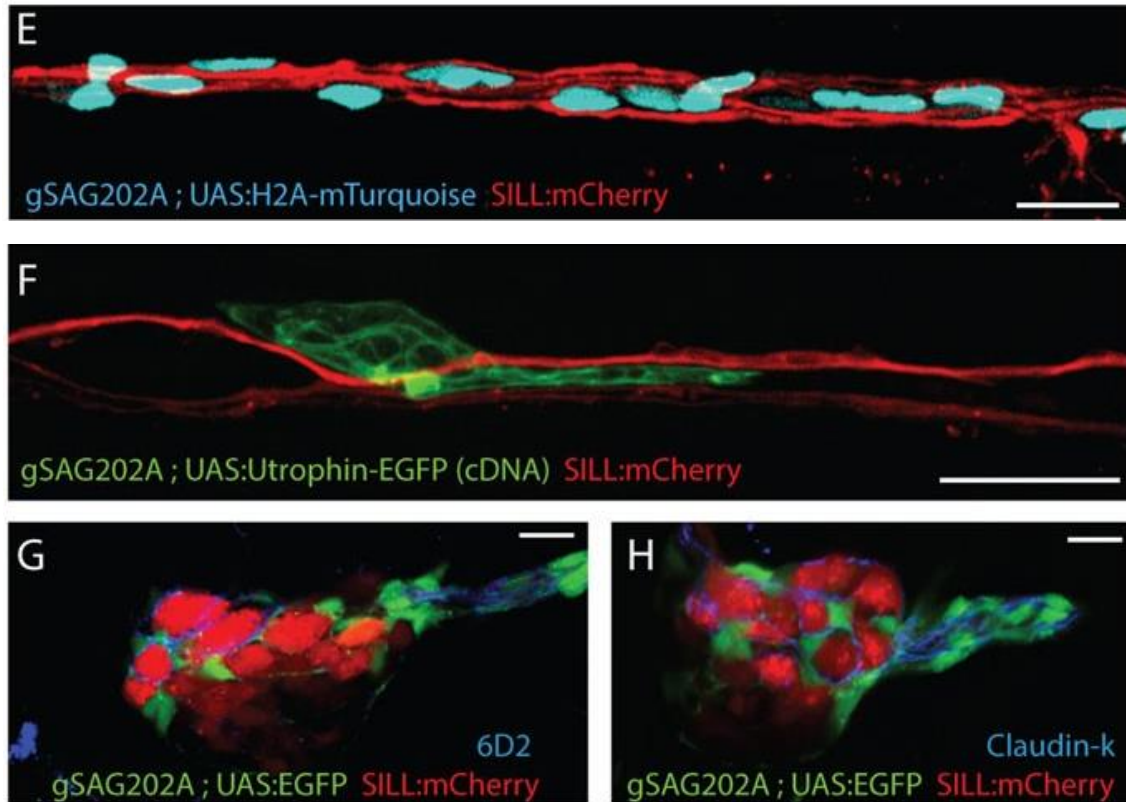


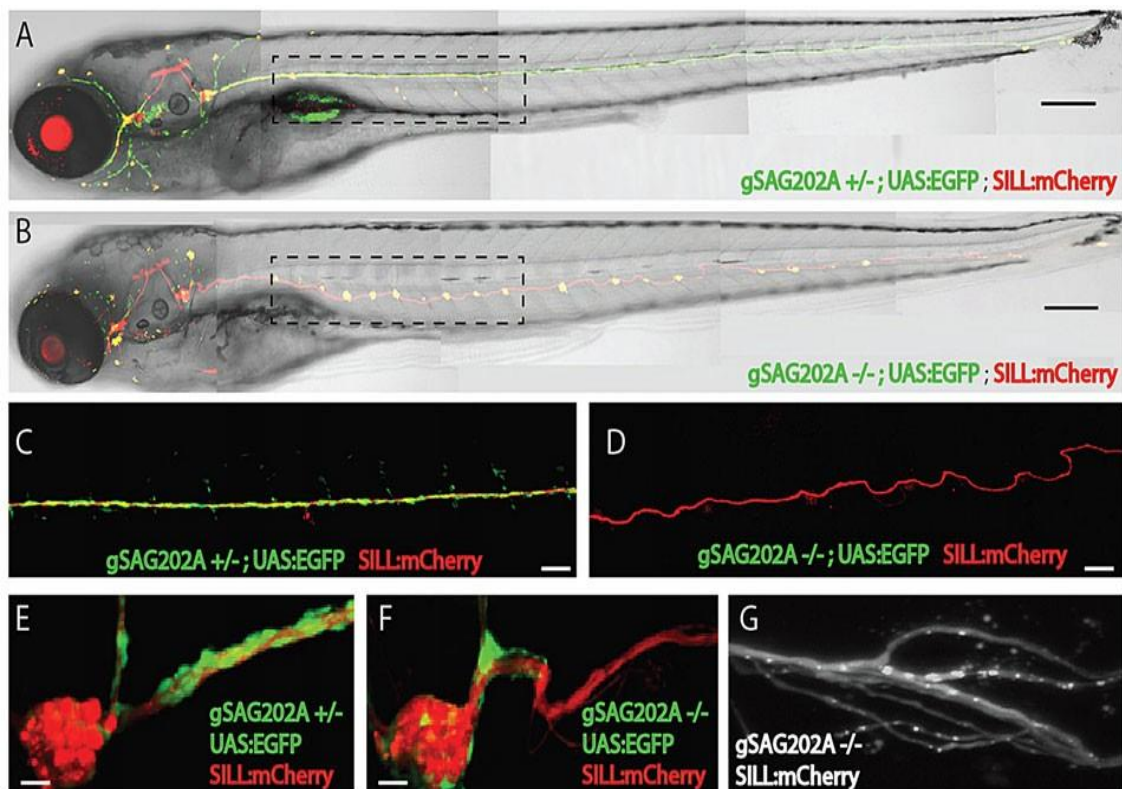
Fig.3.1. Tg[gSAGFF202A] is a specific Gal4 driver in Schwann cells

(A) EGFP expression pattern at 5 dpf by Tg[gSAGFF202A;UAS:EGFP]. (B-D) Triple transgenic Tg[gSAGFF202A;UAS:EGFP;SILL:mCherry] at 5 dpf show that EGFP(+) cells form tubes wrapping around an mCherry (+) axon by confocal (B) and lattice light-sheet imaging (C-D). The white arrow indicates the position of the neuromast. (E) A triple transgenic larva (Tg[gSAGFF202A; UAS:H2AmTurquoise;SILL:mCherry]) at 5 dpf. Nuclei of cells that are in intimate contact with lateralis afferent axons are shown in blue along the trunk. (F) Marking of individual cell shows UtrCH-EGFP expression in a 4 dpf Tg[gSAGFF202A;SILL:mCherry] double transgenic fish injected with UAS:UtrCH-EGFP construct. (G) The marker 6D2 labels EGFP-expressing cells in a lateral plane of posterior ganglion. (H) The marker Claudin-k labels EGFP-expressing cells in a lateral plane of posterior ganglion. In the figures, dorsal is up and anterior is left. Scale bars: 150 μm (A) and 10 μm (B-H).

3.1.2 The Tg[gSAGFF202A] insertion disrupts the *ErbB2* gene

I found that incrossing two heterozygous Tg[gSAGFF202A] fish produced 25% of individuals with more than twice the number of neuromasts found in wild-type animals

(Fig.3.2A-B), suggesting that the insertion is mutagenic. Furthermore, I observed the absence of Schwann cells along the posterior lateral line (Fig.3.2C-F) and axon fasciculation defects of lateral line afferent neurons in Tg[gSAGFF202A] homozygous larva (Fig.3.2 G). Therefore, I checked the online database <https://ztrap.nig.ac.jp/ztrap/> made by the laboratory group of Prof. Dr. Koichi Kawakami (The Graduate University for Advanced Studies, Japan) and found that this transgene bearing a Gal4FF driver was positionally mapped and the insertion site was sequenced (Fig.3.2H). Moreover, I aligned the sequences nucleotides on https://www.ensembl.org/Danio_reio/Info/Index (zebrafish genome reference assembly z10) and found that it was inserted in the first coding exon of the *ErbB2* locus (Fig.3.2I). Thus, the Tg[gSAGFF202A] insertion represented a recessive, fully penetrant and strongly expressive loss-of-function allele of *ErbB2*.



H AAAACTGGACTCTGA~~agagtggc~~GTGAAAATGCGGTGGGCCCCGCGGCCAG
TCGCCGCGTCTTCGGCACCGTAAACGGGTGTCAAC

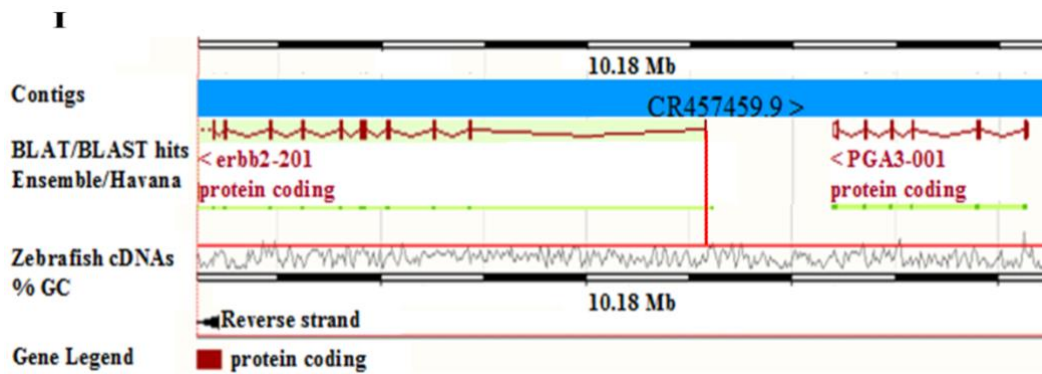


Fig.3.2. The phenotype of homozygous Tg[gSAGFF202A] fish

(A) Heterozygous Tg[gSAGFF202A;UAS:EGFP;SILL:mCherry] 5 dpf larva treated with 4-Di-2-ASP, revealing the normal pattern of neuromasts in its posterior lateral line (5 neuromasts within the dashed rectangle). (B) A homozygous Tg[gSAGFF202A;UAS:EGFP;SILL:mCherry] fish at 5 dpf possesses around twice as many neuromasts (10 neuromasts within the dashed rectangle). (C and E) The normal expression pattern of the posterior ganglion and lateral line in heterozygous Tg[gSAGFF202A;UAS:EGFP;SILL:mCherry] fish 5 dpf. (D and F) At 5 dpf, the abnormal expression pattern of the posterior ganglion and lateral line in homozygous Tg[gSAGFF202A; UAS:EGFP;SILL:mCherry] fish, in which Schwann cells cannot migrate far away from the posterior ganglion. (G) Imaging reveals details of the axonal defasciculation in homozygous Tg[gSAGFF202A;UAS:EGFP;SILL:mCherry] larva at 5 dpf. (H) The integration site indicated by red nucleotides. (I) BLAST (basic local alignment search tool) shows the insertion within the first exon of *ErbB2* gene. Scale bars: 150 μ m (A-B), 50 μ m (C-D) and 10 μ m (E-G).

3.1.3 Differential responses of Schwann cells to acute and chronic denervation

To investigate responses of Schwann cells to neuron injury, I designed a method to generate acute or chronic denervation of Schwann cells in whole animals by axon severing (Fig.3.3A,B) or neuronal ablation (Fig.3.3C-F), respectively. The strategy consisted of inducing plasma-mediated cell damage by directing a pulsed ultraviolet laser (355nm, 400ps/2.5 μ J per pulse) onto the living specimen. The laser was coupled to a spinning-disc inverted microscope and focused to axons for severing (Fig.3.3A) or neuronal soma for ablation (Fig.3.3C-D) in Tg[SILL:mCherry] transgenics. Observation at 1 h after microsurgery confirmed complete severing (Fig.2.3B) or neuronal ablation (Fig.3.3E-F).

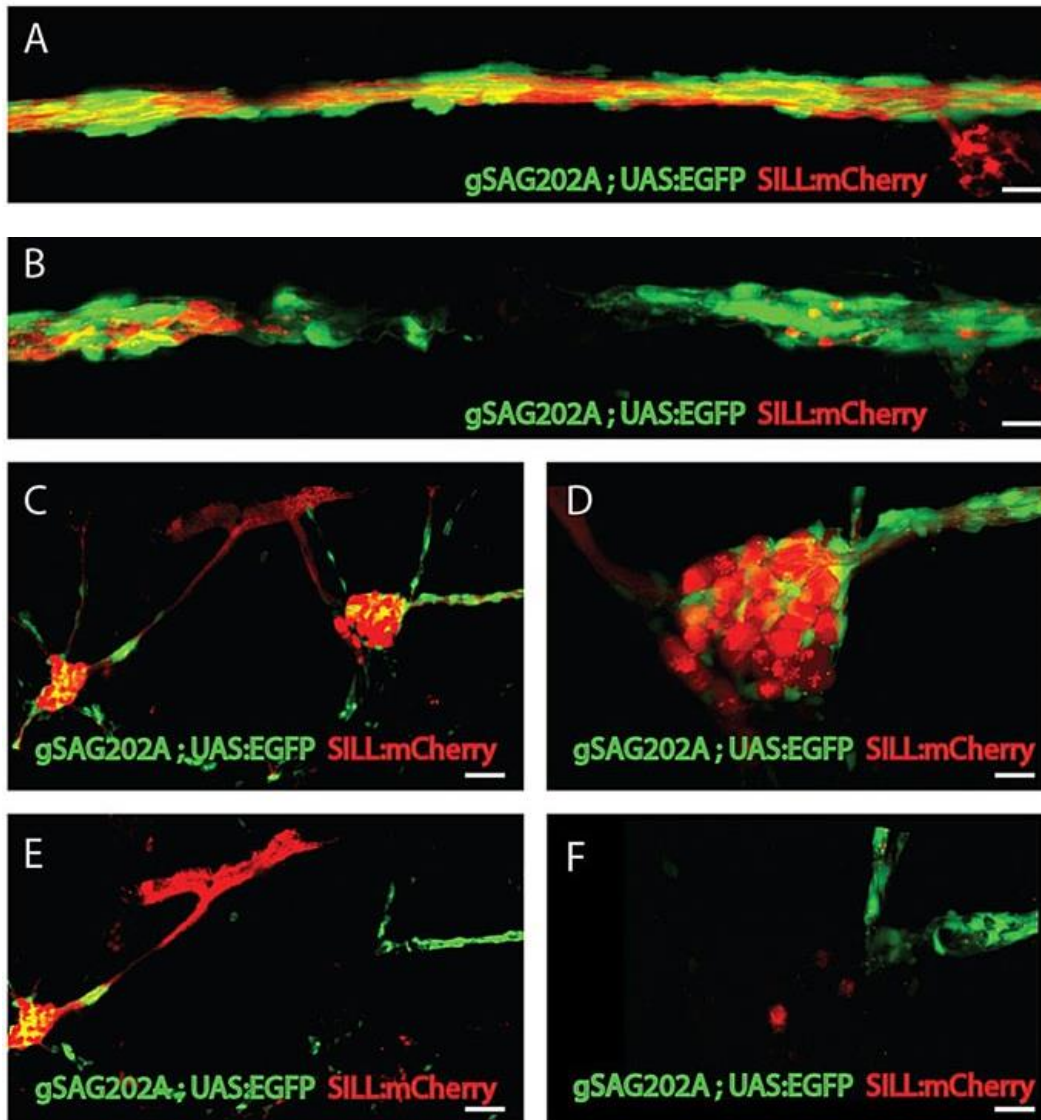


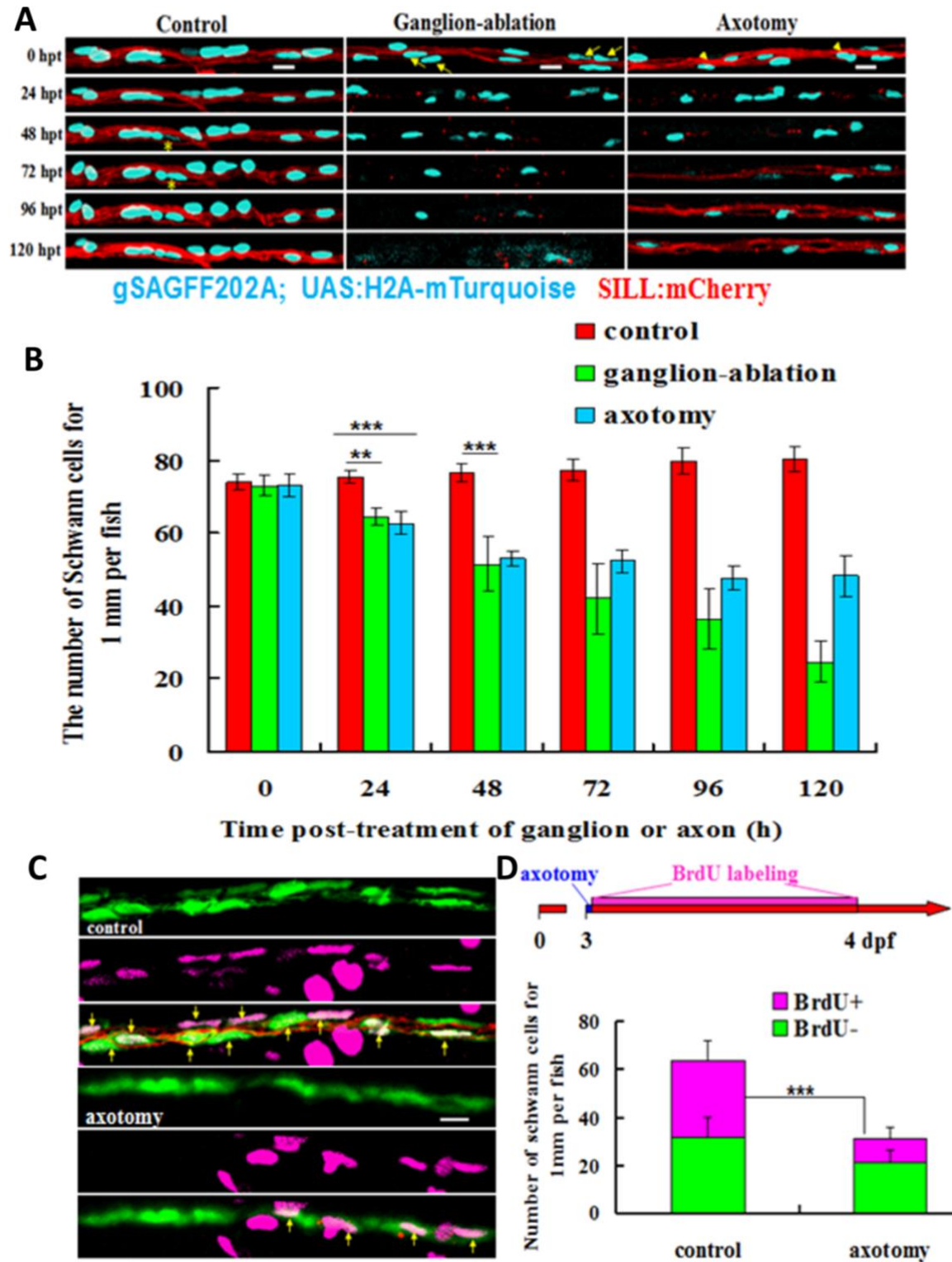
Fig.3.3. Selective axonal severing and neuronal ablation by laser

(A, B) High magnification of the lateral line nerves before laser ablation (A) and after laser ablation (B). The nerve and Schwann cells are precisely and completely severed with no visible damage to the surrounding tissue. (C) The maximal projections of anterior and posterior ganglion before ablation. (D) Higher magnification of posterior ganglion before ablation. (E) The image of the same animal after ablation reveals that the posterior ganglion was totally ablated. (F) Higher magnification of posterior ganglion after ablation. Scale bars: 10 μ m (A, B, D, F) and 50 μ m (C, E).

To better investigate responses of Schwann cells, I used Tg[gSAGFF202A; UAS:H2A-mTurquoise; SILL:mCherry] triple transgenics starting at 5 dpf to quantify Schwann cells after denervation (Fig.3.4A-B). A follow-up period of 5 days showed a

significant decrease in the number of Schwann cells marked with H2A-mTurquoise beginning at 24 hours post-trauma (hpt) (Fig.3.4B). The number of Schwann-cell continued to decrease in the fish lacking afferent neurons but stopped in fish with transected axons at 48 hpt (Fig.3.4A-B). The decrease of Schwann cells upon denervation might be due to the loss of fluorescent-protein expression. However, this possibility was not supported for two reasons. First, I used H2A-mTurquoise as a Schwann-cell marker. Although I have not directly measured the stability of the H2A-mTurquoise fusion protein, histones are known to be some of the most stable proteins in animal cells, with a half-life of several months (Toyama et al., 2013), suggesting that even if Schwann cells ceased to express Gal4 immediately after denervation, fluorescence would persist in nuclei for longer than the 5-days follow-up period. Second, I did not observe widespread loss of H2A-mTurquoise, which would be expected if Schwann cells ceased to express Gal4 after denervation (Fig.3.4A-B). Alternatively, glial depletion upon denervation might result from increased Schwann-cell apoptosis, or by physiological cell death accompanied by abnormally reduced Schwann-cell proliferation. To test these possibilities, I performed a 24 h pulse-chase analysis of DNA synthesis by BrdU incorporation in Schwann cells as a proxy for cellular proliferation, starting at 3 dpf (Fig.3.4C-D). I quantified Schwann cells within 1 mm of the fish trunk and found that approximately 50% of the Schwann cells were BrdU(+) in control animals (BrdU(+) 32.1 ± 5.9 cells; BrdU(-) 31.4 ± 8.2 cells; n=8), suggesting that these cells underwent active proliferation (Fig.3.4D). Upon acute denervation, I observed the reduction in the number of Schwann cells, and that only around 33.6% of the Schwann cells were BrdU(+) (BrdU(+) 10.5 ± 4.5 cells; BrdU(-) 20.8 ± 8.5 cells; n=8 larvæ) (Fig.3.4D). To assess cell death, I used the TUNEL assay in Tg[gSAGFF202A; UAS:H2A-mTurquoise; SILL:mCherry] transgenics starting 24 h after denervation. TUNEL-positive staining in Schwann cells was rarely observed in the control fish (n=5), whereas prominent and widespread TUNEL signal co-localized with H2A-mTurquoise in the experimental animals (TUNEL (+) Schwann cells 11.7 ± 3.8 in larvæ with ablated ganglia, n=8; TUNEL (+) Schwann cells 5.6 ± 1.1 in larva with severed axons, n=8), (Fig.3.4E-F). I also directly visualized Schwann-cell

dynamics by confocal live imaging of the quadruple transgenics, Tg[gSAGFF202A; UAS:EGFP; UAS:H2A-mTurquoise; SILL:mCherry], which clearly showed the mitotic behavior and apoptosis of denervated Schwann cells (Fig.3.4G).



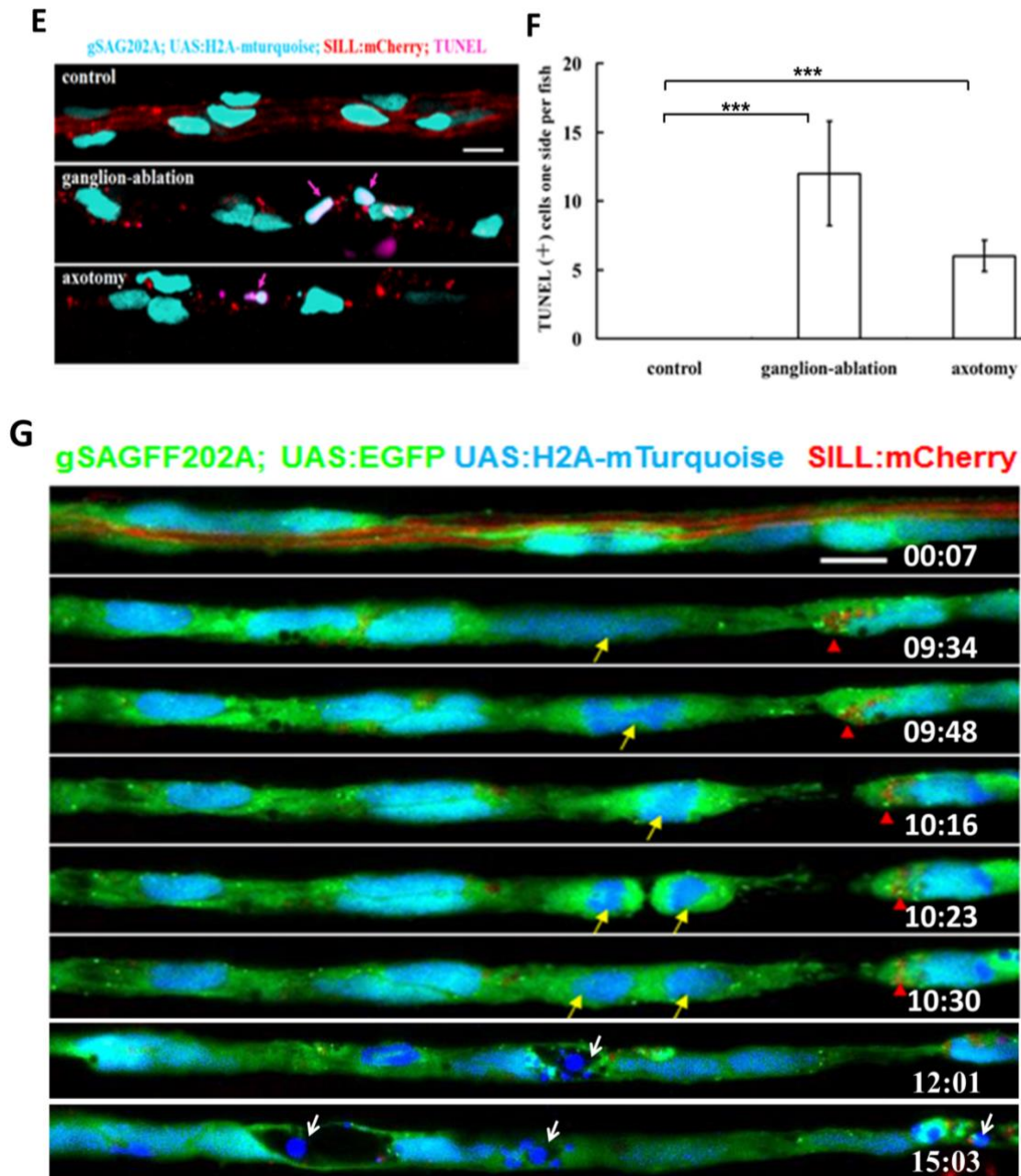


Fig.3.4. Differential responses of Schwann cells to acute and chronic denervation

(A) 24 hpt, 48 hpt, 72 hpt, 96 hpt, 120 hpt in the control, ganglion-ablated and axotomy groups. Yellow asterisk marks the proliferative cells. Yellow arrows and arrowheads indicate the dead cells.

(B) Quantification of Schwann cells, showing a significant reduction in the group with severed axons (n=6) and ganglion-ablated group (n=8) compared with the control group (n=5) (** p<0.001, ***p<0.0001).

(C) Control and axon-transected Tg[gSAGFF202A; UAS:EGFP;SILL:mCherry] larvæ treated with BrdU. (D) The larvæ were subject to axon severing at 3 dpf and treated with BrdU for 24 hours. Fewer BrdU-positive Schwann cells were observed in the axon-transected fish (n=8)

compared to the control group (n=8) (**p<0.0001, two-tailed t test). (E) Examination of apoptotic Schwann cells by TUNEL assay. Pink arrow indicates co-localization of H2A-mTurquoise with TUNEL-positive cells. (F) Quantification of TUNEL positive Schwann cells in the control group, the ganglion-ablation and axon-severed group (**p<0.0001). (G) Frames captured from time lapse images of a Tg[gSAGFF202A; UAS:EGFP;UAS:H2A-mTurquoise; SILL:mCherry] larva with severed axons. Numbers in lower right corners denote time elapsed from the first frame of the movie. Red arrowhead marks axon debris that has been phagocytosed by the Schwann cells. At 10:23 hpt Schwann cells started to divide (yellow arrow) when no intact axon exists. White arrow points to apoptosis of denervated Schwann cells. Error bars are + or ± SD. Scale bars: 10 μm (A, C, E, G).

To assess architectural changes of denervated peripheral glia, I used the 6D2 and the anti-Claudin-k antibodies (Fig.3.5 A-L). In control animals, 6D2 decorated Schwann cells around the lateralis afferent ganglia and neuronal peripheral axons (Fig.3.5A-C). Upon laser ablation of the posterior ganglion (Fig.3.5D), the central axons and projections rapidly degraded. Schwann cells around the ganglion were also ablated with the laser (Fig.3.5D-E). I chose samples that presented no new-born neurons within the period of analysis (Fig.3.5D,G,J). At 24 hpt, Schwann cells devoid of axons began to lose expression of the P0-like myelin glycoprotein (Fig.3.5G-I), and had lost virtually all 6D2 labeling at 48 hpt (Fig.3.5J-L). A detailed visualization of the trunk of the treated specimens showed Claudin-k uniformly distributed along the lateralis nerve (Fig.3.5M). After axonal severing, the Schwann cells around the proximal nerve stump maintained Claudin-k protein, whereas the Schwann cells in contact with the distal degenerating axons began to lose Claudin-k protein expression starting at 8 hpt (Fig.3.5M). The levels of Claudin-k distal to the site of injury remained lower than on the proximal part, even after axonal regeneration at 26 hpt (Fig.3.5M). However, Claudin-k protein levels in Schwann cells returned to normal and were equivalent on both sides of the axonal cuts around 72 hpt (Fig.3.5M).

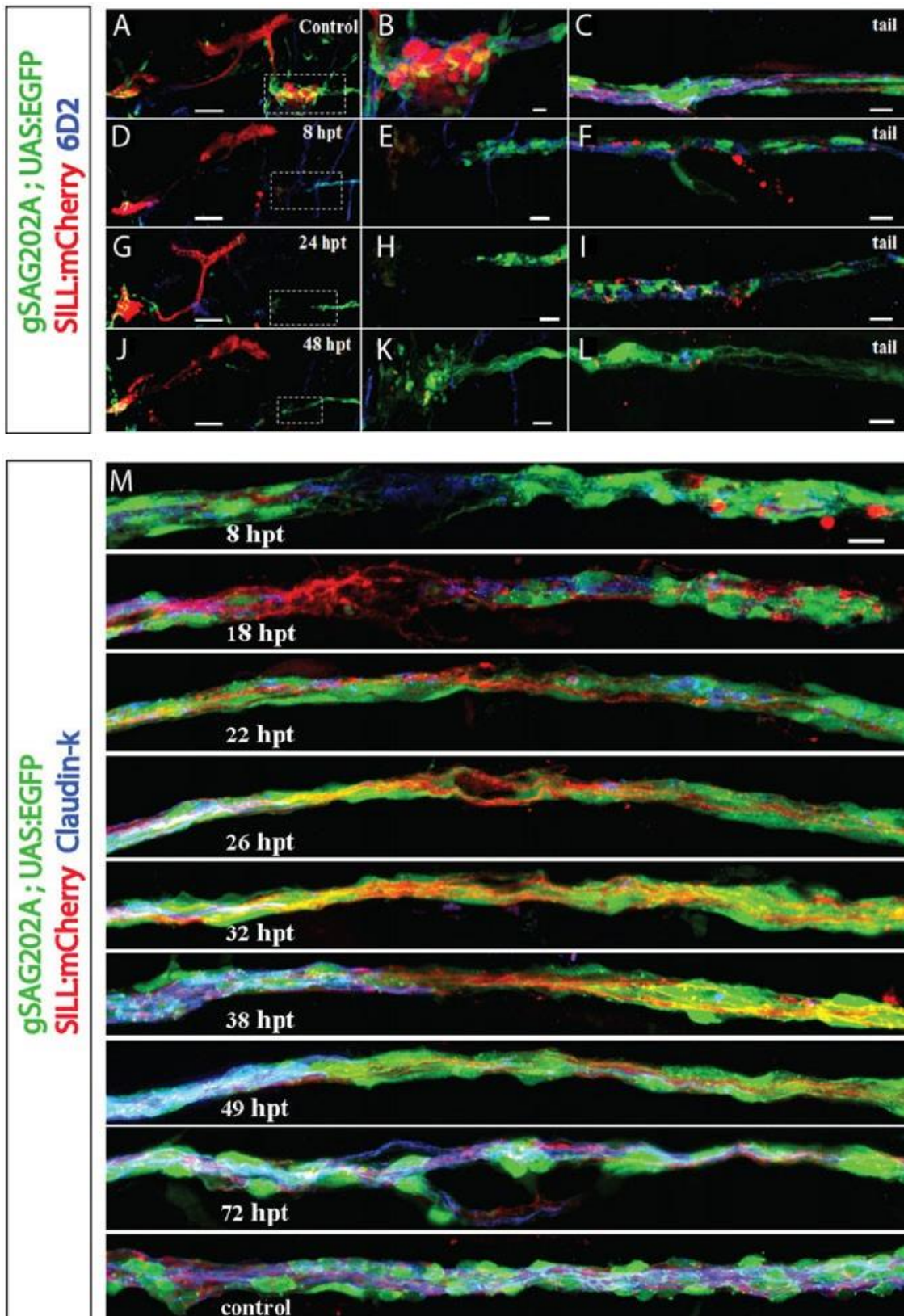


Fig.3.5. Gradual loss of expression of myelin glycoprotein and Claudin-k junctional protein upon axon severing or ganglion ablation

(A-L) Maximal projection of Tg[gSAGFF202A; UAS:EGFP;SILL:mCherry] larvæ immunolabeled

with myelin 6D2 antibody (blue). (A,D,G,J) The cephalic region showing the anterior and posterior ganglion before ganglionostomy (A) and at 8-48 hpt in fish with ganglion ablation (D,G,J). (B,E,H,K) Higher magnification of boxed region in A,D,G,J, respectively. (C,F,I,L) Images of the animal's tail, corresponding to A,D,G,J. (D, G, J) At 8 hpt, 24 hpt, 48 hpt, immunostaining images reveals gradual loss of myelin protein. (F, I, L) Immunostaining of fish tails delineates the loss of myelin and clearance of axon debris in a gradual manner. (M) Time-course analysis of axonal regeneration and Claudin-k junctional protein expression (blue) in the Schwann cells around the site of damage. Claudin-k is present along the perineurium in control fish (lowest panel). A marked reduction of Claudin-k in the perineurium distal to the cutting site can be seen at 8 hpt. Distal Claudin-k protein levels remain lower than on the proximal part of the perineurium even after axonal regeneration at 26 hpt, and only increase around 72 hpt. Scale bars: 50 μm (A,D,G,J), 10 μm (B-C, E-F, H-I, K-M).

3.1.4 Schwann cells facilitate but are dispensable for axonal re-growth

To investigate the influence of Schwann cells on the rate and extent of axon re-growth after injury, I used the double-transgenic larvae Tg[gSAGFF202A; SILL:mCherry] at 5 dpf, when the posterior lateralis ganglion contains around 50 neuronal perikarya. The stereotypic position of this ganglion and the lateral branches of the afferent axons towards the neuromasts were used to precisely define a site of axonal cuts between samples (Fig.3.6B). Additionally, I used the somites along the trunk to quantify the extent of axonal regeneration (Fig.3.6A). All afferent axons were severed between the posterior ganglion and the first neuromast situated between somites 5 to 7. A time-course analysis of axonal regeneration in the wild-type double-transgenic Tg[gSAGFF202A^{+/-}; SILL:mCherry] fish revealed that severed axons began to regrow within the 24 hpt. On average, the fastest growth cones reached 12.7 ± 0.9 somites at 24 hpt, and continued to grow at an average speed of 0.4 ± 0.1 somites per hour until they reached the tip of the tail, which occurred within 72 hpt (Fig. 3.6A-B). By contrast, in Tg[gSAGFF202A^{-/-}] mutants, axons showed a much slower rate of re-growth, advancing on average to the somite 5 by 24 hpt, and stabilizing at around somite 9 by 72 hpt, with negligible further growth and often some retractions during the remainder

of the follow-up period (Fig. 3.6A-B).

The defective circuit recovery in the *ErbB2* mutants might be due to neuronal death. Therefore, I quantified the number of lateral line afferent neurons in wild type and *ErbB2* mutant fish under control and traumatic conditions. I counted the number of neurons using confocal stacks of the posterior lateral line ganglion in Tg[gSAGFF202A; SILL:mCherry]. Wild-type larva at 5 dpf had around 53 neurons, whereas the average number of neurons in *ErbB2* mutants was 51 (Fig.3.6C). Over the course of 5 days, ganglia grew to 65.2 ± 3.1 and 63.2 ± 1.7 neurons by 10 dpf in wild type and *ErbB2* mutants ($p=0.097$), respectively. Axon severing did not affect neuronal number or ganglion growth in wild type animals (48 hpt: control 56.8 ± 2.2 neurons, severed axons 55.8 ± 3.6 neurons, $p=0.81$; 120 hpt: control 65.2 ± 3.1 neurons, severed axons 64.2 ± 3.3 neurons, $p=0.65$). However, axon severing had a profound effect on neuronal viability in the *ErbB2* mutants (48 hpt: control 56.5 ± 3.7 neurons, severed axons 51.3 ± 2.5 neurons, $p<0.05$; 120 hpt: control 63.2 ± 1.7 , severed axons 42.3 ± 3.6 neurons, $p<0.0001$) (Fig.3.6C). Neural-circuit recovery in wild type fish might result either from the efficient re-growth of damaged axons, from the growth of axons of newborn neurons (~ 2 new neurons per day), or from a combination of the two processes. Whole-fascicle severing experiments did not allow the discrimination between axonal regrowth and axonogenesis by newborn neurons. To directly test the growth capacity of severed axons in control and *ErbB2* mutants, I severed the peripheral axon of a single identified afferent neuron marked by microinjection SILL:EGFP plasmid DNA. The transgenic line Tg[gSAGFF202A; SILL:mCherry] was used to identify *ErbB2* mutants with axon defasciculation and to ensure that EGFP expressors were lateralis afferent neurons. The results showed that after laser ablation of the entire axons, the single EGFP-marked axons can efficiently regrow in wild-type larva, but not in *ErbB2* mutants (Fig.3.6D).

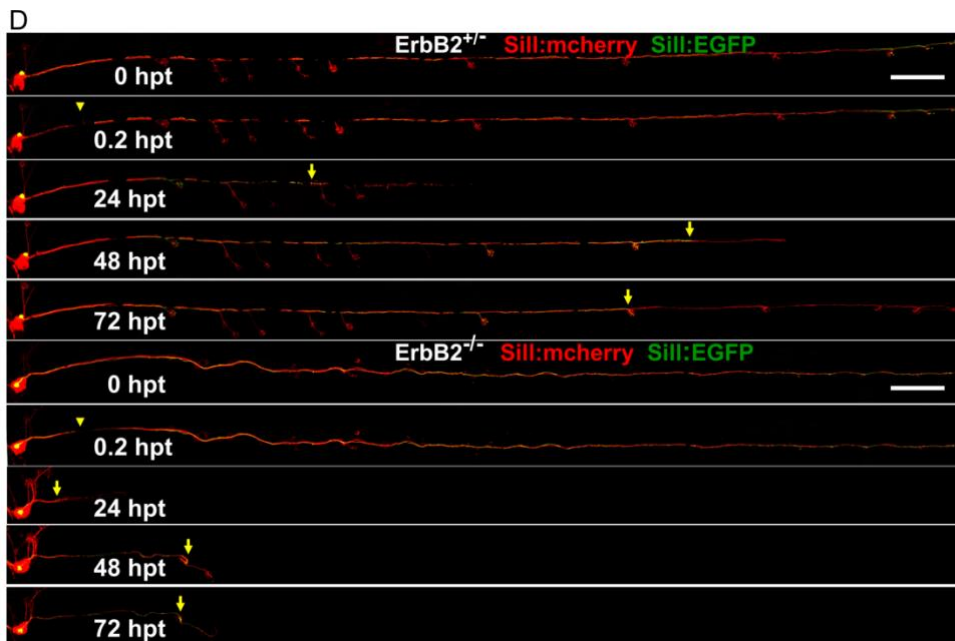
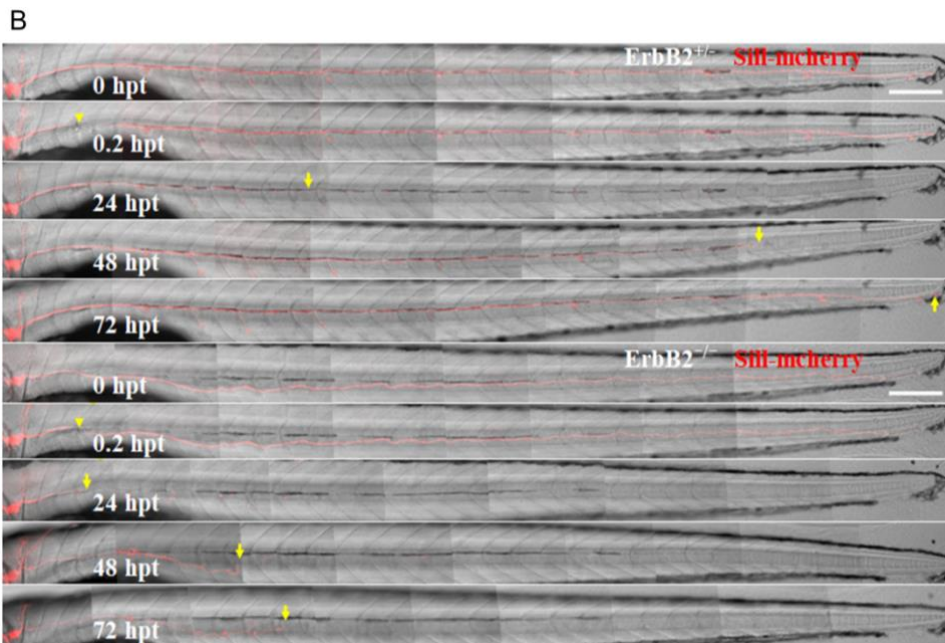
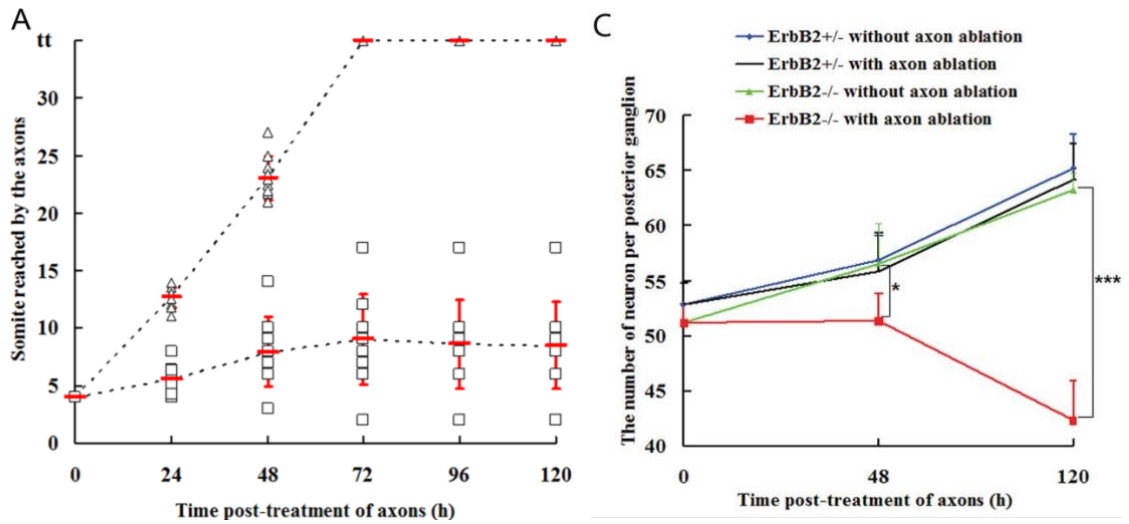


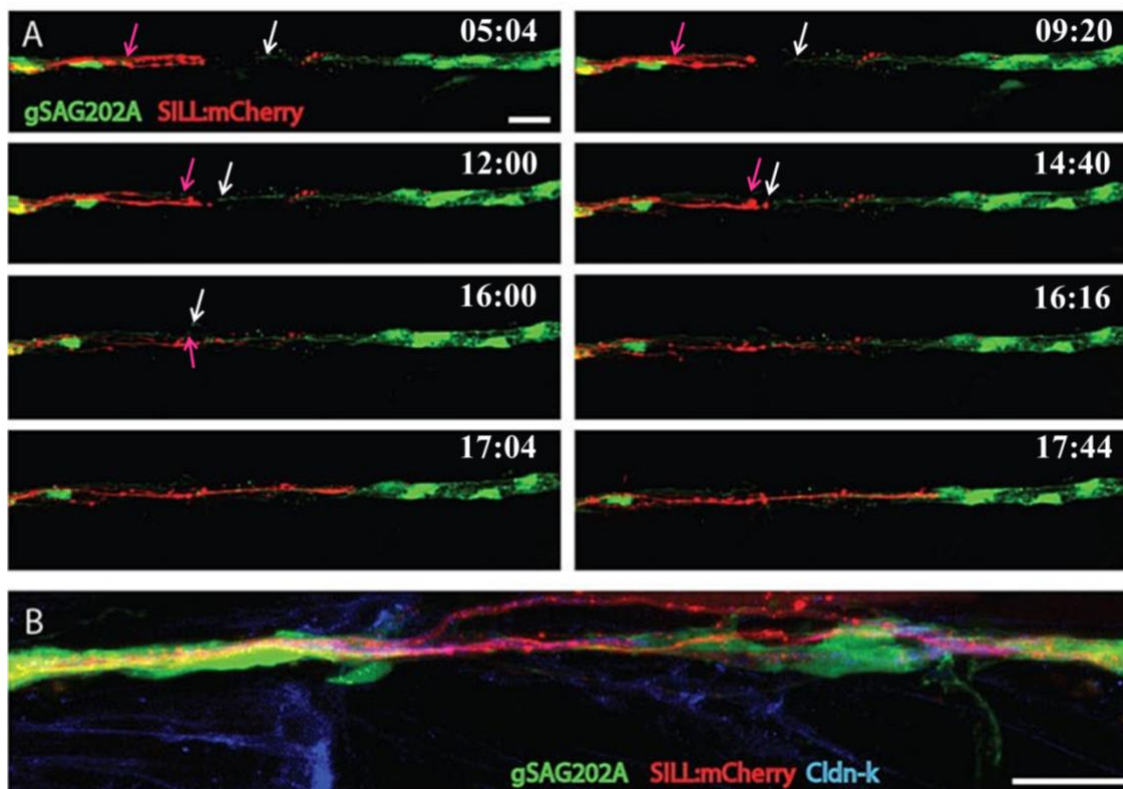
Fig.3.6. Schwann cells facilitate but are dispensable for axonal regeneration

(A) The axons were severed at somite 3 in 5 dpf larvæ. The somite reached by the regenerating nerve was examined at 24, 48, 72, 96, 120 hpt. In all cases (n=10) the axons had reached the tip of the body and re-innervated the terminal neuromasts at 72 hpt in Tg[gSAGFF202A^{+/-}; SILL:mCherry] (triangles). All cases (n=10) of Tg[gSAGFF202A^{-/-};SILL:mCherry] fish revealed an abnormal and lower regeneration rate (squares). (B) Examples of axon regeneration after injury in heterozygous and homozygous Tg[gSAGFF202A;SILL:mCherry]. (C) Sum of neuron numbers in posterior ganglion at 5 dpf and 48 hpt, 120 hpt in Tg[gSAGFF202A^{+/-};SILL:mCherry] and Tg[gSAGFF202A^{-/-}; SILL:mCherry] larvæ upon laser-mediated axon severing or in the untreated group. n=6 fish per group. (*p<0.05, ***p<0.0001) (D) Examples of an identified axon's regeneration after damage in heterozygous and homozygous Tg[gSAGFF202A;SILL:mCherry] fish injected with SILL:EGFP. Yellow arrowheads and arrows point to cutting sites and to the tip of regenerate axons, respectively. Error bars are + or ± SD. Scale bars: 150 µm (B, D).

To assess the dynamic relationship between axons and Schwann cells during axonal regrowth, I performed live imaging in Tg[gSAGFF202A; UAS:EGFP;SILL:mCherry] triple transgenics. Laser mediated axon severing also ablated Schwann cells locally and formed a glial gap (Fig.3.7A). I found that, immediately after injury, there was a retraction of the proximal and distal axon fragments, accompanied by a physiological clearing of distal axonal debris (Fig.3.7A). Distal and proximal Schwann cells adjacent to the injury extended bridging processes towards the glial gap. Axonal growth cones seemed to accompany proximal glial processes, with growth and retraction phases that alternatively leave Schwann-cell processes leading and lagging the growth-cone tips. Regenerating axons were found to preferentially extend growth cones around the Schwann cells and cross the injury site as soon as the glial gap was bridged (Fig.3.7A). When the bridging of the gap by Schwann cells did not occur, re-growing axons stalled, and only resumed growth upon physical contact with the distal Schwann cells (Fig.3.7A). Additionally, I found that regenerating axons were readily myelinated by the distal Schwann cells, but often remained defasciculated over the injury site (Fig.3.7B).

3.1.5 Schwann cells are necessary for the re-innervation of peripheral targets

I observed that “lateral” Schwann cells associated with axon terminal projections below the neuromasts (Fig.3.7C). Therefore, I used these axon terminal projections to investigate whether Schwann cells play a role in the re-innervation of sensory organs by regenerating axons. To this end, I severed axons before two adjacent neuromasts (control and experimental) and ablated the lateral Schwann cells of the more rostral neuromast (experimental). The Tg[gSAGFF202A;UAS:EGFP;SILL:mCherry;Brn3c:mEGFP] animals expressing green fluorescence in hair cells enabled the identification of the experimental and the control neuromasts before and after the damage (Fig.3.7C). A follow-up period of 72 hours showed that Schwann cells at the main axonal bundle did not migrate to replace the ablated lateral Schwann cells, leaving the experimental neuromasts devoid of glia. Further, I found that regenerating axons always re-innervated the control neuromasts, but in 7 out of 9 cases failed to re-innervate the experimental neuromasts devoid of Schwann cells.



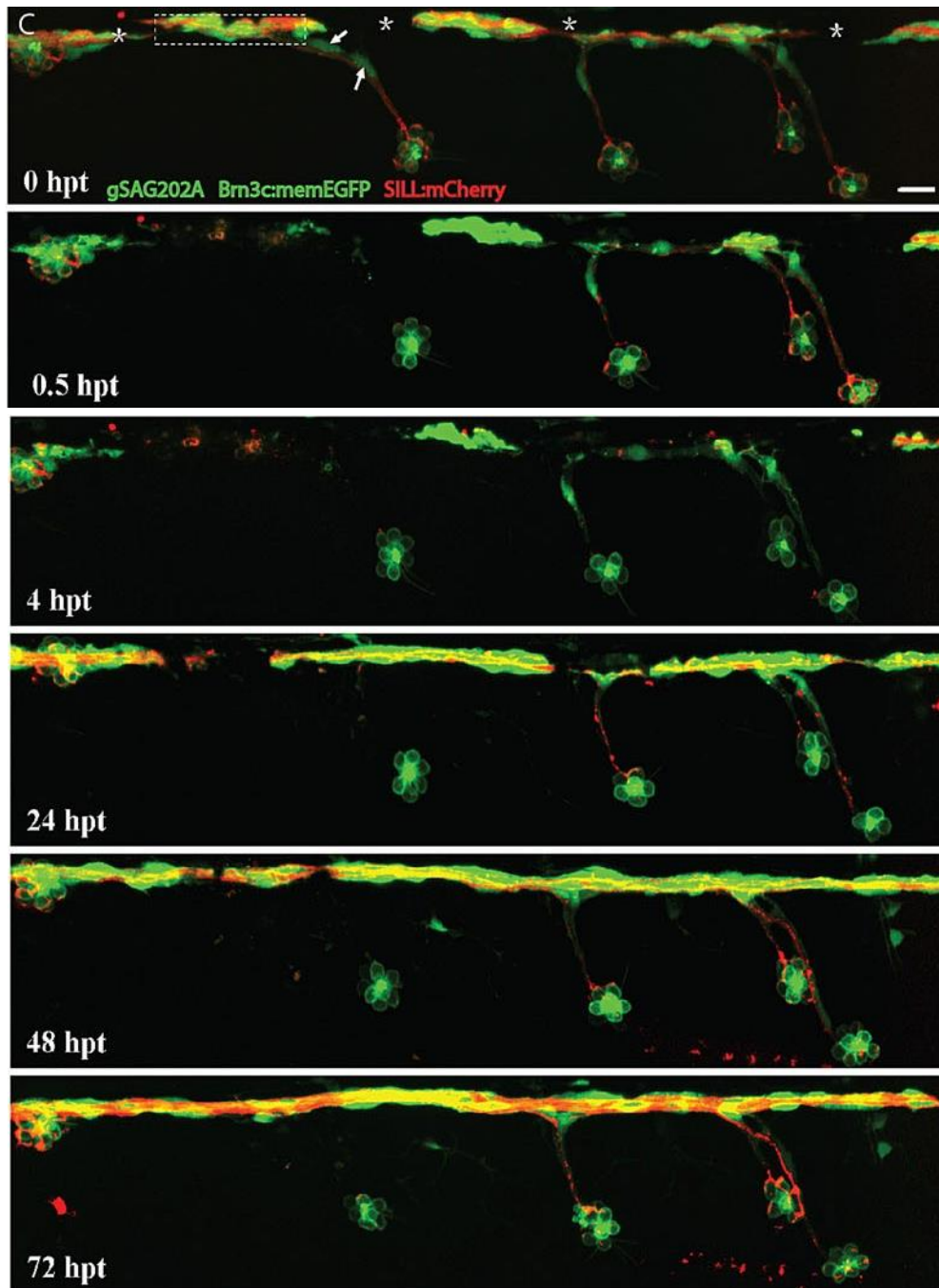


Fig.3.7. Regenerating axons followed Schwann cell processes

(A) Frames captured from time-lapse imaging of a Tg[gSAGFF202A; UAS:EGFP; SILL:mCherry] larva with severed axons, leaving a glial gap. Time elapsed from the first frame of the time-lapse imaging are from left to right and top to bottom: 05:04 h, 09:20 h, 12:00 h, 14:40 h, 16:00 h, 16:16 h, 17:04 h, 17:44 h. Images were taken every 8 min. The pink arrow points to the process tip of proximal Schwann cells and the white arrow points to the process tip of distal Schwann cells. At 16 hpt axons started to regrow when Schwann cells filled the gap. (B) An example of partially defasciculated axons at the site of injury. (C) A quadruple transgenic Tg[gSAGFF202A;

UAS:EGFP;SILL:mCherry;Brn3c:mGFP] larva starting at 6 dpf and following 0.5 hpt, 4 hpt, 24 hpt, 48 hpt, 72 hpt after axon severing and ablation of lateral Schwann cells. At 24 hpt, regenerating axons re-innervated the neuromast with lateral Schwann cells, but failed to re-innervate neuromasts devoid of lateral Schwann cells even at 72 hpt. Asterisk marks pigment cells. Arrows point to ablated lateral Schwann cells. Dash frame indicates the site of the cut. Scale bars: 25 μ m (A-C).

3.2 The development of the central axons in the lateral-line afferent neurons

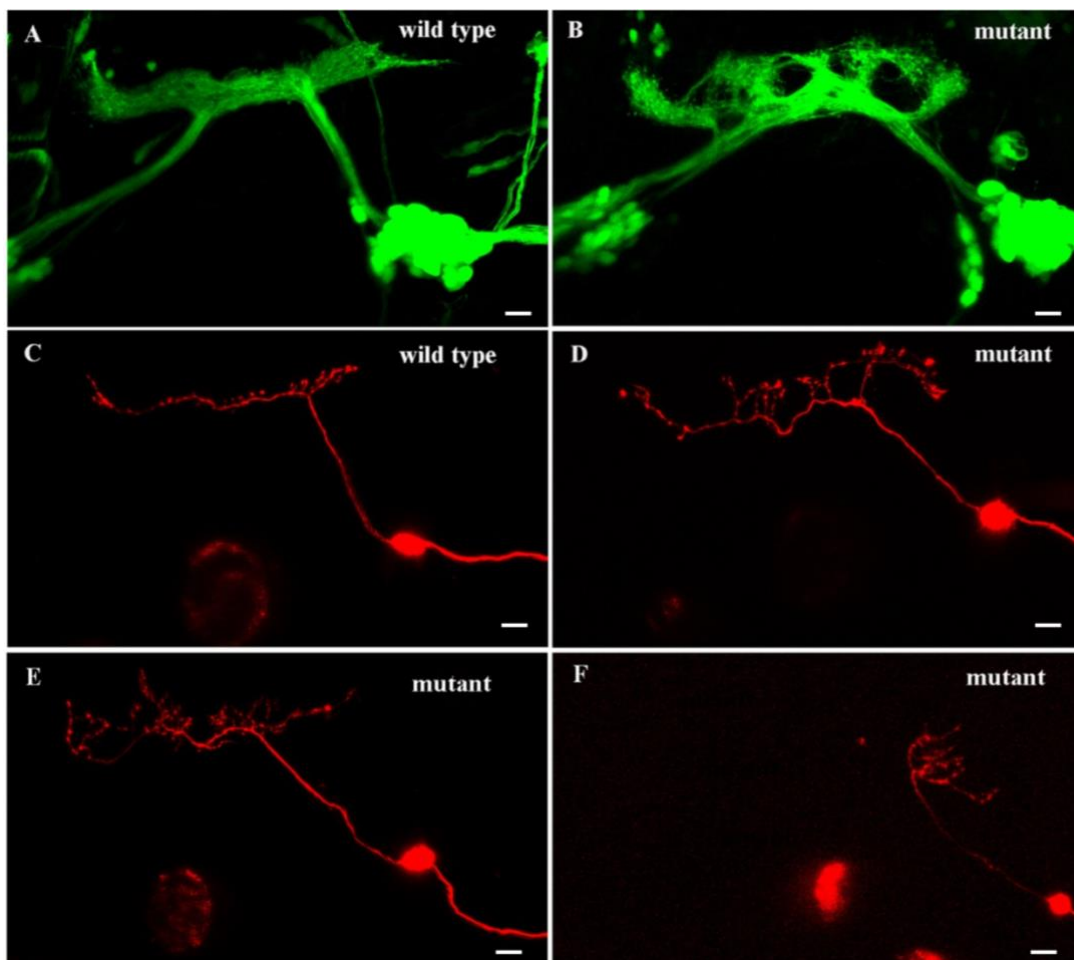
3.2.1 The defect of central axons in the lateral-line afferent neurons

In the lateral-line afferent neurons, the mechanism mediating how central axons of new-born neurons navigate to their targets remains unknown. To identify molecular mechanism controlling axonal pathfinding in the lateral-line central nervous system, I investigated the mutant strain of zebrafish that arose spontaneously. Incrossing between male and female Tg[HGn39D] fish accidentally produced classic Mendelian ratio of phenotypically normal and abnormal progeny with upward curved tails, which indicated that the mutant strain possessed a recessive mutation.

In the wild-type animals, central (parental) axons bifurcated into two daughter branches that extended in opposite directions along the rostrocaudal axis of the hindbrain and grew in a strictly ipsilateral manner (Fig.3.8A). I found that the zebrafish mutant in the Tg[HGn39D] transgenic line showed dramatic morphological defects in the central axons of lateral-line afferent sensory neurons (Fig.3.8B). In particular, the neurons in mutant animals overshoot the target area, whose axons can often be found extending more dorsally into the hindbrain. Interestingly, these axons did not cross the midline to invade territories outside the hindbrain (Fig.3.8B). The number of neurons and the overall structure and localization of the lateral-line posterior ganglia seem normal in the mutant strain (Fig.3.8A-B).

To understand how central axons were affected in the mutant, I directly visualized the projection pattern of aberrant axons at single-cell resolution using microinjection of

DNA coding for the red-fluorescent protein mCherry under the control of the SILL enhancer. This was injected into fertilized eggs of the Tg[HGn39D] transgenic line, which labeled all the afferent neurons of the lateral line with EGFP. The individual central axons in wild-type zebrafish bifurcated into two daughter branches along the rostrocaudal axis in the hindbrain, which can be easily visualized from a lateral perspective (Fig.3.8C). In the mutants, 39% of the neuron produced parental axons that bifurcated normally (Fig.3.8E, H). However, in the remaining 61% of the neurons, one of the daughter branches, either the rostral or the caudal, failed to extend horizontally (Fig.3.8D, F-H). Instead, these branches aberrantly continued to extend in the same direction as the parental axon and grew into the dorsal of hindbrain. Moreover, central axons in the mutant strain possessed significantly longer length, larger branching areas, more branch number and branch order (Fig.3.8I-L)



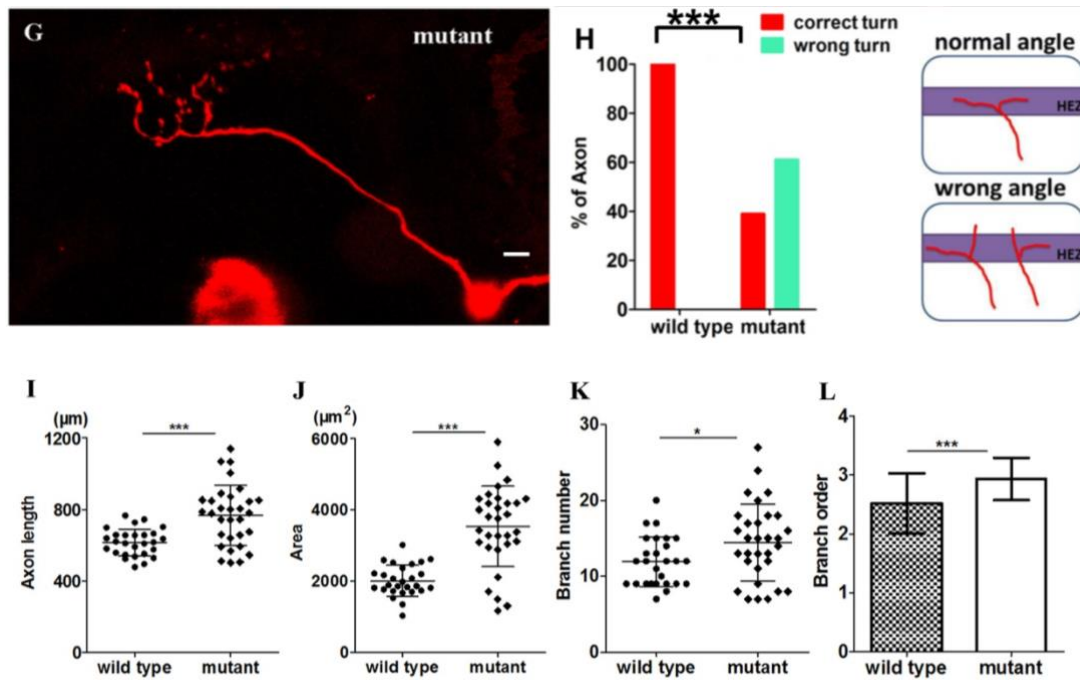


Fig.3.8. Misguidance of central branches in the mutant zebrafish

(A) The stereotypical pattern of central axons is shown in Tg[HGn39D] wild-type zebrafish at 5 dpf. (B) The defect of sensory afferent neurons into the hindbrain is revealed in 5dpf mutant embryos. (C) Marking of solitary neurons in a 5 dpf wild-type embryos by injection with SILL:mCherry plasmid DNA. Normally, sensory axons bifurcate at the hindbrain entry zone (HEZ) and turn to grow along the rostrocaudal axis. However, one of the two horizontal branches in the mutant does not make the right angle turn but instead extends straight along the dorsoventral axis and grows into the hindbrain (D, F-G). In some cases, the daughter branches can make the correct turn and later form longer sprouts from the bifurcated axons (E). (H) The number of afferent neurons that have or have not made the correct turn is quantified and plotted as the percentage of the total labeled neurons. (I-L) The afferent central axons of the mutant (n=30) possess a significant increase in arbor length, arbor area, the number of branch tips, and arbor order compared to wild-type (n=27). Error bars represent SD. * $p < 0.05$, *** $p < 0.001$. Scale bars: 10 μm (A-G).

3.2.2 The different effect in other neurons of hindbrain

In zebrafish, the hindbrain includes serially repeated classes of individually identifiable neurons. The Mauthner cells are two large reticulospinal neurons located in the hindbrain segment 4, near the entry of the VIII cranial nerve. To investigate whether

Mauthner cells are affected or not, I used the monoclonal antibody 3A10 (anti-neurofilament) to examine the axonal projections of Mauthner cells (Burgess *et al.*, 2009). The immunostaining revealed normal Mauthner cell axon-pathfinding in the mutant compared with wild-type sibling larva at 3 dpf (Fig.3.9A-L).

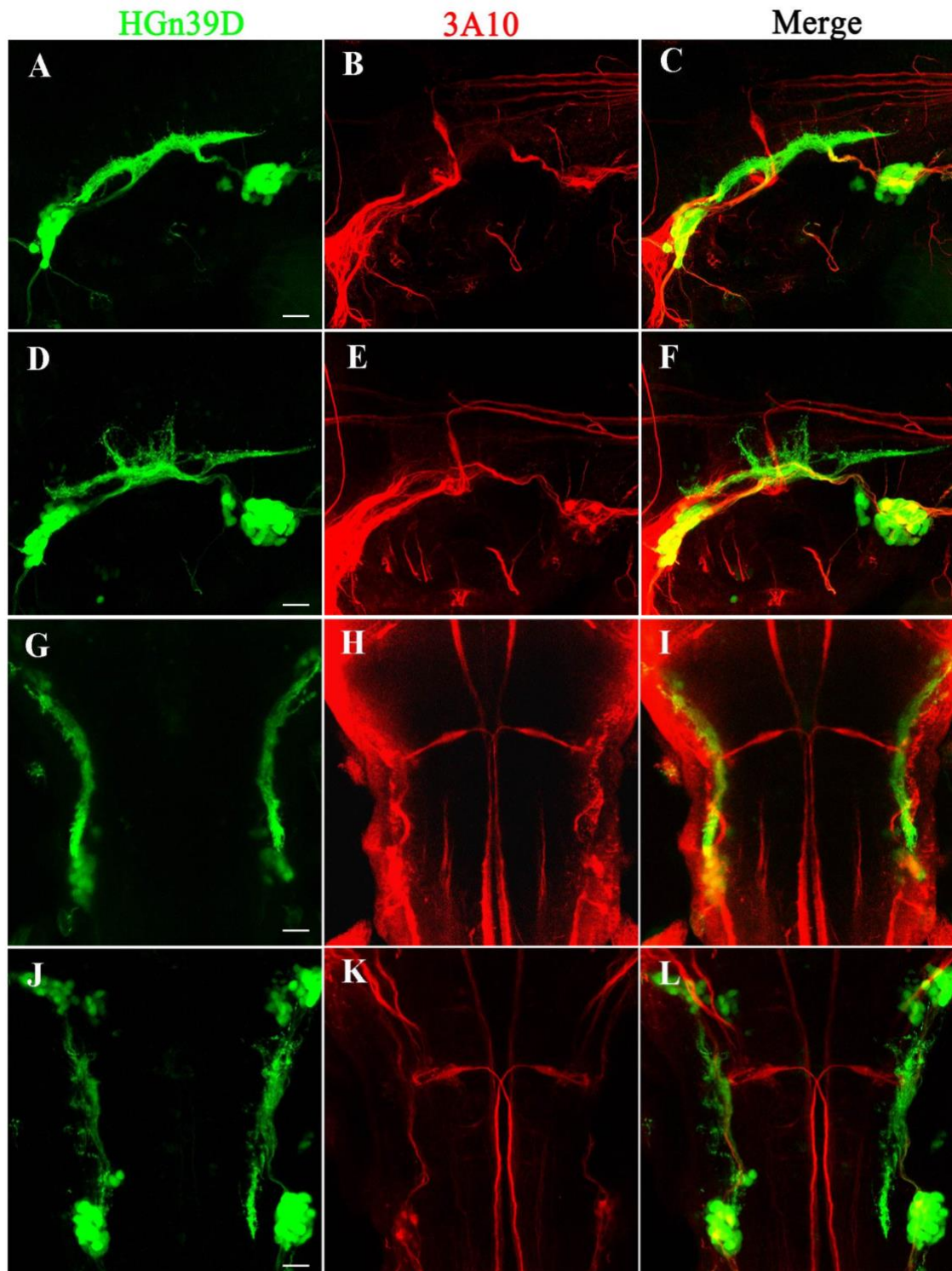
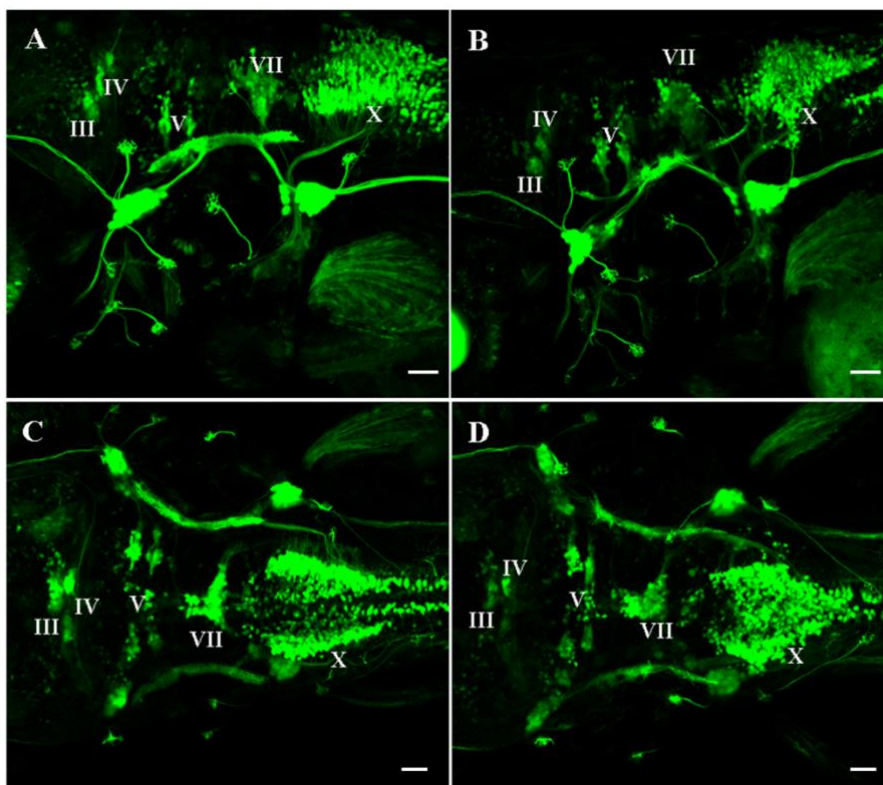


Fig.3.9. Mauthner axons can normally cross the midline in mutant zebrafish.

Immunostaining was performed with the 3A10 antibody (red) to show the similar morphology of Mauthner axons at 3 dpf Tg[HGn39D] (green) wild-type (A-C) and mutant (D-F) in lateral view. Maximal projections of two Mauthner cells in dorsal view demonstrated that they can cross the midline in both wild-type (G-I) and mutant (J-L). Scale bars: 30 μ m (A, D, G, J).

Additionally, the Tg[Islet:GFP] fish was used to visualize other neurons in the hindbrain by crossing with the mutant zebrafish. I found that the overall structure of branchiomic nerves III, IV, V, VII was not affected (Fig.3.10A-D), whereas the soma of branchiomic nerves X presented strongly abnormal uniform distribution through the midline of the hindbrain in the mutant strain (Fig.3.10A-D).

**Fig.3.10. The soma of branchiomic nerve X with abnormal uniform distribution in mutant**

The phenotype can be distinguished by the morphology of central axons in lateral line afferent neurons marked by Tg[HGn39D]. The branchiomic nerves III, IV, V, VII marked by Tg[Islet:GFP] were overall similar between the wide type (A, C) and the mutant (B, D). However, the branchiomic nerves X showed difference between the wide type and the mutant in lateral view (A,

B) and dorsal view (C, D). Scale bars: 30 μ m (A-D).

To further understand the anatomical defects of mutant fish, I used the acetylated tubulin antibody to investigate the structure of the entire nervous system. The immunostaining showed that the mutant at 3 dpf have irregular axon-like fibers in the hindbrain, compared with wild-type fish (Fig.3.11A-F).

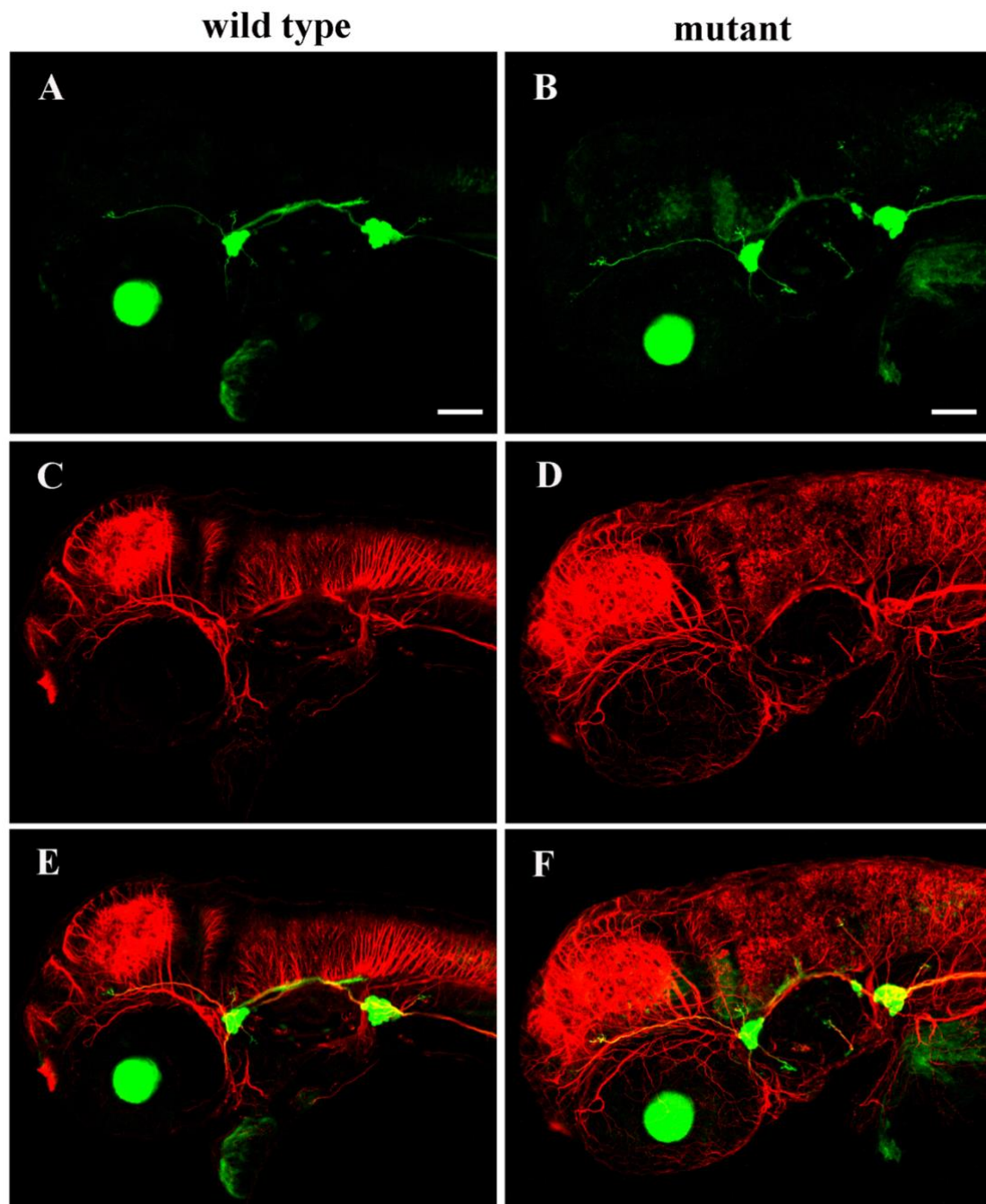


Fig.3.11. The mutant zebrafish with massive defects in the hindbrain

The mutant can be distinguished by the defect of central axons in lateral line afferent neurons marked by Tg[HGn39D] (green) (A, B). The acetylated tubulin staining revealed that the structure was disorganized in the hindbrain of the mutant fish (D, F), whereas wild-type fish possessed structure with regular axon-like fibers (C, E). Scale bars: 75 μ m (A-B).

3.2.3 Cell non-autonomous control central axons growth

The gene mutation disrupted the central projections of the lateral line afferent neurons, and it was not clear whether the effect is intrinsic or extrinsic to these neurons. To address this issue, I generated chimæric zebrafish by transplanting cells from a donor embryo into a host embryo at the appropriate embryonic stage. Donor cells can be targeted to a specific region of the developing blastula or gastrula stage host embryo by choosing a transplantation site in the host embryo based on well-established fate maps (Kemp et al., 2009; Pujol-Martí et al., 2014). When cells were transplanted in low numbers from a transgenic donor into a host embryo, I could image single donor derived and fluorescently labeled lateral line nerves, within a host environment. The lateral line afferent neurons resulting from wild-type cells transplanted into wild type host embryos had a normal morphology (n=16) (Fig.3.12A,C,E). The wild-type neurons in the mutant fish behaved like the mutants (Fig.3.8E), as the neurons formed longer branches from the bifurcated axons (n=8) (Fig.3.12B,D,F). Therefore, the results suggested that the mutated gene acted cell-non-autonomously in axonal navigation to their correct target area in the hindbrain.

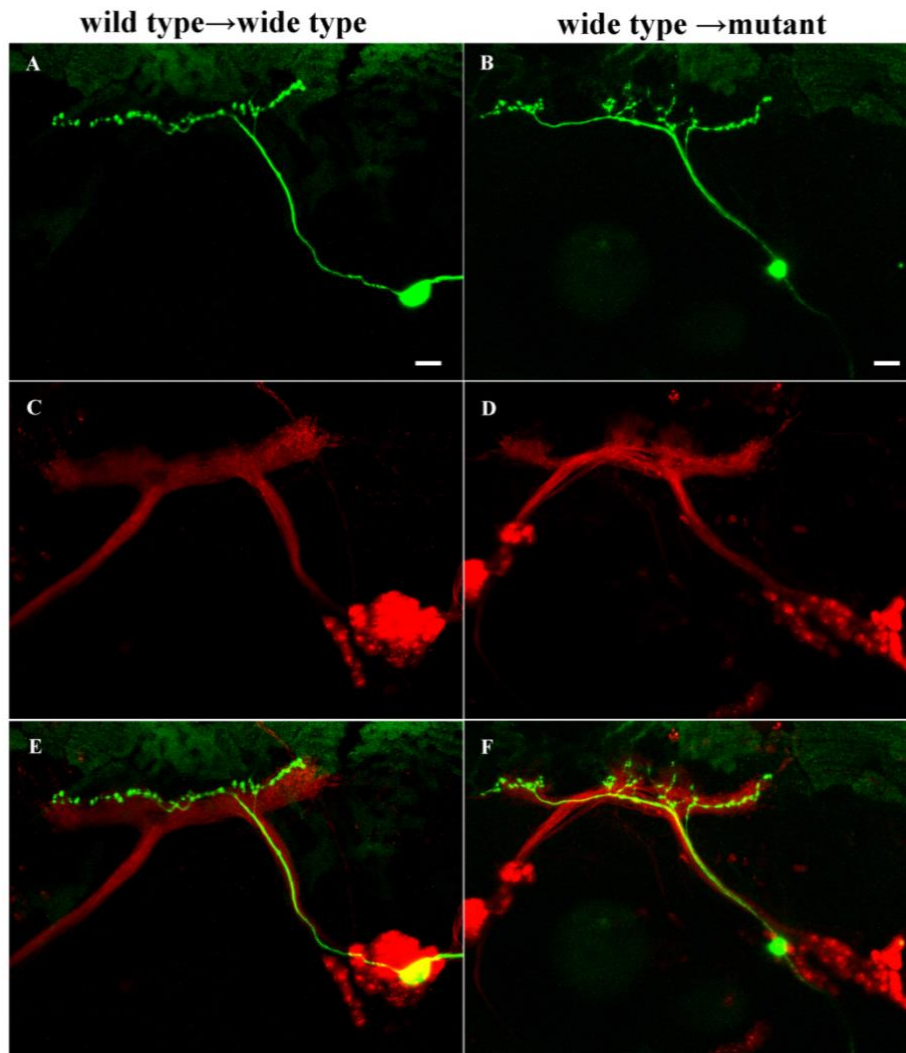


Fig.3.12. The central axon growth in the mutant acts in a cell non-autonomous manner

Representative pictures of single axon transplanted from wild-type donor into the wild-type host (left panel) and into the mutant host (right panel). Individual afferent neuron from the wild-type donor of Tg[HGn39D] (green) transplanted to the wild-type host of Tg[SILL:mCherry] showed normal morphology (A,C,E). However, the wild type donor of Tg[HGn39D] transplanted to the mutant host of Tg[SILL:mCherry] overshoot its target (B,D,F). Scale bars: 10 μ m (A-B).

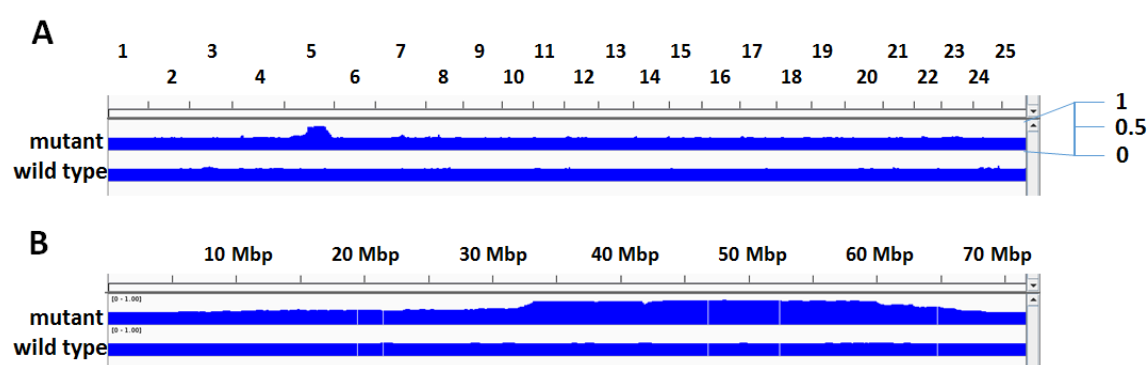
3.2.4 The analysis of causative gene by whole genome sequencing

The mutated gene was a recessive mutation, because incrossings of heterozygous mutant fish produced the classic Mendelian ratio (3:1) of phenotypically normal and abnormal progeny. To identify the mutation on the zebrafish genome, heterozygous mutant fish with the wild-type AB genetic background were outcrossed with the

highly-polymorphic strain WIK, and subsequently the mutant carriers with AB/WIK genetic background were incrossed to generate homozygous mutant embryos and their siblings. I extracted the genomic DNA from a pool of 50 mutants and 50 phenotypical wild-type siblings that was sent to our collaborator (laboratory group of Prof. Dr. Strähle Uwe, Next Generation Sequencing Core facility, Institute of Toxicology and Genetics, Karlsruhe Institute of Technology, Germany) for paired-end Illumina sequencing and analysis. The sequence reads were aligned to the zebrafish genome version 10 (zv10). Totally, 20 Gb sequences were generated including 10 Gb per pool, which was equivalent to a sevenfold genomic coverage (the zebrafish reference genome sequence is 1.4 Gb). Single nucleotide polymorphisms (SNP) with homozygosity score were plotted against their respective position on the annotated genome (Fig.3.13A). Analysis of all the SNP across 25 chromosomes identified the prominent position of homozygosity on chromosome 5 (Fig.3.13A, B) (Voz *et al.*, 2012). Based on a cut-off value of 0.9 for the homozygosity score, only one region on chromosome 5 was selected as the candidate: a 26.9 Mb region from position 33,170,176 to 60,091,309. To identify the mutated *locus* within this interval, the potential transcript-producing genes were searched by exporting annotated transcripts from Ensembl. In total, 334 SNP were located within the gene-coding region. Among these, 5 SNP produced nonsense mutations, 5 SNP were frameshifts (Table 3.1). The remainder represented missense mutations; only one missense mutation was selected for further investigation (Table 3.1). This missense mutation was the repulsive guidance molecule family member b (Rgmb), a glycosylphosphatidylinositol (GPI)-anchored protein that contributed to the patterning of the developing nervous system (Monnier *et al.*, 2002; Liu *et al.*, 2009). Also, the missense mutation in Rgmb was deleterious to protein function by sorting intolerant from tolerant analysis (SIFT), which could predict whether the amino acid substitution would affect protein function, and hence potentially alter phenotype. Additionally, tmem232 was the transmembrane protein 232, which had a yet unknown function and expressed in neurons and glial cells (Zhang *et al.*, 2014). Therefore, I chose Rgmb and tmem232 as the candidate genes for further validation.

Table 3.1 Mutations identified by whole genome sequencing

| Gene | Codons | Amino acids | Function |
|----------|----------------|-------------|---------------------------------------------------------------------------------------------------------|
| FCGBP | tcTGca/tcca | SA/SX | Fc-gamma binding protein covalently attached in mouse and human colon (Johansson et al., 2009) |
| polk | Gga/Tga | G/* | polymerase kappa involved in DNA binding and repair |
| fam169aa | Aga/Tga | R/* | the family with sequence similarity 169 member Aa involved in the fin regeneration (Nolte et al., 2015) |
| Rgmb | gGt/gTt | G/V | a bone morphogenetic protein coreceptor |
| ZMYM1 | Cga/Tga | R/* | |
| ZMYM1 | tCa/tAa | S/* | |
| ZMYM1 | agg/agCATAg | R/SIX | |
| ZMYM1 | ctG/ct | L/X | |
| ZMYM1 | ctg/cACGACAAtg | L/HDNX | |
| ZMYM1 | tTa/tAa | L/* | |
| Tmem232 | -/CTCCTGCTGA | -/LLX | unknown function expressed in neurons and glial cells (Zhang et al., 2014) |

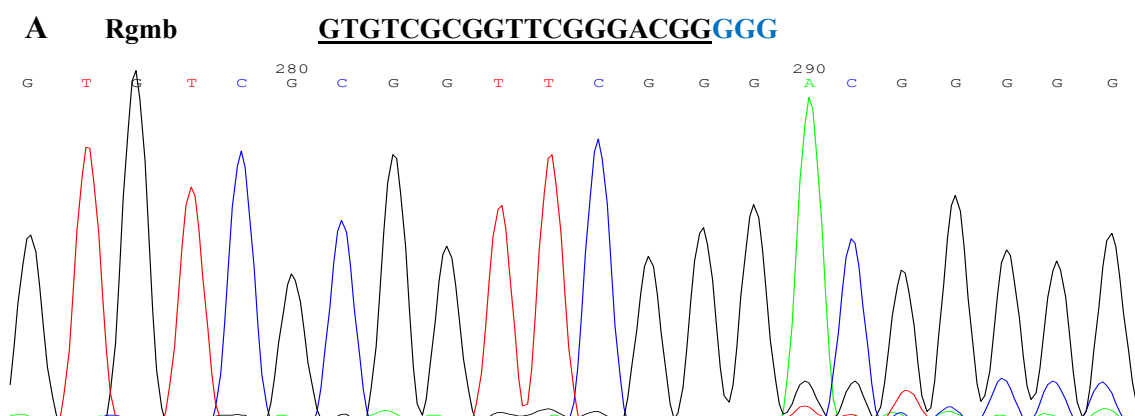
**Fig.3.13. The analysis of the SNP homozygosity scores**

(A) SNP homozygosity scores for the whole genome were plotted against their respective position. It

was clearly identified that the causal mutation region localized on chromosome 5. (B) The causative mutation was carried by the chromosome 5 between the positions 33170176 and 60091309 (score > 0.9).

3.2.5 The validation of the causative gene by CRISPR/Cas9

The CRISPR/Cas9 system has expanded the ability to knock-out genes in different animal models, including zebrafish (Burger *et al.*, 2016; Chang *et al.*, 2013; Hwang *et al.*, 2013; Jao *et al.*, 2013). To validate the causative gene by CRISPR/Cas9-mediated targeted mutagenesis, I designed sgRNAs to target the two potential candidates, which could guide the Cas9 nuclease to the desired genomic locus. I co-injected the sgRNAs with Cas9 protein into one-cell stage embryos and analyzed the targeted genome editing of injected embryos at 48 hpf. PCR products containing the target regions were amplified and then assessed by T7 endonuclease I assay, after which I selected the positive samples for further analysis by sequencing. The sequencing results showed that I successfully generated the mutations at the target sites in the sgRNA/Cas9-injected F0 embryos (Fig.3.14A-B). The future work needs to investigate whether the phenotype in the mutant zebrafish can be recapitulated in F2 embryos with CRISPR/Cas9-induced mutations.



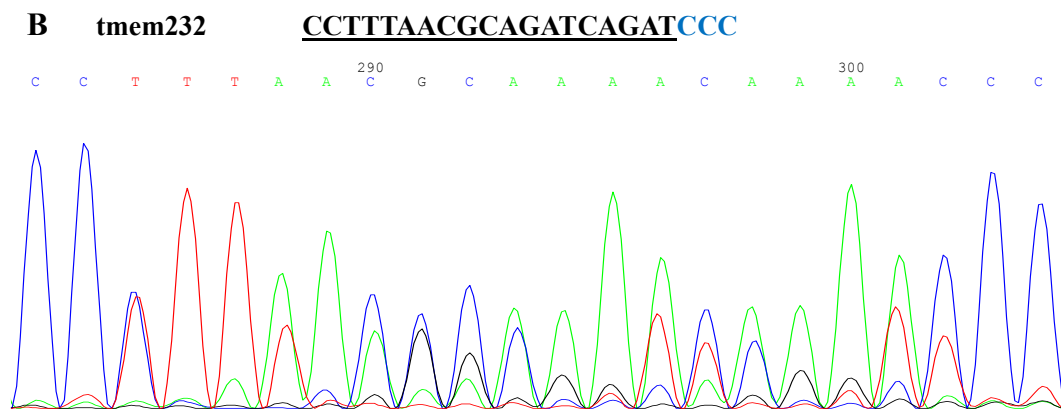


Fig.3.14. The mutations induced by Cas9/sgRNA in F0 embryos

(A-B) Representative Sanger sequencing results of the PCR products from 48 hpf embryos show that mutations are induced in the targeted Rgmb (A) and tmem232 loci (B) by Cas9/sgRNA. The sequences targeted by sgRNAs are underlined.

3.3 The regeneration of central axons in the lateral-line afferent neurons

3.3.1 The regenerative capacity of central axons

In the zebrafish lateral-line nervous system, the individual afferent neuron has one central axon that projects along the anteroposterior axis of the hindbrain, and one peripheral axon that innervates mechanosensory hair cells in superficial receptors called neuromasts (Fig.3.15A-B and 3.16A-C). Many investigations were focused on the development and regeneration of their peripheral nerves. However, the regeneration of central axons in the lateral-line afferent neurons is unknown. To investigate this, I marked these neurons using a 2-kilobase ‘SILL’ enhancer (Pujol-Martí et al., 2012), and either marked single neurons by microinjection of the SILL:mCherry plasmid DNA (Weili Tian did a part of microinjection to mark individual neurons in Dr. Hernán López-Schier lab, Helmholtz Zentrum München) or the entire neuronal population by Tg[HGn39D] stable transgenic line (Fig.3.16J). To induce neuronal damage and probe repair in living zebrafish larvae, I used a nanosecond ultraviolet laser (355nm, 400ps/2.5μJ per pulse) to transect individually identified axons or the entire lateralis nerve. The laser beam was guided by the fluorescence of lateralis neurons in the Tg[HGn39D] stable transgenic line, or by mosaic expression of SILL:mCherry

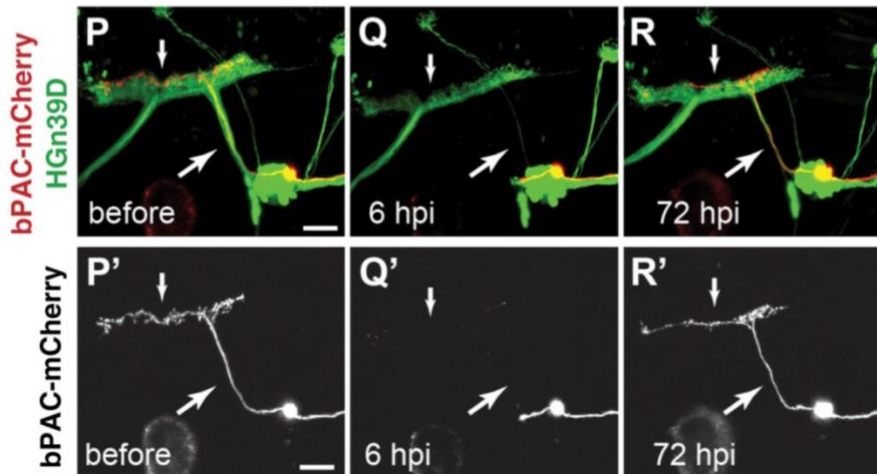
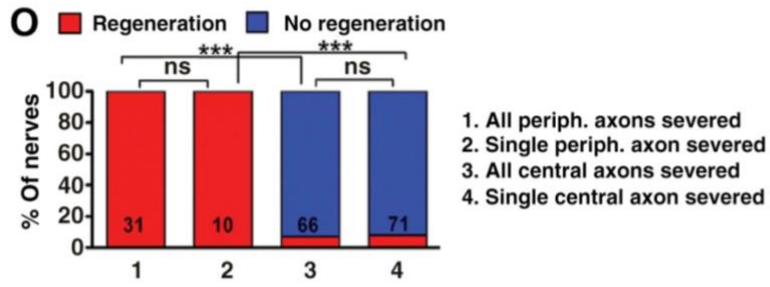
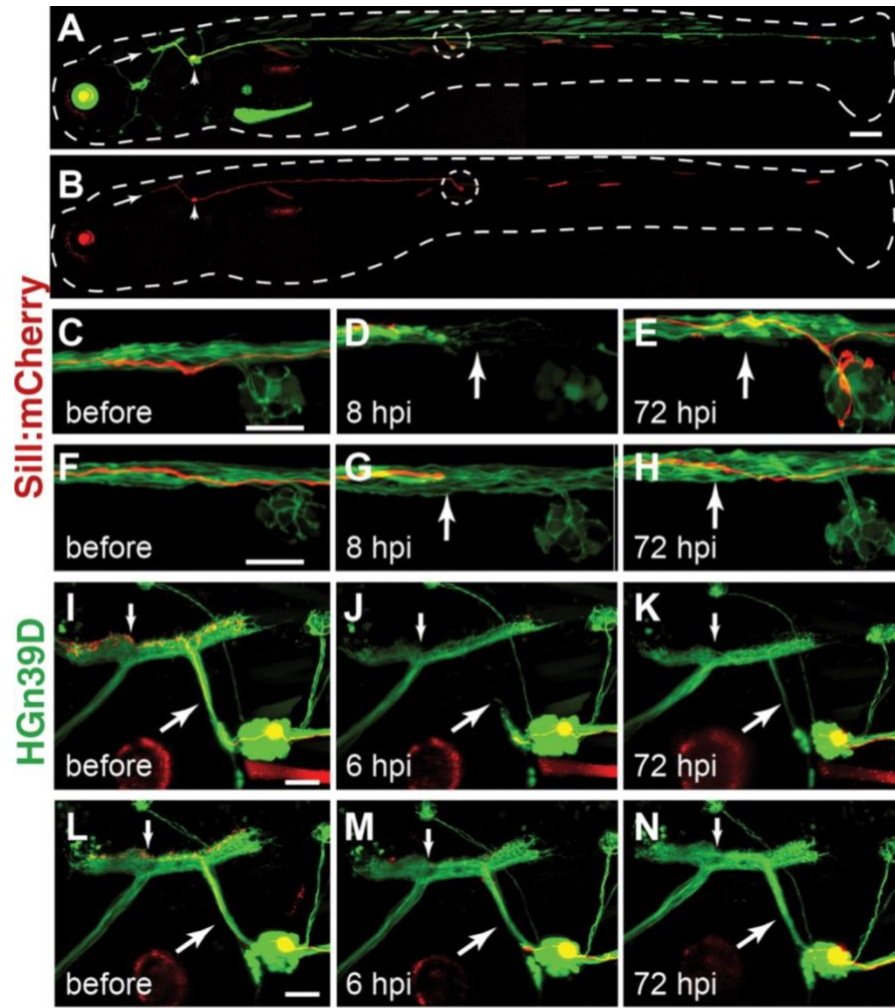
(Fig.3.15C-N, P-R and Fig.3.17A-F). I found that all types of cuts led to a rapid distal degeneration (Fig.3.15D,G,J,M and Fig.3.17A-F). Post-injury quantifications showed that 100% of the severed peripheral axons regenerated and re-innervated neuromasts within 72 hours, equally between the injury of individual nerves and the entire nerves (Fig.3.15O). Unexpectedly, I discovered that only 5% of the central axons regenerated within the same period, regardless of the presence of uncut axons (Fig.3.15O).

3.3.2 The regeneration of central axons promoted by optogenetic stimulation

The pharmacological manipulation of intracellular cAMP in neurons after the lesion was used to promote axonal regeneration in the CNS of mouse and zebrafish (Bhatt et al., 2004; Hannila et al., 2008; Martinez et al., 2014; Neumann et al., 2002; Qiu et al., 2002; Spencer et al., 2004). To explore this new method to enhance axonal regeneration, I used the approach based on the blue-light activatable adenylyl cyclase bPAC, which exists naturally in the soil bacterium *Beggiatoa* and is used to increase cAMP level (Stierl et al., 2011). Using 'SILL' enhancer, I generated zebrafish that mosaically expressed a bPAC-Myc-V2A-mCherry fusion gene (hereafter bPAC-mCherry) alone or together with the presynaptic marker Synapsin1-GFP (Fig.3.16D-F). Control fish co-expressed Synapsin1-GFP and membrane-targeted mCherry (Fig.3.16G-I). The direct comparison between different animals showed that the bPAC(+) neurons did not have any structural defects: there was no significant change in the arborization (bPAC(+) 6.7 ± 2.7 ; bPAC(-) 6.6 ± 2.4 ; $p=0.8$), the length of central axon (bPAC(+) 561 ± 65 ; bPAC(-) 589 ± 88 μm ; $p=0.5$), and the number of synapsin1-GFP puncta (bPAC(+) 57 ± 7 ; bPAC(-) 57 ± 6 ; $p=0.9$) (Fig.3.16K-M).

By microinjecting bPAC-mCherry mRNA into one-cell stage embryos, I confirmed that blue-light stimulation of bPAC-mCherry at 450-490nm raised cAMP levels in zebrafish at 2 dpf or 5 dpf by ELISA (Fig.3.17G). Zebrafish expressing bPAC showed low adenylyl cyclase activity in darkness (non-stimulated), with cAMP levels that did not differ from control group of bPAC(-). Blue-light stimulation of bPAC-expressing specimens resulted in significantly higher cAMP levels, while blue-light illumination of

bPAC(-) did not result in increased cAMP levels (Fig.3.17G). Additionally, neurons expressing mCherry or bPAC-mCherry in 5 dpf fish were photostimulated after severing of peripheral or central axons. I found that all the proximal fragments retracted upon axotomy and the average length of retraction relative to the injury site showed no difference between (bPAC(+)) $77.2\pm 28.9 \mu\text{m}$ and bPAC(-) $73.7\pm 49.7 \mu\text{m}$; $p=0.6$) (Fig.3.17H-I). Additionally, the onset time of peripheral-axon re-growth after injury (bPAC(+)) $10\pm 3.2 \text{ h}$ and bPAC(-) $12.8\pm 2.4 \text{ h}$; $p=0.4$) and the speed of peripheral-axon re-growth (bPAC(+)) $22.6\pm 10.1 \mu\text{m/h}$ and bPAC(-) $28.4\pm 9.9 \mu\text{m/h}$; $p=0.4$) did not differ significantly (Fig. 3.17H,J,K). Remarkably, however, the regeneration of severed central axons of bPAC-mCherry(+) neurons dramatically increased after photostimulation (Fig. 3.15P-S). The axonal regeneration rate of bPAC-mCherry(+) neurons after photostimulation (~27%) was significantly higher than that of bPAC(-) or non-stimulated bPAC-mCherry(+) neurons (~5%) (Fig.3.15S). Additionally, I generated the Tg[SILL:bPAC-mCherry] stable transgenic line, where the expression accumulated in the somata rather than in axons. In order to facilitate quantification of axonal regeneration, the central axons from anterior ganglion were also transected. The results showed that the success rate of central-axon regeneration was increased at 24 hpi in this Tg[SILL:bPAC-mCherry] stable transgenic, although axons labeling is not visible due to faint fluorescent labeling (Fig.3.15T and Fig.3.17L-Q). Pharmacological inhibition assays revealed that central-axon regenerative success was dependent on cAMP-dependent protein kinase-A (Qiu et al., 2002). To test this, I performed pharmacological assays using PKA activators and inhibitors. The results showed that ~30% of bPAC(-) neurons regenerated central axons in fish treated with the PKA activator cAMPSp, and very few regenerated after treatment with the PKA inhibitor H89 (Fig.3.15S). To investigate whether the regenerative axons have potential for functional recovery, I analyzed the reformation of synaptic structures after axonal regeneration. Imaging Synapsin1-GFP expressed in individually-identified neurons before severing and after bPAC-mediated regeneration showed that regenerated central axons re-targeted the correct area of the brain, and re-formed fewer but mature presynaptic structures (Fig.3.15U-V).



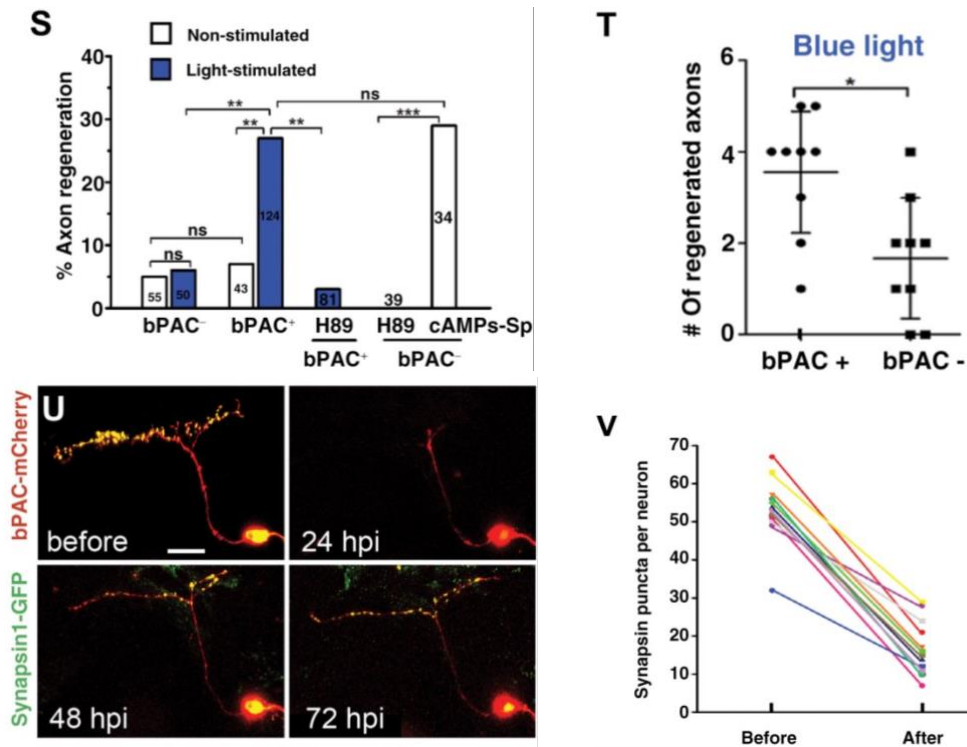
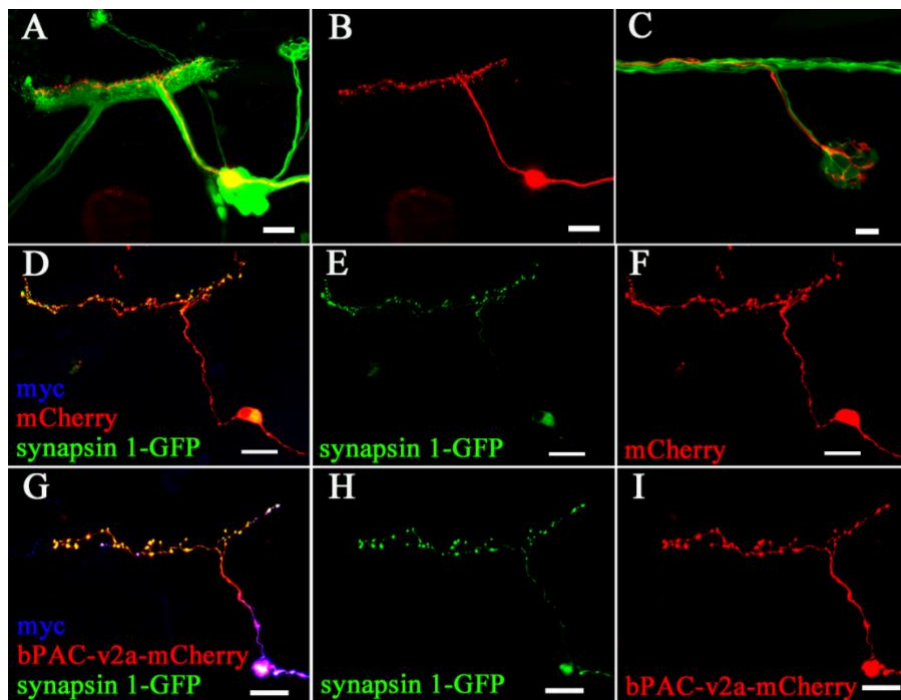


Fig.3.15. Photoactivation of bPAC stimulates the regeneration of refractory axons in lateral line afferent neurons

(A) The Tg[HGn39D] stable transgenic line (green) at 5 dpf, also expressing mCherry in an individual lateralis neuron (red). The arrow points to the central-axon projections in the hindbrain, the arrowhead indicates the posterior lateralis ganglion. Dotted lines outline the fish body, and the circle shows the neuromast innervated by the mCherry-expressing neuron. (B) The same specimen showed the neuron expressing mCherry under the SILL enhancer. (C-E) The peripheral nerves of Tg[HGn39D] (green) and a single axon marked by SILL:mCherry before severing (C), 8 hpi (D), and 72 hpi after whole-nerve severing (E). The arrow indicates the location of nerve transection. The distal axons degenerated rapidly (D), and regenerated completely after 72 hours (E). (F-H) Severing a single peripheral axon expressing mCherry led to distal degeneration (F-G), and regenerated within 72 hpi (H). (I-K) The central projections of anterior and posterior lateralis neurons in Tg[HGn39D] (green) and a mCherry-marked neuron from the posterior lateral line (red) before transection (I). Upon severing the entire central nerve bundle, all distal axonal fragments degenerated 6 hpi (J), and the majority did not re-grow even after 72 hpi (K). Some newborn neurons from a small adjacent ganglion extended axons towards the brain (K). The small white arrow shows the terminal projection along the hindbrain, and the large arrow indicates the site of central-axon transection. (L-N) Severing singly marked axons (red) and leaving most of the other axons intact (green) showed that

uncut axons did not promote the regeneration of the severed axons. (O) Quantification of the peripheral- and central-axon regeneration in two axotomized categories. The number of independent axons examined is shown inside the bars. (P-R) A single neuron expressing bPAC-mCherry (red) in the Tg[HGn39D] stable line (green). After severing the entire central bundle, all distal fragments degenerated 6 hpi. The sole neuron expressing bPAC-mCherry regenerated its central axons after photostimulation. (S) Quantification of the central-axon regeneration of bPAC(+) neurons after photostimulation (~27%), which was significantly higher than that of bPAC(-) or non-stimulated bPAC(+) neurons (~5%). ~30% of bPAC(-) neurons regenerated central axon in fish treated with the PKA activator cAMPSp, and very few regenerated after treatment with the PKA inhibitor H89. (T) Quantification of the central axon regeneration in the Tg[SILL:bPAC] stable transgenic line at 24 hpi. (U) An example of an identified axon expressing bPAC-mCherry (red) and Synapsin1-GFP (green) before severing and after severing upon blue-light stimulation. (V) Counting Synapsin1-GFP puncta before axotomy and after regeneration showed that regenerated axons matured pre-synaptic structures, albeit fewer. * $p < 0.05$, ** $p < 0.01$, *** $p < 0.001$, “ns” indicates non-significant. Scale bars: 150 μm (A-B), 25 μm (C,F,I,L,P,U).



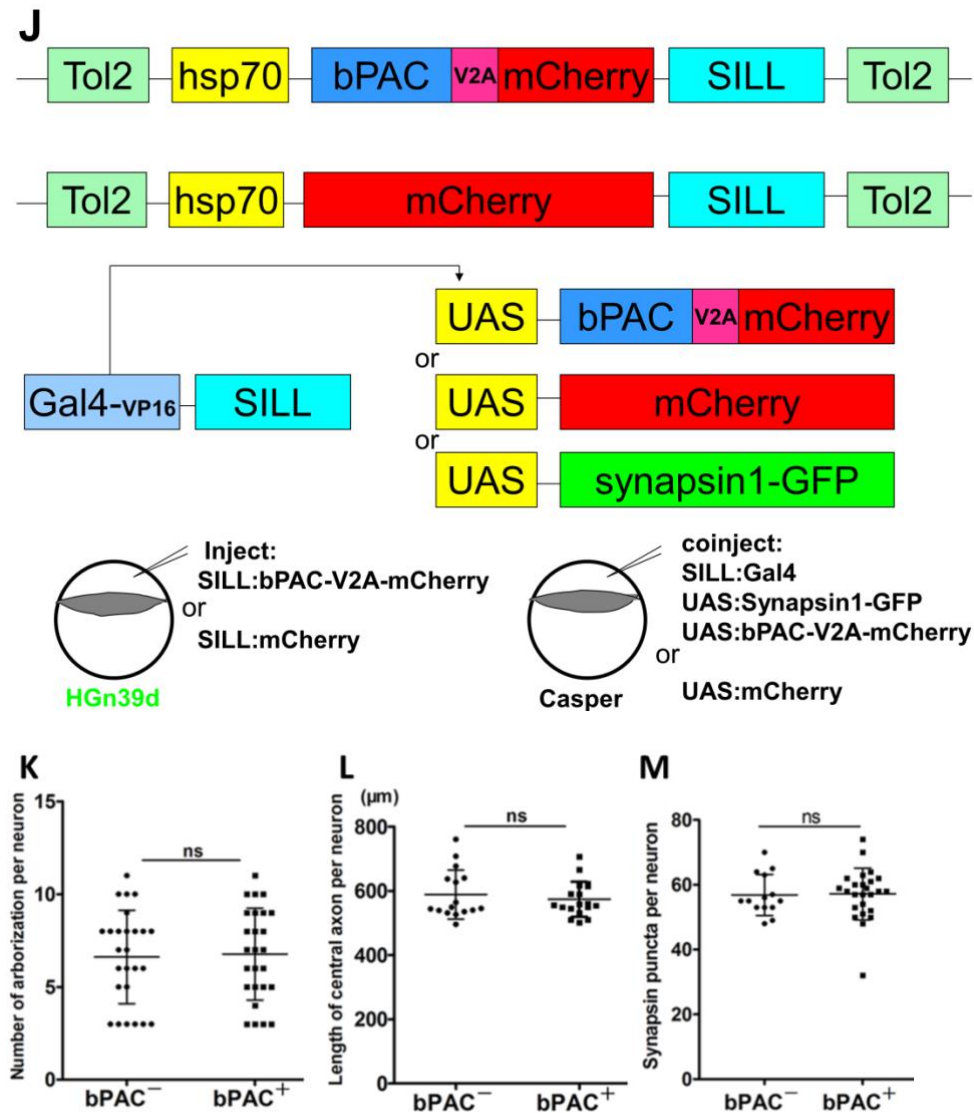
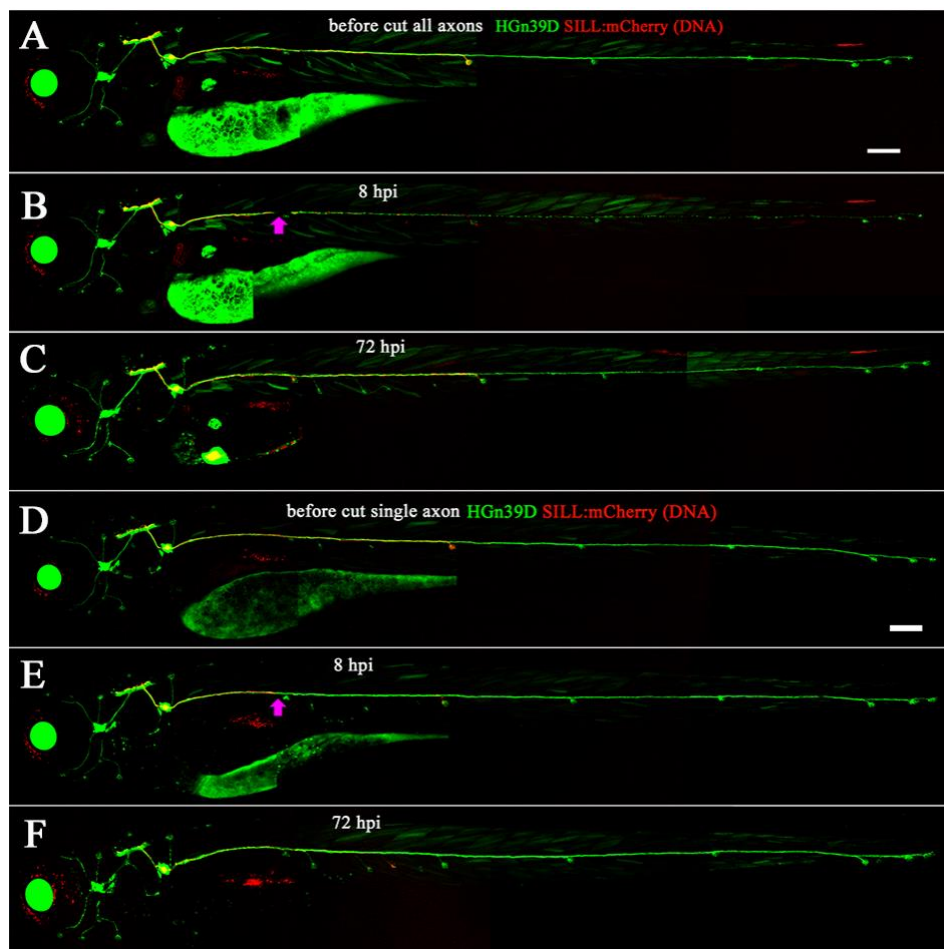


Fig.3.16. bPAC transgene expression in lateralis afferent neurons

(A) Maximal central projections of a confocal-image stack detailing the central projections of the anterior and posterior lateralis ganglia (from Fig.3.15A). (B) Higher magnification of the single neuron marked by SILL:mCherry (Fig.3.15B). (C) Higher magnification of circled region in (Fig. 3.15A-B) depicting peripheral axons innervating a neuromast, with an individual axon labeled by SILL:mCherry expression. (D) The image of an individual central projection of an afferent neuron co-expressing bPAC-mCherry (red) the presynaptic marker synapsin1-GFP (green) and Myc-tagged bPAC, immunolabeled with an antibody to Myc (blue). (E-F) The same axon labeled by synapsin1-GFP (E) and bPAC-mCherry (F). (G) The image of an individual afferent neuron co-expressing mCherry (red) and the presynaptic marker synapsin1-GFP (green), and probed with anti-Myc antibody (negative). (H-I) The same axon marked by synapsin1-GFP (H) and mCherry (I).

(J) Schematic overview of transgene expression strategies in the lateral-line afferent neurons. The SILL:bPAC-V2A-mCherry construct contains the Tol2 transposable element (green), and minimal heat-shock 70 promoter element (yellow), the bPAC-encoding gene fused to a Myc tag (blue), which were also fused to mCherry (red) and followed by the SILL enhancer (turquoise). The bPAC and mCherry are separated by the viral “self-cleaving” 2A-like peptide sequence (magenta). The SILL:mCherry construct expressing only mCherry (red), otherwise color-coded as above. The co-injected constructs were driven by the UAS element and by the transcriptional activator Gal4-vp16 under the control of the SILL enhancer. The lower panels show the strategies to express transgenes in single neurons via cDNA injection in eggs of the Tg[HGn39D] stable transgenic line or the *casper* line that was used as control. (K-M) The bPAC(+) neurons showed the normal development in the number of arborization, the length of central axon and the number of synapsin1-GFP puncta. “ns” indicates non-significant. Error bar represents the SD. Scale bars: 25 μm (A-I).



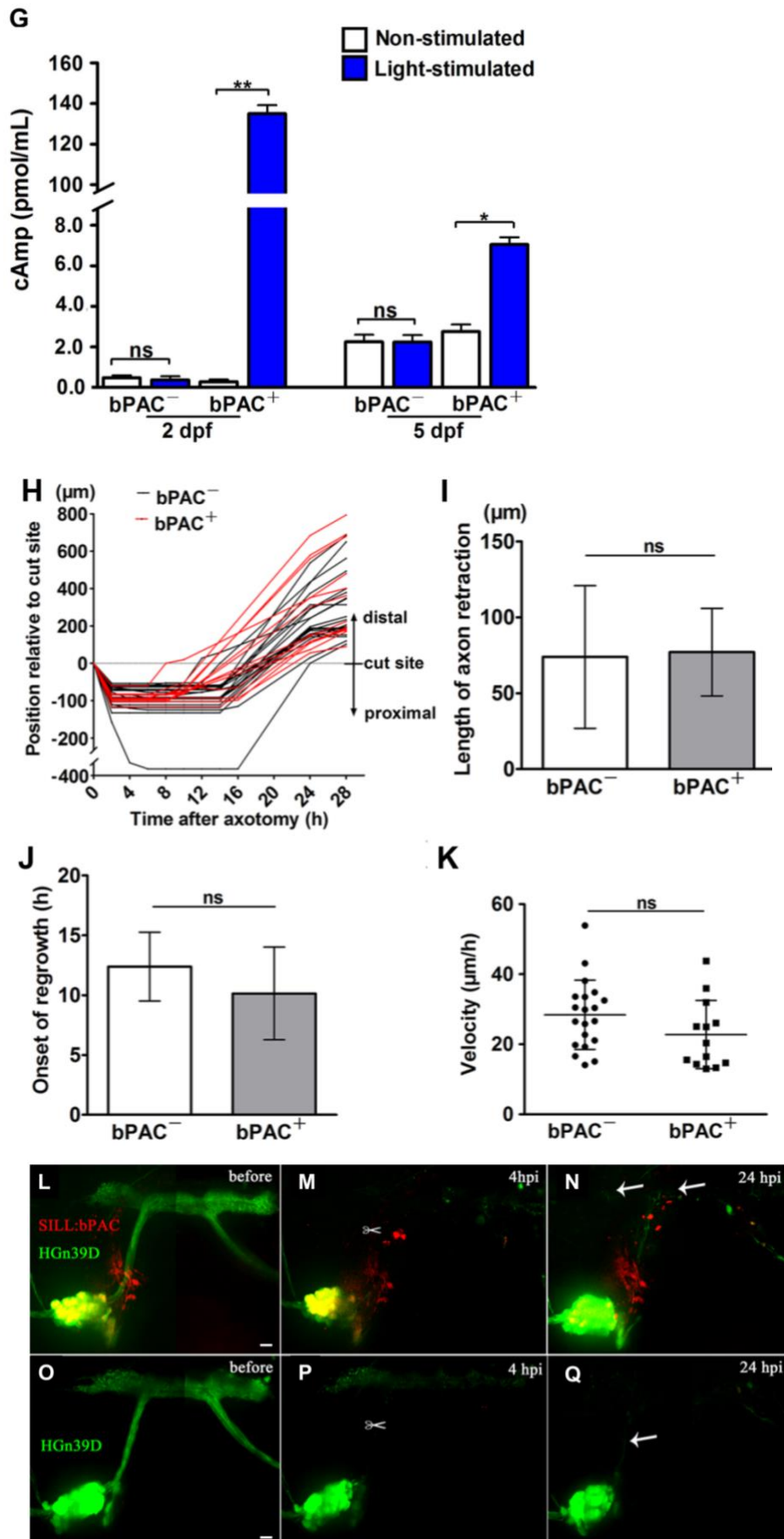


Fig.3.17. The effect of bPAC transgene expression on the regeneration of the peripheral and central axons

(A-C) An example of a 5 dpf zebrafish larva expressing EGFP in all the afferent neurons of the lateral line in the stable transgenic line Tg[HGn39D] (green). A single neuron was made to express mCherry by cDNA injection in the eggs. These images correspond to the high-magnification examples shown in Fig.3.15 C-E. Before axotomy (A), 8 hours post-axotomy of the entire nerves, indicated by the pink arrow (B). Note that the entire distal nerve became fragmented and degenerated. Peripheral axons regenerated completely at 72 hpi and were indistinguishable from the ones prior to severing (C). (D-F) An example similar to (A-C) but in which only an individual axon expressing SILL:mCherry was cut (arrow in E), without damaging other neighboring axons. This single transected axon re-grew and innervated a neuromast within 72 hpi (F). (G) Blue-light stimulation of bPAC increases cAMP levels in zebrafish at 2 dpf or 5 dpf. (H) Relative position of the proximal stump of the peripheral nerve after severing of bPAC(+) (red) and bPAC(-) (black) neurons. Each line represents individual axons: the bPAC-mCherry-expressing neurons (n = 20) and mCherry-expressing neurons (n = 13) stimulated by blue light. All the proximal fragments retracted upon axotomy. (I) The average length of retraction relative to the injury site was measured and the data showed no difference between bPAC(+) and bPAC(-). (J) Axons showed a variable “resting” or lag period between severing and re-growth. The average onset of axon re-growth was calculated and no difference was found between groups bPAC(+) and bPAC(-). (K) Similarly, there was no significant change in the average velocity axonal growth. (L-Q) bPAC expression promotes axonal regeneration in Tg[SILL:bPAC] stable transgenic line upon blue light. Representative images from zebrafish larva with expressing bPAC-mCherry (L-N) or without (O-Q) when all the afferent neurons of the lateral line in the stable transgenic line Tg[HGn39D] before axotomy (L, O), 4 hpi (M, P), 24 hpi (N, Q). The scissor indicates the injury site and arrow points to the tip of regenerated axon. “ns” indicates nonsignificant. Error bars represent SD. Scale bars: 150 μ m (A,D), 10 μ m (L,O).

To investigate downstream effectors of cAMP signaling involving axonal re-growth, I used the native zebrafish ribosomal protein Rpl10a and generated a stable transgenic line expressing EGFP-Rpl10a under the control of SILL enhancer, which can be used for translating ribosome affinity purification (Fig.3.18). Translating ribosome affinity

purification was initially used to tease apart the genes and pathways unique to numerous cell populations comprising the murine brain by affinity purifying EGFP-tagged ribosomal protein and affiliated mRNAs (Heiman et al., 2008). Additionally, it has been demonstrated the capacity to capture mRNA transcripts bound to ribosomes in zebrafish (Tryon et al., 2013). Therefore, further work in identifying downstream effectors of cAMP signaling in axonal re-growth could be performed by combining with bPAC expression.

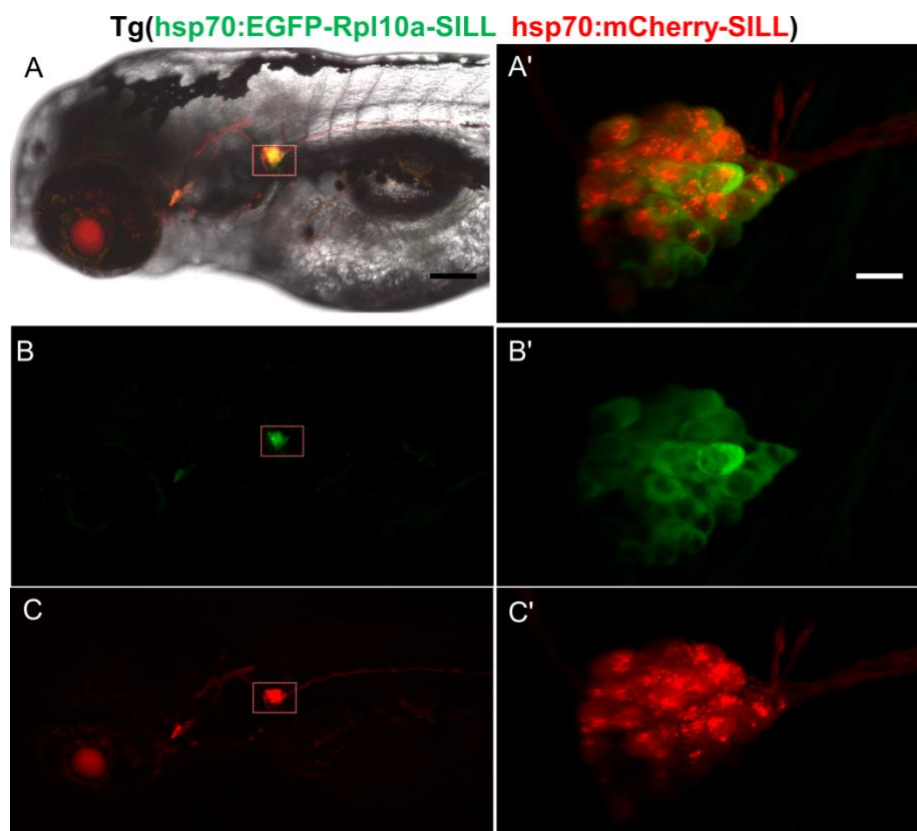


Fig.3.18. Expression of the EGFP-Rpl10a protein in stable transgenic line

(A-C) The Tg(hsp70:EGFP-Rpl10a-SILL) line shows specific expression in the lateral line afferent neurons at 4 dpf, as the expression of GFP is overlapped with mCherry. (A'-C') Higher magnification of lateral line posterior ganglion show that the expression of EGFP-Rpl10a accumulates in the neuronal cell body. Scale bars: 150 μ m (A), 20 μ m (A').

4. Discussion

4.1 Axon-glia interactions during peripheral axon injury

4.1.1 The model of disease and Schwann cells respond to denervation

Neuropathies arising from neuronal or glial damage in the traumatic events can cause severe morbidity and increase mortality in humans (Beirowski, 2013; Scherer and Wrabetz, 2008). Schwann cells are an important glial cell type in the vertebrate peripheral nervous system (Jessen and Mirsky, 2005; Kidd et al., 2013), and the interaction between Schwann cells and neurons is crucial to maintain the integrity and function of neuronal circuits (Arthur-Farraj et al., 2012; Court et al., 2004; Nave, 2010; Rodrigues et al., 2011; Sharghi-Namini et al., 2006; Shy, 2009). Understanding the cellular and molecular mechanisms involved in the onset and progression of neuropathies of glial origin is therefore of utmost importance to devise effective treatments for peripheral neuropathies (Gordon et al., 2003). However, most of the classical experimental animal models are not amenable to explore the fine details of the dynamic interaction between Schwann cells and neurons during injury and repair, because of the inaccessibility of these cells to direct live imaging at high resolution. The zebrafish has emerged as a favourable system to study organ development, homeostasis and regeneration in the whole animal at high resolution (Goessling and North, 2014; Patton et al., 2014). Additionally, zebrafish have a superficial and accessible sensory-neural system called the lateral line, where the peripheral axons of the lateral line afferent neurons are myelinated by Schwann cells (Brösamle and Halpern, 2002; Lyons et al., 2005; Raphael and Talbot, 2011). In this study, I used the zebrafish lateral line system to establish an experimental paradigm of traumatic injury, which combined live imaging with genetic and microsurgical manipulations to study in detail the behavior and function of Schwann cells during the repair of the lateralis afferent neurons. Transgenic zebrafish lines expressing fluorescent proteins was used to study Schwann-cell behavior during embryogenesis (Jung et al., 2010; Lewis and Kucenas, 2013; Munzel et al., 2012; Perlin et al., 2011). However, no Schwann-cell specific Gal4 driver line exists in zebrafish. To overcome this deficiency, I firstly identified the

transgenic line Tg[gSAGFF202A] with a Gal4FF driver marking Schwann cells validating by antibody immunostaining of P0-like myelin glycoprotein and claudin-k junctional protein (Fig.3.1 G-H), which were used as the specific markers for Schwann cells in zebrafish (López-Schier et al., 2005; Munzel et al., 2012). Also, I generated Tg[UAS:H2AmTurquoise] and plasmid UAS:UtrCH-EGFP in the Tg[gSAGFF202A] transgenic line to mark the nuclei and F-actin of the Schwann cells, respectively (Fig. 3.1 E-F). The combination of genetically encoded fluorescent biosensors with the transgenic line Tg[gSAGFF202A] could further be used for the visualization of subcellular physiological responses, other cytoskeletal and organellar dynamics.

Using Tg[gSAGFF202A; UAS:H2A-mTurquoise; SILL:mCherry] triple transgenics, I found that chronic denervation by ablating the neuron somata is lethal for Schwann cells and the number of Schwann cells continued to decrease over the 5 days follow-up period, suggesting that Schwann cells require support from neurons. Although glial depletion also occurred during acute denervation, axonal regrowth stabilized the peripheral glia by preventing further Schwann-cell loss (Fig. 3.4A-B), which indicates that neurons regulate the status of Schwann cells. Further, I did not observe extrusion of Schwann cells from the glial stream, suggesting that the reduction in the number of Schwann cells possibly resulted from cell death or by physiological cell death accompanied by reduced Schwann-cell proliferation. Thus, to prove the hypothesis, I performed TUNEL assay and live-cell time-lapse imaging after axonal injury and demonstrated that Schwann cells underwent apoptosis (Fig.3.4 E-G). This is in line with a dramatic increase in Schwann cell death after axonal degeneration in chicken embryos (Ciutat et al., 1996) and neonatal mice (Petratos et al., 2003). The apoptosis of Schwann cells in the axotomized peripheral nerve is mediated predominantly through neurotrophin receptor p75 signaling and initiated via endogenously produced NGF (Petratos et al., 2003). In future work, it would be interesting to find out the axonal-derived factors for the regulation of Schwann cell survival. Additionally, I found that Schwann cell proliferation decreased upon axon severing (Fig.3.4C-D), suggesting that Schwann cell proliferation can be regulated by non-cell-autonomous mediators. It

was reported that death receptor 6 released from neurons acted cell non-autonomously to suppress Schwann cell proliferation in the PNS of mouse models (Colombo et al., 2018). It is tempting to suppose that death receptor 6 might have similar functions. However, these still need to be elucidated in the zebrafish lateral line system.

I found that, during the initial loss of contact with the axolemma, Schwann cells downregulated the expression of the P0-like myelin glycoprotein and junctional Claudin-k (Fig.3.5A-M), suggesting that they de-differentiated (Scherer, 1997). Thus, Schwann cells in zebrafish and in mammals behave similarly upon denervation (Harrisingh et al., 2004). Additionally, the results showed that an axon-induced proximal-distal gradient of Schwann cell de-differentiation might represent a directional cue for regenerating axons to grow towards distal sites (Fig.3.5M). This way, growth cones were induced to extend directionally along de-differentiated Schwann cells that are located exclusively distal to the site of damage (Allodi et al., 2012). It has previously been shown in mammals that dedifferentiated Schwann cells promoted axonal growth, and that Schwann cells re-differentiated after entering into contact with re-growing axons (Arthur-Farraj et al., 2012). The results showed that Schwann cells in zebrafish re-differentiated and re-myelinated upon entering into contact with re-growing axons (Fig.3.5). Taken together, these results further supported the strong conservation of the cellular processes underlying axon-glia interactions across vertebrates.

Additionally, although I have focused on axonal and circuit repair, the disease model can be easily adapted to visualize and probe other injury responses, such as inflammation, infection, immune reactions and scarring.

4.1.2 Schwann cells and neurons are mutually dependent

I found that an incrossing between Tg[gSAGFF202A] fish produced 25% of individuals with much more neuromasts than that in wild-type animals (Fig.3.2A-B), suggesting that the insertion is mutagenic. The Ngn1 mutant zebrafish lacking Schwann cells

showed this phenotype, in addition to axon defasciculation due to loss of myelination (López-Schier et al., 2005). Also, I found that the transgene with Gal4FF driver in Tg[gSAGFF202A] was inserted in the first coding exon of the *ErbB2* locus, and Schwann cells in homozygous Tg[gSAGFF202A] zebrafish cannot migrate far away from the posterior ganglion (Fig.3.2C-I). Therefore, the ErbB2 receptor tyrosine kinase is essential for the migration of Schwann cells along zebrafish lateral line afferent axons during development (Lush and Piotrowski, 2014; Lyons et al., 2005). In mouse model, knockdown of ErbB3 using a Schwann cell-specific promoter in mice inhibited migration of Schwann cells (Torii et al., 2014), which is consistent with the results in this study, suggesting a genetically conservative role of ErbB family in Schwann cell migration.

In this study, I designed a method to generate acute or chronic denervation of Schwann cells in whole animals by axon severing or neuronal ablation. The lateral-line peripheral axons of zebrafish sensory neurons are able to quickly regenerate after injury. By contrast, neuronal ablation abolishes lateral-line innervation for a longer period. Time-course analyses of axons after severing showed that the distal segments degenerated, and Schwann cells quickly cleared distal-axonal fragments by phagocytosis (Fig.3.4G). Previous studies demonstrate that, shortly after nerve damage in zebrafish, macrophages are recruited to injured lesions and play a major role in debris clearance (Peri et al., 2008; Rosenberg et al., 2012; Villegas et al., 2012). The model in this study can be easily combined with transgenic zebrafish marking macrophages for the future work to investigate macrophage responses after nerve injury. Additionally, I found that neurons remained viable in animals with severed axons, in which the severed axons began to regrow within 24 h post-damage (Fig.3.6). However, axonal severing induced neuronal death (Fig.3.6C) and axons failed to regenerate effectively in *ErbB2* mutant fish (Fig.3.6D), indicating that Schwann cells play an important role during regenerative axonal growth. Together with the above-discussed results that after axonal injury Schwann cells undergo apoptosis and reduce proliferation, it can be concluded that the Schwann cells and lateral line afferent neurons are mutually dependent.

Moreover, the loss of ErbB2 blocked migration and survival of most Schwann cells, suggesting that the peripheral glia might protect injured neurons from dying upon axonal damage. Notably, the survival of sensory spiral ganglion neurons required ErbB signaling in the inner ear of mice (Stankovic et al., 2004). Because neuronal perikarya remain associated with Schwann cells in *ErbB2* mutant animals, a Schwann-cell independent role of ErbB2 in neuronal survival remained a possibility. One way to test this idea will be to make inducible loss of ErbB2 in Schwann cells after axon injury.

4.1.3 The identity of the directional cues for axonal re-growth

I found that, after the physiological clearance of the degenerating distal axon fragments, the Schwann cells maintained endoneurial tubes, called bands of Büngner. It has been proposed that these tubes provide a permissive environment for axonal regeneration (Fawcett and Keynes, 1990; Parrinello et al., 2010). However, they might also play an instructive role by inducing regrowing axons to extend growth cones in a directional manner. In rodents, nerve cuts triggered coordinated changes in behavior of fibroblasts and Schwann cells (Fawcett and Keynes, 1990; Parrinello et al., 2010). This induced the collective migration of the Schwann cells towards the injury, guiding regrowing axons across the injury gap. Furthermore, if the collective migration of Schwann cells was impaired, axons take an abnormal path during regrowth (Fawcett and Keynes, 1990; Feneley et al., 1991; Parrinello et al., 2010). Notably, the afferent neurons of the lateral line extend pioneer axons independently of Schwann cells during embryonic development (Gilmour et al., 2002), suggesting differences between developmental axonogenesis and axonal regrowth. Using high-resolution intravital imaging, I complemented and extended this model of glia-dependent axonal guidance during regeneration by showing that Schwann cells on both sides of the injury extended processes that rapidly bridge the gap (Fig.3.7A). I also showed that the directionality of this process was independent of the axons, suggesting that it emerged from the collective behavior of the Schwann cells. Axonal regeneration was slow before glial processes close the injury gap, but accelerated upon growth-cone contact with distal

Schwann cells (Fig.3.7A). In addition, in the absence of Schwann cells, regenerating axons grew at slower rates and their growth cones strayed and took random paths (Fig.3.6A and Fig.3.7B). This was consistent with the results that regenerating axons frequently failed to cross the injury site and strayed along aberrant trajectories in spinal cord of zebrafish mutant *erbb2^{st50}* and *erbb3^{st48}* lacking Schwann cells (Rosenberg et al., 2014). Furthermore, Schwann cells were found to serve as a cue and substratum for the growth cone of regenerating axons, and that the glia were essential for the regenerative innervation of peripheral sensory organs (Fig.3.7C). These observations demonstrated similarities in multiple aspects of the role of the Schwann cells during axonal regeneration between mammals and fish (Allodi et al., 2012; Bradke et al., 2012). However, whether these similarities extend to fibroblasts are unknown, but live imaging in the zebrafish model of injury in combination with transgenic markers of fibroblasts might be able to address this question in the future. Importantly, the results strongly suggested that regenerating axons used haptotaxis with Schwann cells for directional growth. Therefore, Schwann cells have a powerful influence on the architecture of the repairing neural circuit by controlling the kinetics and directionality of axonal regrowth.

4.1.4 Different modes of axonal repair

A protracted degeneration of distal axonal fragments could affect neuronal repair in two opposite ways: it might block axonal re-growth until the distal portion of the damaged fibers are completely cleared, but might also facilitate fast neuronal repair by axolemmal resealing (David et al., 1997; Spira et al., 1993). Sensory neurons are known to be under mechanical tension (Chada et al., 1997; Lafont and Prochiantz, 1994; Smith, 1988). In addition to trophic support (Soares et al., 2014), Schwann cells might control the mechanical forces acting on axons, which could bias the frequency of either regenerative pathway. In the future it will be important to characterize the physical environment of sensory neurons and the influence of the Schwann cells on the behavior of injured axons under different regimens of mechanical tension. To this end, the highly reproducible *in vivo* model of axonal injury that I presented in this study, and the

anatomical simplicity and superficial localization of the zebrafish lateral line can be combined with genetically encoded sensors to visualize the mechanical properties of axons upon injury and repair in their natural context.

4.1.5 Clinical implications

Peripheral neuropathies are nerve pathologies caused by genetic disorders or physical trauma, which can cause transient sensory and motor dysfunction (Nave, 2010; Cashman et al., 2015). Comorbidity of traumatic and metabolic peripheral neuropathies is common in humans. Experimental and population-based studies have shown that lower-limb amputations due to neural dysfunction are prominent in individuals (Lombardo et al., 2014). This invariably leads to a decrease in the quality of life of the affected individuals and puts an enormous long-term burden on healthcare systems. Notwithstanding recent progress, the knowledge about the influence of the glia on the degeneration and regeneration of the peripheral nervous system remains incomplete to the point that therapies against neural injury are usually ineffective (Faber et al., 2015). Additionally, differential cell vulnerability to denervation further complicates efforts to elucidate the basis of degeneration and regeneration. Therefore, studies aimed at deepening the understanding of the dynamic interactions between neurons and Schwann cells in the natural context would be important to develop therapeutic strategies aimed at sensory or motor function recovery in humans suffering from traumatic injury. Collectively, the results show that denervation induces progressive destruction of the peripheral glia by increasing the apoptosis and inducing de-differentiation of Schwann cells (Fig.3.4). These negative effects of denervation are reversible, however, because axon regrowth prevents further glial destruction (Fig.3.4). An important corollary of the results in this study was the dominant influence of the Schwann cells on the onset and directionality of axonal regeneration. This had obvious clinical implications because strategies aimed at neural-circuit repair might benefit from preventing the death or disassembly of the peripheral glia during periods of denervation (Dedkov et al., 2002; Meier et al., 1999; Painter et al., 2014). Therefore, characterizing the axonal signals that

control the differentiation status, entry into proliferation, and survival of Schwann cells will provide multiple “druggable” targets with therapeutic potential. One additional promising avenue is the screening of molecular libraries to identify drug leads. The genetic, anatomical and histopathological similarities of the peripheral glia among vertebrates suggested that the zebrafish model that I had developed in this study was well suited for these approaches.

4.2 The guidance cue of central axons in lateral-line afferent neurons

4.2.1 The axonal pathfinding in lateral-line afferent neurons

During the development of the nervous system, axons often branch in stereotypic manners to connect with many synaptic targets. Over the last century, a large body of work has enhanced the understanding of the diversity of axonal architecture and the mechanisms that how new-born neurons make the spatial navigation and synaptic connections. Multiple axon-guidance cues with attractive and repulsive properties have been found to control axon branching such as the Ephrins, Semaphorins, Slit and the Netrins (Bonanomi et al., 2010; Campbell et al., 2007; Gatto et al., 2014; Hilario et al., 2009; Kadison et al., 2006; Ma et al., 2007; Oliva et al., 2016; Sakai et al., 2006; Xiao et al., 2003; Xiao et al., 2011; Zhang et al., 2012). Many of these cues are conserved in zebrafish. For example, Slit acts as a ligand for the Roundabout-2 (Robo2) receptor controlling axonal pathfinding of anterior dorsal telencephalic neuron in zebrafish forebrain (Zhang et al., 2012), and the axonal arborization of the RGC axons in zebrafish optic tectum (Campbell et al., 2007; Xiao et al., 2011). However, the catalog of proteins that control central-axons pathfinding in the lateral line afferent neurons remains unknown. In this study I detected a zebrafish mutant disrupting the central projections of lateral-line afferent neurons, giving clues as to the molecular mechanisms controlling axonal pathfinding in the lateral-line central nervous system.

The zebrafish mutant strain arose spontaneously by incrossing Tg[HGn39D] fish, which often produced phenotypically normal embryos, and accidentally produced a 3:1

Mendelian ratio of phenotypically normal and abnormal progeny with upward curved tails. This suggested that the mutant strain possessed a recessive mutation and it was not caused by Tg[HGn39D] transgenic itself, where the gene trap of hsp70 promoter and the GFP was inserted within a locus coding for zebrafish homolog of the contactin associated protein-like 2 (Faucherre et al., 2009; Pujol-Martí et al., 2012). If the gene trap insertion caused the mutation, it should always produce the Mendelian ratio of phenotypically normal and abnormal progeny by incrossing Tg[HGn39D] fish. But here, that was not the case. In the wild-type zebrafish, central parental axons bifurcated into two daughter branches that extended in opposite directions along the anterior-posterior axis in the hindbrain forming T-shaped axons (Fig.3.8A,C). However, I found that the central projections of the lateral-line afferent neurons overshoot the target area and extended more dorsally into the hindbrain in the zebrafish mutant embryos (Fig.3.8B, D-G). Therefore, these results indicated that the role of the mutated gene was to guide the branches after parental-axon bifurcation. The explanation could be that, at the early stages of neurogenesis, the mutated gene should have negatively regulated the entry of the branches along the normal anterior-posterior axis in the hindbrain, confining them to an extension pathway towards the dorsal hindbrain. DRG sensory axons in the mouse spinal cord have similar morphology to the lateral line afferent neurons. The peripheral axons of DRG projected to the skin or muscle, whereas the central axons projected to the spinal cord and bifurcated to extend in opposite directions along the anterior-posterior axis (Ma et al., 2007). It was reported that Slit/Robo signaling involved in the formation of central axons of DRG (Ma et al., 2007). In mutant mice lacking Slit or Robo, the DRG central axons still bifurcated but no longer had the normal orientation of the T-shaped bifurcation fork, as half of the neurons one daughter branch followed the normal trajectory whereas the others entered the spinal cord (Ma et al., 2007). In the spontaneous mutants analyzed in this study, 39% of the neurons produced parental axons that bifurcated normally, whereas in the remaining 61% of the neurons, one of the daughter branches (either the rostral or the caudal) entered the hindbrain (Fig. 3.8D, F-H). This similar phenotype suggested that Slit/Robo signaling might also be involved in the formation of central axons of lateral-line afferent neurons.

Furthermore, a recent study showed that slit1/Robo2 signals guided later-differentiated statoacoustic nerves toward the hindbrain, which positioned ventrally but closely to lateral line afferent nerves (Zecca et al., 2015). Future studies could be performed to test whether the guidance cue slit1/Robo2 is conserved in zebrafish lateral line afferent nerves. Additionally, I found that these central axons did not cross the midline to the other side of the hindbrain, and the number of the lateral-line afferent neurons was normal in the mutants (Fig.3.8I-L). These results revealed that the mutated gene in the mutant did not control neurogenesis and central axons navigating to the ipsilateral hindbrain.

Further analysis of the axonal projection pattern at single-cell resolution revealed that the individual central axons in wildtype zebrafish bifurcated into two daughter branches along the anterior-posterior axis with single layer in the hindbrain (Fig.3.8C). However, one of the daughter branches in the mutants, either the rostral or the caudal, failed to extend horizontally and the axons possessed significantly longer axons, larger branching areas, more branch number and branch order. This might also be similar to RGC terminals that are precisely targeting single laminae when they grow into the tectal neuropil (Donato et al., 2018; Xiao et al., 2011). In the zebrafish tectal neuropil, Reelin was demonstrated to form a superficial-to-deep concentration gradient as the attractive cue for ingrowing RGC axons (Donato et al., 2018), whereas Slit1 was distributed in a superficial-to-deep concentration gradient as the repulsive cue for robo2-expressing RGC axons (Xiao et al., 2011). Future experiments might be interesting to investigate the role of Reelin and Slit in the lateral line afferent neurons targeting single layer.

4.2.2 The regulation of cell non-autonomous in central axons growth

When lateral-line afferent neurons from wild-type cells were transplanted into wild type hosts, the neurons had a normal appearance, whereas wild-type neurons in mutant fish behaved like mutant neurons (Fig.3.12). Therefore, the results suggested that the product of the mutated gene acted cell-non-autonomously during axonal projection to

their correct target area in the hindbrain. It was reported that extrinsic molecules can act as local cues to inhibit branch formation along axons. For example, semaphorin 3a in embryonic hamster cortical axons inhibited branching by collapsing microtubule arrays (Dent et al., 2004). Moreover, central axons in the mutants possessed significantly longer branches, larger branching areas, more branch number and branch order (Fig.3.8I-L). Therefore, the mutated gene can be extrinsic to neurons and acted cell-non-autonomously to inhibit branching.

Immunostaining with 3A10 antibody revealed normal Mauthner axon-pathfinding in the mutant compared with wild-type sibling embryos. Previous study showed that the Mauthner axons were disrupted in *robo3* mutant (Burgess et al., 2009), suggesting that the mutated gene in this study is not the *robo3* gene. Additionally, the immunostaining with the acetylated tubulin antibody showed that the mutant zebrafish have irregular axon-like fibers and massive defects in the hindbrain, indicating that the mutated gene is widely expressed and regulates the axonal pathfinding in the hindbrain.

To identify the mutation by whole genome sequencing, 334 amino-acid changing candidates SNP were found to locate at chromosome 5. Polk, fam169aa, ZMYM1 had nonsense mutations and FCGBP, ZMYM1, tmem232 were frameshifts (Table 3.1). Among these, only tmem232 was selected for further investigation, and other genes were discarded because of no relation with the development of nervous system, according to existing literature (Nolte et al., 2015; Jen et al., 2016; Johansson et al., 2009). Tmem232 (transmembrane protein 232) was expressed in neurons and glial cells with a yet unknown function referring to the literature (Zhang et al., 2014), where the transcriptome database was generated by RNA sequencing for acutely purified populations of glial cells and neurons from mouse cerebral cortex. The formation of the central nervous system depends on the coordinated development of neurons and glial cells. Defects in glial patterning were always associated with axon defects, supporting an important role for axon-glial interactions during axon scaffold development (Barresi et al., 2010). Astroglia-encoded semaphoring 3a through plexin A/neuropilin 1 receptor

complexes was required for proper motor neuron and sensory neuron circuit organization in the mouse model (Molofsky et al., 2014). Also, radial glia was required for localization of Slit and ablation of these radial glia resulted in RGC axon laminar targeting defects of the zebrafish tectal neuropil (Xiao et al., 2011). Therefore, *tmem232* may be expressed in glial cells for regulating axon development. Additionally, *Rgmb* with a missense mutation was selected for further investigation, because the missense mutation G261V changed hydrophilic glycine to hydrophobic valine and it was predicted to be deleterious to protein function by SIFT analysis. Moreover, it was reported that *Rgmb* as a GPI-anchored plasma membrane protein induced collapse of temporal retinal axons growth cones and inhibited the neurite outgrowth of cerebellar granule neurons (Monnier et al., 2002; Liu et al., 2009). Therefore, *tmem232* and *Rgmb* were selected as two potential candidate genes to validate by mutagenesis using the CRISPR/Cas9 technique to generate additional alleles. I successfully generated mutations at the target sites in the sgRNA/Cas9-injected embryos (Fig.3.14). The injected zebrafish embryos (F0) in fact are mosaics, therefore induced mutations in their germline must be identified by a second screening-step in the F1 embryos. Moreover, the F2 progeny must be generated, grown and genotyped for homozygous mutation. Future experiments will further investigate whether the phenotype in original mutant can be recapitulated in F2 embryos with CRISPR/Cas9-induced mutations.

4.3 Optogenetic stimulation of central axonal regeneration

4.3.1 The limited regenerative capacity of central axons

RGC in zebrafish can survive after injury and their axons regrow and reinnervate termination targets in the optic tectum (Becker et al., 2000; Nagashima et al., 2011; Zou et al., 2005). However, Mauthner cells and ascending axons of DRG neurons fail to regenerate axons after damage (Bhatt et al., 2004; Vajn et al., 2013). Therefore, not all injured CNS axons in zebrafish can regenerate and CNS axons show variable regenerative capacity. However, whether the ascending central axons in the lateral line afferent neurons can regenerate is unclear. To explore the regenerative capacity of these

axons, a nanosecond ultraviolet laser was used to cut the entire lateral line nerve or individually identified axons at selected locations in living zebrafish larvae. I found that the severed peripheral axons always regenerated and re-innervated neuromasts within 72 hpi, equally between cutting all axons and individual axons. However, only 5% of the central axons regenerated within 72 hpi, regardless of the presence of uncut axons, suggesting that uncut axons did not promote axon regrowth as a supportive structure (Fig. 3.15). This was different from the results that in the presence of Schwann cells, a continuous physical bridge consisting of nontransected axons was permissive to regrowth in zebrafish spinal cord (Rosenberg et al., 2014). Further, these results indicated that lateral line afferent neurons were similar to many mammalian neurons, which can regenerate their peripheral axons efficiently, but regenerate very poorly their central projections to the brain (Bradke et al., 2012).

4.3.2 The enhanced axonal regeneration by increasing neuronal cAMP level

Environmental insult, disease or trauma can affect the physical integrity of neuronal circuits, and the inability of many neurons to regenerate injured axons invariably leads to irreversible neural dysfunction. Increasing neuronal levels of the second messenger cAMP by pharmacological approaches after a lesion can promote axonal regeneration in the CNS of mouse and zebrafish (Bhatt et al., 2004; Hannila et al., 2008; Neumann et al., 2002; Qiu et al., 2002; Spencer et al., 2004). Additionally, elevating cAMP by overexpressing soluble adenylyl cyclase can overcome myelin-associated-glycoprotein dependent inhibition and promote axonal regeneration in mouse neurons (Martinez et al., 2014). However, pharmacological or genetic approaches increasing intracellular levels of cAMP were often inadequate for precise neural-circuit reconstruction, because their activity cannot be easily timed to specific target cells. These shortcomings have prevented the controlled repair of pre-defined neurons at selected time points in whole specimens. Thus, technologies to guide neuronal repair in time and space would enable neural-circuit reconstitution and studies of functional recovery with unprecedented resolution. Towards this aim, I investigated and found an optogenetic method could

promote the selective regeneration of refractory axons in a living vertebrate.

The approach was based on the blue-light activatable adenylyl cyclase bPAC, which occurs naturally in the soil bacterium *Beggiatoa* and was firstly demonstrated to increase cAMP level (Stierl et al., 2011). The bPAC-mCherry expression did not affect the development, synaptogenesis, or stability of these lateral line afferent neurons (Fig.3.16). This suggested that expressing exogenous bPAC was not toxic to neurons. Photostimulation of bPAC-mCherry raised cAMP levels in 2 dpf and 5 dpf zebrafish, which resulted from injecting bPAC-mCherry mRNA into fertilized eggs. This result was consistent with the fact that bPAC expression in the pituitary corticotroph cells of zebrafish can optogenetically elevate cAMP level leading to enhanced locomotion after stressor exposure (De Marco et al., 2013). Additionally, the onset and speed of peripheral-axon re-growth did not differ significantly between control and bPAC-mCherry-expressing neurons (Fig.3.17). This may be because the normally strong regenerative capacity of these axons did not benefit from further increase of intracellular cAMP levels, or because processes occurring upstream of cAMP signaling were rate-limiting. Remarkably, however, the regeneration of severed central axons of bPAC-mCherry(+) neurons dramatically increased after photostimulation. The central-axon regeneration of bPAC(+) neurons after photostimulation (~27%) was significantly higher than that of bPAC(-) or non-stimulated bPAC(+) neurons (~5%). The success rates of central-axons regeneration in the lateral line nervous system was also increased using the Tg[SILL:bPAC-mCherry] stable transgenic line, although bPAC expression accumulated in the neuron somata rather than in axons, suggesting that elevating cAMP levels localized in neuron somata is sufficient to promote axon regeneration. These results also demonstrated that optogenetically elevating cAMP level by bPAC firstly enhanced the regeneration of central axons. Pharmacological inhibition assays revealed that central-axon regenerative success was dependent on cAMP-dependent protein kinase-A (Qiu et al., 2002). ~30% of bPAC(-) neurons regenerated central axon in fish treated with the PKA activator cAMPSp, and very few regenerated after treatment with the PKA inhibitor H89, which was consistent with

the conclusion that pharmacologically increasing cAMP in neurons after a lesion can promote axonal regeneration in the CNS of mouse and zebrafish (Bhatt et al., 2004; Hannila et al., 2008; Neumann et al., 2002; Qiu et al., 2002; Spencer et al., 2004). Imaging Synapsin1-GFP expressed in individually-identified neurons before severing and after bPAC-mediated regeneration showed that regenerated central axons re-targeted the correct area of the brain, and re-formed fewer but mature presynaptic structures, indicating that they have the potential for functional recovery. It would be interesting to test the ability of bPAC to promote the repair of other neurons, such as the Mauthner cells. Towards this end, I have generated a stable transgenic line that can express bPAC-V2A-mCherry under the control of a UAS promoter (data not shown), which can be used in combination with GAL4-driver lines expressed in diverse neurons. Additionally, a direct assessment of functional recovery could be performed after establishing the setup for behavioral analysis.

The biological novelty arising from these results was the discovery that under permissive conditions given by elevation of neuronal cAMP, there was no critical period for lateralis-neuron axonogenesis, regenerative pathfinding to the correct brain area, and synaptogenesis. Yet, the most salient aspect was the demonstration of a simple and versatile optogenetic approach that achieved the desired aim of promoting the regeneration of refractory axons in the whole animal. This approach was superior to classical pharmacological or genetic methods to increase cAMP levels, because light had higher spatiotemporal resolution. It is also generally applicable because bPAC-mediated elevation of cAMP works across species and does not need additional exogenous factors (Stierl et al., 2011). In its current implementation, this approach will be immediately suitable to probe the capacity of defined neural circuits to reclaim functionality after the time-selected repair of individual or multiple neurons. Its potential may be further increased by using adenylyl cyclases sensitive to longer wavelengths for better penetration and lower toxicity (Ryu et al., 2014). Additionally, adaptation of this method to molecular-screening platforms may help to identify cell-autonomous and non-autonomous effectors of axonal re-growth downstream of

cAMP signaling, to find molecules with therapeutic potential (Richter et al., 2015). In summary, the control of neuronal repair by optogenetics represented a powerful tool that could find broader uses in neurobiological research and biomedicine.

In addition, downstream effectors of cAMP signaling involving axonal re-growth were largely unexplored. Toward this end, I generated a stable transgenic line expressing EGFP-Rp110a in the lateral line afferent neurons, which would be used for translating ribosome affinity purification (Fig.3.18). This method was based on the expression of an epitope-tagged version of a ribosomal protein (EGFP-Rp110a) and the affinity purification of ribosomes and associated mRNAs using antibodies conjugated to agarose beads. Quantitative assessment of the transcriptome could be achieved by direct RNA sequencing and the capacity to capture mRNA transcripts bound to ribosomes was demonstrated in mouse and zebrafish (Heiman et al., 2008; Tryon et al., 2013). Therefore, further work in identifying downstream effectors of cAMP signaling in axonal re-growth is feasible by combining with bPAC expression.

5. Conclusions and Outlook

This study established an experimental model of neurotrauma to study the fundamental mechanisms that underlie neuronal and glial interactions *in vivo* at high spatiotemporal resolution. I developed an *in vivo* assay using the zebrafish, an animal model that combined long-fiber sensory neurons and their associated glia (Schwann cells) with the availability of both live imaging and genetic and microsurgical manipulations. I conducted a comprehensive characterization of Schwann cells and neurons during homeostasis, physical injury and repair by intravital imaging. Results showed that denervation caused progressive loss of Schwann cells by inducing cell apoptosis and reducing cell proliferation. In addition, the negative effects of denervation are reversible because Schwann-cell re-innervation prevented further glial destruction. Dynamic processes in the nervous system should be studied *in toto*, because the cells in their natural context provide the ideal framework for evaluating changes associated with physical injury. Neuronal-circuit regeneration began when Schwann cells extended bridging processes to close the injury gap. Regenerating axons grew faster and directionally after the physiological clearing of distal debris by the Schwann cells. Further, in the absence of Schwann cells, regenerating axons were misrouted, impairing the re-innervation of sensory organs. These results might have direct clinical implications because they demonstrated the dominant influence of the Schwann cells on the onset and directionality of axonal regeneration after injury. Thus, strategies aimed at neural-circuit repair would benefit from preventing the disassembly of the glia during periods of denervation. Therefore, the open question of this study is the identification of molecular mechanism and drugs that can maintain the integrity of the glia to treat traumatic neuropathies.

Another intriguing yet enigmatic issue is the molecular mechanism of how the central axons of the lateral line afferent neurons navigate to their target in the hindbrain. A mutant zebrafish strain was identified, where the central projections of lateral-line afferent neurons overshoot the target area and extended more dorsally into the hindbrain.

Additionally, the mutated gene was found to be extrinsic for neurons to inhibit branching by cell transplantation experiments. Moreover, 334 amino-acid changing candidates SNP were found by whole genome sequencing. This revealed that the identification of the mutation was complicated and laborious. To avoid this limitation, injection of the mutagenic agent with transposon into one-cell embryos might be an option for mutagenesis, as the targeted locus can be readily identified by inverse or ligation-mediated PCR using the insertional element as an amplification tag (Lawson et al., 2011). However, *Rgmb* and *tmem232* might be good candidate genes to validate by CRISPR/Cas9 technique, as *Rgmb* induced collapse of temporal retinal axons growth cones and inhibited the neurite outgrowth of cerebellar granule neurons (Monnier et al., 2002; Liu et al., 2009), and *tmem232* (with a yet unidentified function) was expressed in neurons and glial cells (Zhang et al., 2014). Furthermore, I successfully generated mutations at the target sites of these two genes in the sgRNA/Cas9-injected F0 embryos. The future work needs to investigate whether the phenotype in the mutant can be recapitulated in F2 embryos.

Lastly, this study provided the first line of evidence that the regenerative capacity of central axons in the lateral line afferent neurons was limited and can be enhanced by optogenetically increasing cAMP level based on the expression of exogenous bPAC. Moreover, regenerated central axons re-targeted the correct area of the brain, and re-formed presynaptic structures. However, the assessment of function recovery is still missing. To this aim, I have generated a stable transgenic line expressing bPAC-V2A-mCherry under the control of a UAS promoter (data not shown), which can be used in combination with GAL4-driver lines expressed in diverse neurons. For example, it would be interesting to test the ability of bPAC to promote the repair of Mauthner cells, which can be assessed by the functional recovery of the well-established escape behavior (Bhatt et al., 2004). In addition, downstream effectors of cAMP signaling involving axonal re-growth were largely unexplored. Toward this end, I generated a stable transgenic line expressing EGFP-rpl10a under the control of SILL enhancer, which can be used for translating ribosome affinity purification.

Therefore, further work in identifying downstream effectors of cAMP signaling in axonal re-growth is warranted by combining with bPAC expression.

In conclusion, the findings presented in this thesis demonstrate the essential function of Schwann cells for promoting peripheral neurorepair, extrinsic axonal guidance cues for central axon branching, and optogenetically elevated cAMP level by expressing exogenous bPAC to enhance regenerative capacity of the central axons in the lateral line afferent neurons. I believe that these findings contribute to the understanding of the development and regeneration of the lateral line afferent neurons. Future identification of novel regulators for the regeneration may provide potential strategies for combating traumatic neuropathies.

REFERENCES

- Alexandre, D., Ghysen, A.,** (1999). Somatotopy of the lateral line projection in larval zebrafish. Proc Natl Acad Sci USA 96,7558-7562.
- Allodi, I., Udina, E., Navarro, X.,** (2012). Specificity of peripheral nerve regeneration: interactions at the axon level. Prog Neurobiol 98, 16-37.
- Andermann, P., Ungos, J., Raible, D.W.,** (2002). Neurogenin 1 defines zebrafish cranial sensory ganglia precursors. Dev Biol 251, 45-58.
- Arthur-Farraj, P.J., Latouche, M., Wilton, D.K., Quintes, S., Chabrol, E., Banerjee, A., Woodhoo, A., Jenkins, B., Rahman, M., Turmaine, M., Wicher, G.K., Mitter, R., Greensmith, L., Behrens, A., Raivich, G., Mirsky, R., Jessen, K.R.,** (2012). c-Jun reprograms Schwann cells of injured nerves to generate a repair cell essential for regeneration. Neuron 75, 633-647.
- Asakawa, K., Suster, M.L., Mizusawa, K., Nagayoshi, S., Kotani, T., Urasaki, A., Kishimoto, Y., Hibi, M., Kawakami, K.,** (2008). Genetic dissection of neural circuits by Tol2 transposon-mediated Gal4 gene and enhancer trapping in zebrafish. Proc Nat Acad Sci USA 105, 1255-1260.
- Barresi, M.J., Sean Burton, S., DiPietrantonio, K., Adam Amsterdam, A., Nancy Hopkins, N., Karlstrom, R.O.,** (2010). Essential genes for astroglial development and axon pathfinding during zebrafish embryogenesis. Dev Dyn 239, 2603-2618.
- Becker, C.G., Lieberoth, B.C., Morellini, F., Feldner, J., Becker, T., Schachner, M.,** (2004). L1.1 is involved in spinal cord regeneration in adult zebrafish. J Neurosci 24, 7837-7842.
- Becker, C.G., Meyer, R.L., Becker, T.,** (2000). Gradients of ephrin-A2 and ephrin-A5b mRNA during retinotopic regeneration of the optic projection in adult zebrafish. J Comp Neurol 427, 469-483.
- Becker, T., Bernhardt, R.R., Reinhard, E., Wullimann, M.F., Tongiorgi, E., Schachner, M.,** (1998). Readiness of zebrafish brain neurons to regenerate a spinal axon correlates with differential expression of specific cell recognition molecules. J Neurosci 18, 5789-5803.
- Becker, T., Becker, C.G., Schachner, M., Bernhardt, R.R.,** (2001). Antibody to the HNK-1 glycoepitope affects fasciculation and axonal pathfinding in the developing posterior lateral line nerve of embryonic zebrafish. Mech Dev 109, 37-49.
- Becker, T., Becker, C.G.,** (2014). Axonal regeneration in zebrafish. Curr Opin Neurobiol 27,

186-191.

Beirowski, B., (2013). Concepts for regulation of axon integrity by enwrapping glia. Frontiers in Cellular Neuroscience 7, 256.

Bhatt D.H., Otto, S.J., Depoister, B., Fetcho, J.R., (2004). Cyclic AMP-induced repair of zebrafish spinal circuits. Science 305, 254-258.

Birchmeier, C., (2009). ErbB receptors and the development of the nervous system. Exp Cell Res 315, 611-618.

Bonanomi, D., Pfaff, S.L., (2010). Motor axon pathfinding. Cold Spring Harb Perspect Biol 2, a001735

Boivin, A., Pineau, I., Barrette, B., Filali, M., Vallieres, N., Rivest, S., Lacroix, S., (2007). Toll-like receptor signaling is critical for wallerian degeneration and functional recovery after peripheral nerve injury. J Neurosci 27, 12565-12576.

Bourgeois, F., Ben-Yakar, A., (2008). Femtosecond laser nanoaxotomy properties and their effect on axonal recovery in *C. elegans*. Optics Express 16, 5963.

Bradke, F., Fawcett, J.W., Spira, M.E., (2012). Assembly of a new growth cone after axotomy: the precursor to axon regeneration. Nature Rev Neuroscience 13, 183-193.

Briona, L.K., Dorsky, R.I., (2014). Radial glial progenitors repair the zebrafish spinal cord following transection. Exp Neurol 256, 81-92.

Brösamle, C., Halpern, M.E., (2002). Characterization of myelination in the developing zebrafish. Glia 39, 47-57.

Buckley, C.E., Marguerie, A., Alderton, W.K., Franklin, R.J., (2010). Temporal dynamics of myelination in the zebrafish spinal cord. Glia 58,802-812.

Burger, A., Lindsay, H., Felker, A., Hess, C., Anders, C., Chiavacci, E., Zaugg, J., Weber, L.M., Catena, R., Jinek, M., Robinson, M.D., Mosimann, C., (2016). Maximizing mutagenesis with solubilized CRISPR-Cas9 ribonucleoprotein complexes. Development 1, 025-37.

Burgess, H.A., Johnson, S.L., Granato M., (2009). Unidirectional startle responses and disrupted left-right coordination of motor behaviors in robo3 mutant zebrafish. Genes Brain Behav 8, 500-511.

Campbell, D.S., Stringham, S.A., Timm, A., Xiao, T., Law, M.Y., Baier, H., Nonet, M.L., Chien, C.B., (2007). Slit1a inhibits retinal ganglion cell arborization and synaptogenesis via Robo2-dependent and -independent pathways. Neuron 19, 231-245.

- Cashman, C.R., Höke A.,** (2015). Mechanisms of distal axonal degeneration in peripheral neuropathies. Neurosci Lett 596, 33-50.
- Ceci, M.L., Mardones-Krsulovic, C., Sánchez, M., Valdivia. L.E., Allende. M.L.,** (2014). Axon-Schwann cell interactions during peripheral nerve regeneration in zebrafish larvae. Neural Dev 9:22.
- Chada, S., Lamoureux, P., Buxbaum, R.E., Heidemann, S.R.,** (1997). Cytomechanics of neurite outgrowth from chick brain neurons. J Cell Sci 110, 1179-1186.
- Chang N.N., Sun , C.H., Gao L., Zhu D., Xu X.F., Zhu X.J., Xiong J.W., Xi J.J.,** (2013). Genome editing with RNA-guided Cas9 nuclease in Zebrafish embryos. Cell Res 23, 465-472.
- Chen, B.C., Legant, W.R., Wang, K., Shao, L., Milkie, D.E., Davidson, M.W., Janetopoulos, C., Wu, X.S., Hammer, J.A. 3rd, Liu, Z., English, B.P., Mimori-Kiyosue, Y., Romero, D.P., Ritter, A.T., Lippincott-Schwartz, J., Fritz-Laylin, L., Mullins, R.D., Mitchell, D.M., Bembenek, J.N., Reymann, A.C., Böhme, R., Grill, S.W., Wang, J.T., Seydoux, G., Tulu, U.S., Kiehart, D.P., Betzig, E.,** (2014). Lattice light-sheet microscopy: imaging molecules to embryos at high spatiotemporal resolution. Science 346, 1257998.
- Chen, C.H., Puliafito, A., Cox, B.D., Primo L., Fang, Y., Talia, S.D., Poss, K.D.,** (2016). multicolor cell barcoding technology for long-term surveillance of epithelial regeneration in Zebrafish. Dev cell 36, 668-680.
- Chen, Z.L., Yu, W.M., Strickland, S.,** (2007). Peripheral regeneration. Annu Rev Neurosci 30, 209-233.
- Chien, C.B., Piotrowski, T.,** (2002). How the lateral line gets its glia. Trends Neurosci 25, 544-546.
- Chierzi, S., Ratto, G.M., Verma, P., Fawcett, J.W.,** (2005). The ability of axons to regenerate their growth cones depends on axonal type and age, and is regulated by calcium, cAMP and ERK. Eur J Neurosci 21, 2051-2062.
- Ciba-Foundation,** (1991). Regeneration of Vertebrate Sensory Receptor Cells. John Wiley & Sons, Chichester, UK.
- Citri, A., Skaria, K.B., Yarden, Y.,** (2003). The deaf and the dumb: the biology of ErbB-2 and ErbB-3. Exp Cell Res 284, 54-65.
- Ciutat D., Cladero J., Oppenheim R.W., Esquerda J.E.** (1996). Schwann cell apoptosis during normal development and after axonal degeneration induced by neurotoxins in the chick embryo. J

Neurosci **16**, 3979-3990.

Colombo, A., Hsia, H.E., Wang, M.Z., Kuhn, P.H., Brill, M.S., Canevazzi, P., Feederle, R., Taveggia, C., Misgeld, T., Lichtenthaler, S.F., (2018) Non-cell-autonomous function of DR6 in Schwann cell proliferation. EMBO J. **37**: e97390

Coombs, S., Montgomery, J.C., (1999). The enigmatic lateral line system. In Comparative hearing: Fish and amphibians **11**, 319-362.

Court, F.A., Sherman, D.L., Pratt, T., Garry, E.M., Ribchester, R.R., Cottrell, D.F., Fleetwood-Walker, S.M., Brophy, P.J., (2004). Restricted growth of Schwann cells lacking Cajal bands slows conduction in myelinated nerves. Nature **431**, 191-195.

Cramer, S.C., (2010). Brain repair after stroke. N Engl J Med **362**, 1827-1829.

Curado, S., Stainier, D.Y., (2006). The Heart of regeneration. Cell **127**, 462-464.

Czopka, T., Lyons, D.A., (2011). Dissecting mechanisms of myelinated axon formation using zebrafish. Methods Cell Biol **105**, 25-62.

Dahm, R., Geisler, R., (2006). Learning from small fry: the zebrafish as a genetic model organism for aquaculture fish species. Marine Biotechnol **8**, 329-345.

David, G., Barrett, J.N., Barrett, E.F., (1997). Spatiotemporal gradients of intra-axonal [Na⁺] after transection and resealing in lizard peripheral myelinated axons. J Physiol **498**, 295-307.

David, N., Sapede, D., St-Etienne, L., Thisse, C., Thisse, B., Dambly-Chaudiere, C., Rosa, F., Ghysen, A., (2002). Molecular basis of cell migration in the fish lateral line: role of the chemokine receptor CXCR4 and of its ligand, SDF1. Proc Natl Acad Sci USA **99**, 16297-16302.

De Marco, R.J., Groneberg, A.H., Yeh, C.M., (2013). Optogenetic elevation of endogenous glucocorticoid level in larval zebrafish. Frontiers in Neural Circuits **7**, 82.

Dedkov, E.I., Kostrominova, T.Y., Borisov, A.B., Carlson, B.M., (2002). Survival of Schwann cells in chronically denervated skeletal muscles. Acta Neuropath **103**, 565.

Dent, E.W., Barnes, A.M., Tang, F.J., Kalil, K., (2004). Netrin-1 and Semaphorin 3A Promote or Inhibit Cortical Axon Branching, Respectively, by Reorganization of the Cytoskeleton. J Neurosci **24**, 3002-3012.

Deshmukh, V.A., Tardif, V., Lyssiotis, C.A., (2013). A regenerative approach to the treatment of multiple sclerosis. Nature **502**, 327-332.

Diep, C.Q., Ma, D., Deo, R.C., Holm, T.M., Naylor, R.W., Arora, N., Wingert, R.A., Bollig, F., Djordjevic, G., Lichman, B., Zhu, H., Ikenaga, T., Ono, F., Englert, C., Cowan, C.A., Hukriede,

- N.A., Handin, R.I., Davidson, A.J.,** (2011). Identification of adult nephron progenitors capable of kidney regeneration in zebrafish. Nature 470, 95-100.
- Dijkgraaf, S.,** (1963). The functioning and significance of the lateral-line organs. Biol Rev Camb Philos Soc 38, 51-105.
- Donato, V.D., Santis, F.D., Albadri, S., Auer, T.O., Duroure, K., Charpentier, M., Gebhardt, C., Del Bene, F.,** (2018). An attractive Reelin gradient establishes synaptic lamination in the vertebrate visual system. Neuron 1049-1062.e6
- Drerup, C.M., Nechiporuk, A.V.,** (2013). JNK-interacting protein 3 mediates the retrograde transport of activated c-Jun N-terminal kinase and lysosomes. PLoS Genet 9:e1003303.
- Dutton, J.R., Antonellis, A., Carney, T.J., Rodrigues, F.S., Pavan, W.J., Ward, A., Kelshet, R.N.,** (2008). An evolutionarily conserved intronic region controls the spatiotemporal expression of the transcription factor Sox10. BMC Dev Biol 8:105.
- Erturk, A., Mauch, C.P., Hellal, F., Forstner, F., Keck, T., Becker, K., Jahrling, N., Steffens, H., Richter, M., Hubener, M., Kramer, E., Kirchhoff, F., Dodt, H.U., Bradke, F.,** (2012). Three-dimensional imaging of the unsectioned adult spinal cord to assess axon regeneration and glial responses after injury. Nat Med 18, 166-171.
- Faber, C.G., Merkies I.S.,** (2015). Peripheral neuropathies: Moving closer to mechanism. Neurosci Lett 596, 1-2.
- Falls, D.L.,** (2003). Neuregulins: functions, forms, and signaling strategies. Exp Cell Res 284, 14-30.
- Fame, R.M., Brajon, C., Ghysen, A.,** (2006). Second-order projection from the posterior lateral line in the early zebrafish brain. Neural Dev 1, 4.
- Faucherre, A., Pujol-Martí, J., Kawakami, López-Schier, H.,** (2009). Afferent neurons of the zebrafish lateral line are strict selectors of hair-cell orientation. PLoS ONE 4, e4477.
- Faucherre, A., López-Schier, H.,** (2011). Delaying Gal4-driven gene expression in the zebrafish with morpholinos and Gal80. PLoS ONE 6, e16587.
- Faucherre, A., López-Schier, H.,** (2014). Dynamic neuroanatomy at subcellular resolution in the zebrafish. Methods Mol Biol 1082, 187-195.
- Fawcett, J.W., Keynes, R.J.,** (1990). Peripheral nerve regeneration. Ann Rev Neurosci 13, 43-60.
- Feneley, M.R., Fawcett, J.W., Keynes, R.J.,** (1991). The role of Schwann cells in the regeneration

of peripheral nerve axons through muscle basal lamina grafts. Experimental Neurology 114, 275-285.

Fenno, L., Yizhar, O., Deisseroth, K., (2011). The development and application of optogenetics. Ann Rev Neurosci 34, 389-412.

Fontana, X., Hristova, M., Da Costa, C., Patodia, S., Thei, L., Makwana, M., Spencer-Dene, B., Latouche, M., Mirsky, R., Jessen, K.R., Klein, R., Raivich, G., Behrens, A., (2012). C-jun in Schwann cells promotes axonal regeneration and motoneuron survival via paracrine signaling. J Cell Biol 198, 127-141.

Finzsch, M., Schreiner, S., Kichko, T., Reeh, P., Tamm, E.R., Bösl, M.R., Meijer, D., Wegner, M., (2010). Sox10 is required for Schwann cell identity and progression beyond the immature Schwann cell stage. J Cell Biol 189, 701-712.

Fleck, D., Bebbler, F.V., Colombo, A., Galante, C., Schwenk, B.M., Rabe, L., Hampel, H., Novak, B., Kremmer, E., Tahirovic, S., Edbauer, D., Lichtenthaler, S.F., Schmid, B., Willem, M., Haass, C., (2013). Dual cleavage of neuregulin 1 type III by BACE1 and ADAM17 liberates its EGF-like domain and allows paracrine signaling J Neurosci 33, 7856-7869.

Freeman, M.R., Doherty, J., (2006). Glial cell biology in *Drosophila* and vertebrates. Trends Neurosci 29,82-90.

Fricker, F.R., Bennett, D.L, (2011). The role of neuregulin-1 in the response to nerve injury. Future Neurol 6, 809-822.

Fritz, A., Rozowski, M., Walker C., Westerfield M., (1996). Identification of selected gamma-ray induced deficiencies in zebrafish using multiplex polymerase chain reaction. Genetics 144, 1735-1745.

Gaj T., Gersbach C.A., Barbas C.F., (2013). ZFN, TALEN, and CRISPR/Cas-based methods for genome engineering. Trends Biotechnol 31, 397-405.

Gao, L., Shao, Chen, B.C., Betzig, E., (2014). 3D live fluorescence imaging of cellular dynamics using Bessel beam plane illumination microscopy. Nat Prot 9, 1083.

Garratt, A.N., Voiculescu, O., Topilko,P., Charnay, P., Birchmeier, C., (2000). A dual role of erbB2 in myelination and in expansion of the schwann cell precursor pool. J Cell Biol 148, 1035-1046.

Gatto, G., Morales, D., Kania, A., Klein, R., (2014). EphA4 receptor shedding regulates spinal

motor axon guidance. Curr Biol 24, 2355-65.

Gaudet, A.D., Popovich, P.G., Ramer, M.S., (2011). Wallerian degeneration: gaining perspective on inflammatory events after peripheral nerve injury. J Neuro inflammation 8:110.

Ghosh-Roy, A., Wu, Z., Goncharov, A., Jin, Y., Chisholm, A.D., (2010). Calcium and cyclic AMP promote axonal regeneration in *Caenorhabditis elegans* and require DLK-1 kinase. J Neurosci 30, 3175-3183.

Ghysen, A., Dambly-Chaudière, C., (2004). Development of the zebrafish lateral line. Curr Opin Neurobiol 14, 67-73.

Ghysen, A., Dambly-Chaudière, C., (2007). The lateral line microcosmos. Genes Dev 21, 2118-2130.

Gilmour, D.T., Maischein, H.M., Nusslein-Volhard, C., (2002). Migration and function of a glial subtype in the vertebrate peripheral nervous system. Neuron 34, 577-588.

Gilmour, D., Knaut, H., Maischein, H.M., Nusslein-Volhard, C., (2004). Towing of sensory axons by their migrating target cells in vivo. Nat Neurosci 7, 491-492.

Glenn, T.D., Talbot, W.S., (2013). Signals regulating myelination in peripheral nerves and the Schwann cell response to injury. Curr Opin Neurobiol 23,1041-1048.

Goessling, W., North, T.E., (2014). Repairing quite swimmingly: advances in regenerative medicine using zebrafish. Dis Model Mech 7, 769-776.

Goldshmit, Y., Sztal, T.E., Jusuf, P.R., Hall, T.E., Nguyen-Chi, M., Currie, P.D., (2012). Fgf-dependent glial cell bridges facilitate spinal cord regeneration in zebrafish. J Neurosci 32, 7477-7492

Gompel, N., Dambly-Chaudière, C., Ghysen, A., (2001). Neuronal differences prefigure somatotopy in the zebrafish lateral line. Development 128, 387-393.

Gordon, T., Sulaiman, O., Boyd, J.G., (2003). Experimental strategies to promote functional recovery after peripheral nerve injuries. J Peripher Nerv Syst 8, 236-250.

Graciarena, M., Dambly-Chaudière, C., Ghysen, A., (2014). Dynamics of axonal regeneration in adult and aging zebrafish reveal the promoting effect of a first lesion. Proc Nat Acad Sci USA 111, 1610-1615.

Grant, K.A., Raible, D.W., Piotrowski, T., (2005). Regulation of latent sensory hair cell precursors by glia in the zebrafish lateral line. Neuron 45, 69-80.

- Hahn, A. F., Chang, Y., Webster, H. D.,** (1987). Development of myelinated nerve fibers in the sixth cranial nerve of the rat: a quantitative electron microscope study. *J Comp Neurol* 260, 491-500.
- Hall, S.,** (2005). The response to injury in the peripheral nervous system. *J Bone Joint Surg Br* 87, 1309-1319.
- Hall, S.M.,** (1999). The biology of chronically denervated Schwann cells. *Annals of the New York Academy of Sciences* 883, 215-233.
- Han, M.H., Plao, Y.J., Guo, D.W., Ogawa, K.,** (1989). The role of Schwann cells and macrophages in the removal of myelin during Wallerian degeneration. *Acta Histochem Cytochem* 22, 161-172.
- Hannila, S.S., Filbin, M.T.,** (2008). The role of cyclic AMP signaling in promoting axonal regeneration after spinal cord injury. *Exp Neurol* 209, 321-332.
- Harrisingh, M.C., Perez-Nadales, E., Parkinson, D.B., Malcolm, D.S., Mudge, A.W., Lloyd, A.C.,** (2004). The Ras/Raf/ERK signalling pathway drives Schwann cell dedifferentiation. *EMBO J* 23, 3061-3071.
- Harrison, P.J., Law A.J.,** (2006). Neuregulin 1 and Schizophrenia: Genetics, Gene Expression, and Neurobiology. *Biol Psychiatry* 60, 132-140.
- Harrison, R.G.,** (1904). Experimental analyses of the development of lateral line sense organs in amphibians. *Arch Mikrosk Anat Entwicklungmech* 63,35-149.
- Heiman, M., Schaefer, A., Gong, S., Peterson, J.D, Day, M., Ramsey, K.E., Suárez-Fariñas, M., Schwarz, C., Stephan, D.A., Surmeier, D.J., Greengard, P., Heintz, N.,** (2008). A translational profiling approach for the molecular characterization of CNS cell types. *Cell* 135:738-748.
- Hernández, P.P., Olivari, F.A., Sarrazin, A.F., Sandoval, P.C., Allende, M.L.,** (2007). Regeneration in zebrafish lateralline neuromasts: Expression of the neural progenitor cell marker sox2 and proliferation-dependent and-independent mechanisms of hair cell renewal. *Dev Neurobiol* 67, 637-654.
- Higashijima, S., Hotta, Y., Okamoto, H.,** (2000). Visualization of cranial motor neurons in live transgenic zebrafish expressing green fluorescent protein under the control of the islet-1 promoter/enhancer. *J Neurosci* 20, 206-18.
- Hilario, J.D., Rodino-Klapac, L.R., Wang, C., Beattie C.E.,** (2009). Semaphorin 5A is a bifunctional axon guidance cue for axial motoneurons in vivo. *Dev Biol* 326, 190-200.
- Hoke, A., Redett, R., Hameed, H., Jari, R., Zhou, C., Li, Z.B., Griffin, J.W., Brushart, T.M.,**

- (2006). Schwann cells express motor and sensory phenotypes that regulate axon regeneration. J Neurosci 26, 9646-9655.
- Hruscha, A., Krawitz, P., Rechenberg, A., Heinrich, V., Hecht, J., Haass, C., Schmid, B., (2013).** Efficient CRISPR/Cas9 genome editing with low off-target effects in zebrafish. Development 140, 4982-4987.
- Huang, C.C., Lawson, N.D., Weinstein, B.M., Johnson, S.L., (2003).** reg6 is required for branching morphogenesis during blood vessel regeneration in zebrafish caudal fins. Dev Biol 1, 263-274.
- Hubener, M., Bonhoeffer, T., (2014).** Neuronal plasticity: beyond the critical period. Cell 159, 727-737.
- Hui, S.P., Dutta, A., Ghosh, S., (2010).** Cellular response after crush injury in adult zebrafish spinal cord. Dev Dyn 239, 2962-79.
- Hwang, W.Y., Fu, Y.F., Reyon D., Maeder, M.L., Tsai, S.Q., Sander, J.D., Peterson1, R.T., Joanna Yeh, J.R., Joung, J.K., (2013).** Efficient genome editing in zebrafish using a CRISPR-Cas system. Nat Biotechnol 31, 227-229.
- Ide, C., (1996).** Peripheral nerve regeneration. Neurosci Res 25, 101-121.
- Jao, L.E., Wentz, S.R., Chen W.B., (2013).** Efficient multiplex biallelic zebrafish genome editing using a CRISPR nuclease system. Proc Natl Acad Sci USA 20, 13904-13909.
- Jen, J., Wang, Y.C., (2016).** Zinc finger proteins in cancer progression. J Biomed Sci 23:53.
- Jessen, K.R., Brennan, A., Morgan, L., Mirsky, R., Kent, A., Hashimoto, Y., Gavrilovic, J., (1994).** The Schwann cell precursor and its fate: a study of cell death and differentiation during gliogenesis in rat embryonic nerves. Neuron 12, 509-527.
- Jessen, K.R., Mirsky, R., (2005).** The origin and development of glial cells in peripheral nerves. Nat Rev Neurosci 6, 671-682.
- Jiang, L., Romero-Carvajal, A., Haug, J.S., Seidel, C.W., Piotrowski, T., (2014).** Gene-expression analysis of hair cell regeneration in the zebrafish lateral line. Proc Natl Acad Sci USA 8, 1383-1392.
- Johansson, M.E., Thomsson, K.A., Hansson, G.C., (2009).** Proteomic analyses of the two mucus layers of the colon barrier reveal that their main component, the Muc2 mucin, is strongly bound to the Fcgbp protein. J Proteome Res 8:3549-3557.
- Jopling, C., Sleep, E., Raya, M., Marti, M., Raya, A., Izpisua Belmonte J.C., (2010).** Zebrafish

- heart regeneration occurs by cardiomyocyte dedifferentiation and proliferation. Nature 464, 606-609.
- Jung, S.H., Kim, S., Chung, A.Y., Kim, H.T., So, J.H., Ryu, J., Park, H.C., Kim, C.H.,** (2010). Visualization of myelination in GFP-transgenic zebrafish. Dev Dyn 239, 592.
- Kadison, S.R., Mäkinen, T., Klein, R., Henkemeyer, M., Kaprielian, Z.,** (2006). EphB receptors and ephrin-B3 regulate axon guidance at the ventral midline of the embryonic mouse spinal cord. J Neurosci 26(35):8909-14.
- Kang, H., Lichtman, J.W.,** (2013). Motor axon regeneration and muscle reinnervation in young adult and aged animals. J Neurosci 33, 19480-19491.
- Kang, H., Tian, L., Mikesch, M., Lichtman, J.W., Thompson, W.J.,** (2014). Terminal Schwann cells participate in neuromuscular synapse remodeling during reinnervation following nerve injury. J Neurosci 34, 6323-6333.
- Karanth, S., Yang, G., Yeh, J., Richardson, P.M.,** (2006). Nature of signals that initiate the immune response during wallerian degeneration of peripheral nerves. Exp Neurol 202, 161-166.
- Kemp, H.A., Carmany-Rampey A., Moens, C.,** (2009). Generating chimeric zebrafish embryos by transplantation. J Vis Exp pii:1394. 10.3791/1394
- Kerschensteiner, M., Schwab, M.E., Lichtman, J.W., Misgeld, T.,** (2005). In vivo imaging of axonal degeneration and regeneration in the injured spinal cord. Nat Med 11, 572-577.
- Kidd, G.J., Ohno, N., Trapp, B.D.,** (2013). Biology of Schwann cells. Handbook of Clinical Neurology 115, 55-79.
- Kilmer, S.L., Carlsen, R.C.,** (1984) Forskolin activation of adenylate cyclase in vivo stimulates nerve regeneration. Nature 307, 455-457.
- Kirby, B.B., Takada, N., Latimer A.J., Shin, J., Carney, T.J., Kelsh, R.N., Appel, B.,** (2006). In vivo time-lapse imaging shows dynamic oligodendrocyte progenitor behavior during zebrafish development. Nat Neurosci 9, 1506-1511.
- Knöferle, J., Koch, J.C., Ostendorf, T., Michel, U., Planchamp, V., Vutova, P., Tönges, L., Stadelmann, C., Brück, W., Bähr, M., Lingor, P.,** (2010). Mechanisms of acute axonal degeneration in the optic nerve in vivo. Proc Natl Acad Sci USA 107, 6064-6069.
- Kok, F.O., Shin, M., Ni, C., Gupta, A., Grosse, A.S., van Impel, A., Kirchmaier, B.C., Peterson-Maduro, J., Kourkoulis, G., Male, I., DeSantis, D.F., Sheppard-Tindell, S., Ebarasi, L., Betsholtz, C., Schulte-Merker, S., Wolfe, S.A., Lawson, N.D.,** (2014). Reverse genetic

screening reveals poor correlation between morpholino-induced and mutant phenotypes in zebrafish. Dev Cell 32, 97-108.

Kucenas, S., Wang, W.D., Knapik, E.W., Appel, B., (2009). A selective glial barrier at motor axon exit points prevents oligodendrocyte migration from the spinal cord. J Neurosci 29, 15187-15194.

Kwan, K.M., Fujimoto, E., Grabher, C., Mangum, B.D., Hardy, M.E., Campbell, D.S., Parant, J.M., Yost, H.J., Kanki, J.P., Chien, C.B., (2007). The Tol2kit: a multisite gateway-based construction kit for Tol2 transposon transgenesis constructs. Dev Dyn 236, 3088-99.

Lafont, F., Prochiantz, A., (1994). Region-specific neuroastroglial interactions in neuronal morphogenesis and polarity: from homeogenic induction to cellular cytomechanics. Persp Dev Neurobiol 2, 259-268.

Lago, N., Navarro, X., (2006). Correlation between target reinnervation and distribution of motor axons in the injured rat sciatic nerve. J Neurotrauma 23, 227-240.

LaPlaca, M.C., Simon, C.M., Prado, G.R., Cullen, D.K., (2007). CNS injury biomechanics and experimental models. Prog Brain Res 161, 13-26.

Lawson, N.D., Wolfe, S.A., (2011). Forward and reverse genetic approaches for the analysis of vertebrate development in the Zebrafish. Dev Cell 21,48-64.

LeClair, E.E., Topczewski, J., (2010). Development and regeneration of the zebrafish maxillary barbel: a novel study system for vertebrate tissue growth and repair. PLoS One 5, e8737.

Ledent, V., (2002). Postembryonic development of the posterior lateral line in zebrafish. Development 129, 597-604.

Lee, H., Jo, E.K., Choi, S.Y., Oh, S.B., Park, K., Kim, J.S., Lee, S.J., (2006). Necrotic neuronal cells induce inflammatory Schwann cell activation via TLR2 and TLR3: Implication in wallerian degeneration. Biochem Biophys Res Commun 350, 742-747.

Lewis, G.M., Kucenas, S., (2013). Motor nerve transection and time-lapse imaging of glial cell behaviors in live zebrafish. J Vis Exp 20,doi:10.3791/50621.

Liao, J.C., (2010). Organization and physiology of posterior lateral line afferent neurons in larval zebrafish. Biol Lett 6, 402-405.

Lippincott-Schwartz J, Fritz-Laylin L, Mullins RD, Mitchell DM, Bembenek JN, Reymann AC, Böhme R, Grill SW, Wang JT, Seydoux, G., Tulu, US, Kiehart, D.P., Betzig, E., (2014). Lattice light-sheet microscopy: imaging molecules to embryos at high spatiotemporal resolution. Science

346(6208):1257998

Liu, H.M., Yang, L.H., Yang, Y.J., (1995). Schwann cell properties: 3.C-fos expression, bFGF production, phagocytosis and proliferation during Wallerian degeneration. J Neuropathol Exp Neurol 54, 487-496.

Liu, K., Tedeschi, A., Park, K.K., He, Z., (2011). Neuronal intrinsic mechanisms of axon regeneration. Ann Rev Neurosci 34, 131-152.

Liu, X., Hashimoto, M., Horii, H., Yamaguchi, A., Naito, K., Yamashita, T., (2009). Repulsive guidance molecule b inhibits neurite growth and is increased after spinal cord injury. Biochem Biophys Res Commun 15, 382(4):795-800.

Lombardo, F.L., Maggini, M., De Bellis, A., Seghieri, G., Anichini, R., (2014). Lower extremity amputations in persons with and without diabetes in Italy: 2001-2010. PLoS One 9(1):e86405.

López-Schier, H., Hudspeth, A.J., (2005). Supernumerary neuromasts in the posterior lateral line of zebrafish lacking peripheral glia. Proc Nat Acad Sci USA 102, 1496-1501.

Lush, M.E., Piotrowski, T., (2014). ErbB expressing Schwann cells control lateral line progenitor cells via non-cell-autonomous regulation of Wnt/beta-catenin. eLife 3, e01832.

Lutz, B.A., Barres, B.A., (2014) Contrasting the glial response to axon injury in the central and peripheral nervous systems. Dev Cell 28, 7-17.

Lyons, D.A., Pogoda, H.M., Voas, M.G., Woods, I.G., Diamond, B., Nix, R., Arana, N., Jacobs, J., Talbot, W.S., (2005). *erbb3* and *erbb2* are essential for schwann cell migration and myelination in zebrafish. Curr Biol 15, 513-524.

Lyons, D.A., Talbot, W.S., (2014). Glial cell development and function in zebrafish. Cold Spring Harb Perspect Biol 7(2): a020586.

Ma L., Tessier-Lavigne M., (2007). Dual branch-promoting and branch-repelling actions of Slit/Robo signaling on peripheral and central branches of developing sensory axons. J Neurosci 27, 6843-6851.

Madison, R.D., Sofroniew M.V., Robinson G.A., (2009). Schwann cell influence on motor neuron regeneration accuracy. Neuroscience 163, 213-221.

Mahar, M., Cavalli, V., (2018) Intrinsic mechanisms of neuronal axon regeneration. Nat Rev Neurosci 19(6): 323-337.

Mar, F.M., Bonni, A., Sousa, M.M., (2014). Cell intrinsic control of axon regeneration. EMBO

Reports 15, 254-263.

Martensson, L., Gustavsson, P., Dahlin, L.B., Kanje, M., (2007). Activation of extracellular signal regulated kinase-1/2 precedes and is required for injury-induced Schwann cell proliferation.

Neuroreport 18, 957-961.

Martinez, J., Stessin, A.M., Campana, A., Hou, J., Nikulina, E., Buck, J., Levin, L.R., Filbin, M.T., (2014). Soluble adenylyl cyclase is necessary and sufficient to overcome the block of axonal growth by myelin-associated factors. J Neurosci 34, 9281-9289.

McCurley, A.T., Callard, G.V., (2010). Time course analysis of gene expression patterns in zebrafish eye during optic nerve regeneration. J Exp Neurosci 4, 17-33.

McCampbell, K.K., Wingert, R.A., (2014). New tides: using zebrafish to study renal regeneration. Transl Res 163, 109-122.

Meier, C., Parmantier, E., Brennan, A., Mirsky, R., Jessen, K.R., (1999). Developing Schwann cells acquire the ability to survive without axons by establishing an autocrine circuit involving insulin-like growth factor, neurotrophin-3, and platelet-derived growth factor-BB. J Neurosci 19, 3847-3859.

Metcalf, W.K., (1985). Sensory neuron growth cones comigrate with posterior lateral line primordial cells in zebrafish. J Comp Neurol 238, 218-224.

Metcalf, W.K., Myers, P.Z., Trevarrow, B., Bass, M.B., Kimmel, C.B., (1990). Primary neurons that express the L2/HNK-1 carbohydrate during early development in the zebrafish. Development 110, 491-504.

Misgeld, T., Nikic, I., Kerschensteiner, M., (2007). In vivo imaging of single axons in the mouse spinal cord. Nat Prot 2, 263-268.

Mishra, B., Carson, R., Hume, R.I., Collins, C.A., (2013). Sodium and potassium currents influence Wallerian degeneration of injured *Drosophila* axons. J Neurosci 33, 18728-18739.

Molofsky, A.V., Kelley, K.W., Tsai, H.H., Redmond, S.A., Chang, S.M., Madireddy, L., Chan, J.R., Baranzini, S.E., Ullian, E.M., Rowitch, D.H. (2014) Astrocyte-encoded positional cues maintain sensorimotor circuit integrity. Nature 509, 189-194.

Monk, K.R., Naylor, S.G., Glenn, T.D., Mercurio, S., Perlin, J.R., Dominguez, C., Moens, C.B., Talbot, W.S., (2009). A G protein-coupled receptor is essential for Schwann cells to initiate myelination. Science 325, 1402-1405.

- Monk, K.R., Voas, M.G., Franzini-Armstrong, C., Hakkinen, I.S., Talbot, W.S.,** (2013). Mutation of sec63 in zebrafish causes defects in myelinated axons and liver pathology. Dis Model Mech 6, 135-145.
- Monnier, P.P., Sierra, A., Macchi, P., Deitinghoff, L., Andersen, J.S., Mann M., Flad, M., Hornberger, M.R., Stahl, B., Bonhoeffer, F., Mueller, B.K.,** (2002). RGM is a repulsive guidance molecule for retinal axons. Nature 419, 392-395.
- Morrissey, T.K., Levi, A.D., Nuijens, A., Sliwkowski, M.X., Bunge, R.P.,** (1995). Axon-induced mitogenesis of human Schwann cells involves heregulin and p185erbB2. Proc Natl Acad Sci USA 92, 1431-1435.
- Moreno-Mateos, M.A., Vejnar, C.E., Beaudoin, J.D., Fernandez, J.P., Mis, E.K., Khokha, M.K., Giraldez, A.J.,** (2015). CRISPRscan: designing highly efficient sgRNAs for CRISPR-Cas9 targeting in vivo. Nat Methods 12, 982-988.
- Munderloh, C., Solis, G.P., Bodrikov, V., Jaeger, F.A., Wiechers M., Málaga-Trillo, E., Stuermer C.A.O.,** (2009). Reggies/Flotillins regulate retinal axon regeneration in the Zebrafish optic nerve and differentiation of hippocampal and N2a neurons. J Neurosci 29, 6607-6615.
- Munzel, E.J., Schaefer, K., Obirei, B., Kremmer, E., Burton, E.A., Kuscha, V., Becker, C.G., Brosamle, C., Williams, A., Becker, T.,** (2012). Claudin k is specifically expressed in cells that form myelin during development of the nervous system and regeneration of the optic nerve in adult zebrafish. Glia 60, 253-270.
- Murphey, R.D., Zon, L.I.,** (2006). Small molecule screening in the zebrafish. Methods 39, 255-261.
- Nagashima, M., Fujikawa, C., Mawatari, K., Mori ,Y., Kato, S.,** (2011). HSP70, the earliest-induced gene in the zebrafish retina during optic nerve regeneration: its role in cell survival. Neurochem Int 58, 888-895.
- Napoli, I., Noon, L.A., Ribeiro, S., Kerai, A.P., Parrinello, S., Rosenberg, L.H., Collins, M.J., Harrisingh, M.C., White, I.J., Woodhoo, A., Lloyd, A.C.,** (2012). A central role for the erk-signaling pathway in controlling Schwann cell plasticity and peripheral nerve regeneration in vivo. Neuron 73, 729-742.
- Nave, K.A.,** (2010). Myelination and support of axonal integrity by glia. Nature 468, 244-252.
- Nelson, C.M., Ackerman, K.M., O'Hayer, P., Bailey, T.J., Gorsuch, R.A., Hyde, D.R.,** (2013).

- Tumor necrosis factor-alpha is produced by dying retinal neurons and is required for Muller glia proliferation during zebrafish retinal regeneration. J Neurosci 10, 6524-6539.
- Neumann, S., Bradke, F., Tessier-Lavigne, M., Basbaum, A.I.,** (2002). Regeneration of sensory axons within the injured spinal cord induced by intraganglionic cAMP elevation. Neuron 34, 885-893.
- Neve, L.D., Savage, A.A., Koke, J.R., Garcia, D.M.,** (2012). Activating transcription factor 3 and reactive astrocytes following optic nerve injury in zebrafish. Comp Biochem Physiol C Toxicol Pharmacol 155, 213-218.
- Newbern, J., Birchmeier, C.,** (2010). Nrg1/ErbB signaling networks in Schwann cell development and myelination. Semin Cell Dev Biol 21, 922-928.
- Nolte, H., Hölper, S., Housley, M.P., Islam, S., Piller, T., Konzer, A., Stainier, D.Y., Braun, T., Krüger, M** (2015). Dynamics of zebrafish fin regeneration using a pulsed SILAC approach. Proteomics 15, 739-751.
- Notterpek, L.,** (2003). Neurotrophins in myelination: a new role for a puzzling receptor. Trends Neurosci 26, 232-234.
- O'Brien, G.S., Rieger, S., Martin, S.M., Cavanaugh, A.M., Portera-Cailliau, C., Sagasti, A.,** (2009). Two-photon axotomy and time-lapse confocal imaging in live zebrafish embryos. JoVE 24.
- Oliva, C., Soldano, A., Mora, N., De Geest, N., Claeys, A., Erfurth, M.L., Sierralta, J., Ramaekers, A., Dascenco, D., Ejsmont, R.K., Schmucker, D., Sanchez-Soriano, N., Hassan B.A.,** (2016). Regulation of Drosophila brain wiring by neuropil interactions via a Slit-Robo-RPTP signaling complex. Dev Cell 39, 267-278.
- Ogai, K., Kuwana, A., Hisano, S., Nagashima, M., Koriyama, Y., Sugitani, K., Mawatari, K., Hiroshi Nakashima, H., Katoet, S.,** (2014). Upregulation of leukemia inhibitory factor (LIF) during the early stage of optic nerve regeneration in zebrafish. PLoS One 9:e106010.
- Oteiza, P., Odstrcil, I., Lauder, G., Portugues, R. & Engert, F.** (2017). A novel mechanism for mechanosensory based rheotaxis in larval zebrafish. Nature 547:445-448.
- Painter, M.W., Brosius Lutz, A., Cheng, Y.C., Latremoliere, A., Duong, K., Miller, C.M., Posada, S., Cobos, E.J., Zhang, A.X., Wagers, A.J., Havton, L.A., Barres, B., Omura, T., Woolf, C.J.,** (2014). Diminished Schwann cell repair responses underlie age-associated impaired axonal regeneration. Neuron 83, 331-343.

- Pardo-Martin, C., Chang, T.Y., Koo, B.K., Gilleland, C.L., Wasserman, S.C., Yanik, M.F.,** (2010). High-throughput in vivo vertebrate screening. Nat Methods 7, 634-636.
- Parkinson, D.B., Bhaskaran, A., Droggiti, A., Dickinson, S., D'Antonio, M., Mirsky, R., Jessen, K.R.,** (2004). Krox-20 inhibits Jun-NH2-terminal kinase/c-Jun to control Schwann cell proliferation and death. J Cell Biol 164, 385-394.
- Park, K.K., Liu, K., Hu Y., Smith, P.D., C. Wang, C., He, Z.G.,** (2008) Promoting axon regeneration in the adult CNS by modulation of the PTEN/mTOR pathway. Science 322, 963-966.
- Parrinello, S., Napoli, I., Ribeiro, S., Wingfield Digby, P., Fedorova, M., Parkinson, D.B., Doddrell, R.D., Nakayama, M., Adams, R.H., Lloyd, A.C.,** (2010). EphB signaling directs peripheral nerve regeneration through Sox2-dependent Schwann cell sorting. Cell 143, 145-155.
- Paskin, T.R., Iqbal, T.R., Byrd-Jacobs C.A.,** (2011). Olfactory bulb recovery following reversible deafferentation with repeated detergent application in the adult zebrafish. Neuroscience 196, 276-284.
- Patton, E.E., Dhillon, P., Amatruda, J.F., Ramakrishnan, L.,** (2014). Spotlight on zebrafish: translational impact. Dis Model Mech 7, 731-733.
- Peri, F., Nüsslein-Volhard, C.,** (2008). Live imaging of neuronal degradation by microglia reveals a role for v0-ATPase a1 in phagosomal fusion in vivo. Cell 30, 916-927.
- Perlin, J.R., Lush, M.E., Stephens, Piotrowski, T., Talbot, W.S.,** (2011). Neuronal Neuregulin 1 type III directs Schwann cell migration. Development 138, 4639-4648.
- Petratos, S., Butzkueven, H., Shipham, K., Cooper, H., Bucci, T., Reid, K., Lopes, E., Emery, B., Cheema, S.S., Kilpatrick, T.J.,** (2003). Schwann cell apoptosis in the postnatal axotomized sciatic nerve is mediated via NGF through the low- affinity neurotrophin receptor. J Neuropathol Exp Neurol 62:398-411.
- Pinto-Teixeira, F., Muzzopappa, M., Swoger, J., Mineo, A., Sharpe, J., López-Schier, H.,** (2013). Intravital imaging of hair-cell development and regeneration in the zebrafish. Front Neuroanat 7:33.
- Pinto-Teixeira, F., Viader-Llargués, O., Torres-Mejía, E., Turan, M., González-Gualda, E., Pola-Morell, L., López-Schier, H.,** (2015). Inexhaustible hair-cell regeneration in young and aged zebrafish. Biol Open 22, 903-909.
- Planchon, T.A., Gao, L., Milkie, D.E., Davidson, M.W., Galbraith, J.A., Galbraith, C.G., Betzig, E.,** (2011). Rapid three-dimensional isotropic imaging of living cells using Bessel beam plane

illumination. *Nat Methods* 8, 417-423.

Pogoda, H.M., Sternheim, N., Lyons, D.A., Diamond, B., Hawkins, T.A., Woods, I.G., Bhatt, D.H., Franzini-Armstrong, C., Dominguez, C., Arana, N., Jacobs, J., Nix, R., Fetcho, J.R., Talbot, W.S., (2006). A genetic screen identifies genes essential for development of myelinated axons in zebrafish. *Dev Biol* 298, 118-131.

Pope, H.M., Voigt, M.M., (2014). Peripheral glia have a pivotal role in the initial response to axon degeneration of peripheral sensory neurons in zebrafish. *PLoS One* 9:e103283.

Pujol-Martí, J., Baudoin, J.P., Faucherre, A., Kawakami, K., López-Schier, H., (2010). Progressive neurogenesis defines lateralis somatotopy. *Dev Dyn* 239, 1919-1930.

Pujol-Martí, J., Zecca, Baudoin, Faucherre, Asakawa, K., Kawakami, K., López-Schier, H., (2012). Neuronal birth order identifies a dimorphic sensorineural map. *J Neurosci* 32, 2976-2987.

Pujol-Martí, J., López-Schier, H., (2013). Developmental and architectural principles of the lateral-line neural map. *Frontiers in Neural Circuits* 7, 47.

Pujol-Martí, J., Faucherre, A., Aziz-Bose, R., Asgharsharghi, A., Colombelli, J., Trapani, J.G., López-Schier, H., (2014). Converging axons collectively initiate and maintain synaptic selectivity in a constantly remodeling sensory organ. *Curr Biology* 24, 2968-2974.

Qiu, J., Cai, D., Dai, H., McAtee, M., Hoffman, P.N., Bregman, B.S., Filbin, M.T., (2002). Spinal axon regeneration induced by elevation of cyclic AMP. *Neuron* 34, 895-903.

Raft, S., Koundakjian, E.J., Quinones, H., Jayasena, C.S., Goodrich, L.V., Johnson, J.E., Segil, N., Groves A.K., (2007). Cross-regulation of Ngn1 and Math1 coordinates the production of neurons and sensory hair cells during inner ear development. *Development* 134, 4405-4415.

Raivich, G., Hellweg, R., Kreutzberg, G.W., (1991). NGF receptor-mediated reduction in axonal NGF uptake and retrograde transport following sciatic nerve injury and during regeneration. *Neuron* 7, 151-164.

Raphael, A.R., Talbot, W.S., (2011). New insights into signaling during myelination in zebrafish. *Current Topics Dev Biol* 97, 1-19.

Raphael, A.R., Perlin, J.R., Talbot, W.S., (2010). Schwann cells reposition a peripheral nerve to isolate it from postembryonic remodeling of its targets. *Development* 137, 3643-3649.

Reimer, M.M., Sorensen, I., Kuscha, V., Frank, R.E., Liu, C., Becker, C.G., Becker, T., (2008). Motor neuron regeneration in adult zebrafish. *J Neurosci* 28,8510-8516.

- Reimer, M.M., Norris, A., Ohnmacht, J., Patani, R., Zhong, Z., Dias, T.B., Kuscha, V., Scott, A.L., Chen, Y.C., Rozov, S., Frazer, S.L., Wyatt, C., Higashijima, S., Patton, E.E., Panula, P., Chandran, S., Becker, T., Becker, C.G.,** (2013). Dopamine from the brain promotes spinal motor neuron generation during development and adult regeneration. Dev Cell 25, 478-491.
- Richter, F., Scheib, U.S., Mehlhorn, J., Schubert, R., Wietek, J., Gernetzki, O., Hegemann, P., Mathes, T., Möglich, A.,** (2015). Upgrading a microplate reader for photobiology and all-optical experiments. Photochem Photobiol Sci 14, 270-279.
- Riethmacher, D., Sonnenberg-Riethmacher, E., Brinkmann, V., Yamaai, T., Lewin, G.R., Birchmeier, C.,** (1997). Severe neuropathies in mice with targeted mutations in the ErbB3 receptor. Nature 389, 725-730.
- Robinson, G.A., Madison, R.D.,** (2003). Preferential motor reinnervation in the mouse: comparison of femoral nerve repair using a fibrin sealant or suture. Muscle Nerve 28, 227-231.
- Rodrigues, F., Schmidt, I., Klambt, C.,** (2011). Comparing peripheral glial cell differentiation in Drosophila and vertebrates. Cell Mol Life Sci 68, 55-69.
- Rosen, B., Chemnitz, A., Weibull, A., Andersson, G., Dahlin, L.B., Bjorkman, A.,** (2012). Cerebral changes after injury to the median nerve: A long-term follow up. J Plast Surg Hand Surg 46, 106-112.
- Rosenberg, A.F., Wolman, M.A., Franzini-Armstrong, C., Granato, M.,** (2012). In vivo nerve-macrophage interactions following peripheral nerve injury. J Neurosci 32:3898 -3909.
- Rosenberg, A.F., Isaacman-Beck, J., Franzini-Armstrong, C., Granato, M.,** (2014). Schwann cells and deleted in colorectal carcinoma direct regenerating motor axons towards their original path. J Neurosci 34, 14668-14681.
- Rossi, F., Casano, A.M., Henke, K., Richter, K., Peri, F.,** (2015). The SLC7A7 transporter identifies microglial precursors prior to entry into the brain. Cell Rep 19,1008-1017.
- Ruohonen, S., Khademi, M., Jagodic, M., Taskinen, H.S., Olsson, T., Roytta, M.,** (2005). Cytokine responses during chronic denervation. J Neuroinfl 2, 26.
- Ryu, M.H., Kang, I.H., Nelson, M.D., Jensen, T.M., Lyuksyutova, A.I., Siltberg-Liberles, J., Raizen, D.M., Gomelsky, M.,** (2014). Engineering adenylate cyclases regulated by near-infrared window light. Proc Natl Acad Sci USA 111, 10167-10172.
- Sakai, J.A., Halloran M.C.,** (2006). Semaphorin 3d guides laterality of retinal ganglion cell

- projections in zebrafish. Development 133,1035-1044.
- Santoriello, C., Zon, L.I.,** (2012). Hooked! Modeling human disease in zebrafish. The Journal of clinical investigation 122, 2337-2343.
- Sarrazín, A. F., Nunez, V.A., Sapede, D., Tassin, V., Dambly-Chaudière, C., Ghysen, A.,** (2010). Origin and early development of the posterior lateral line system of zebrafish. J Neurosci 30, 8234-8244.
- Sauka-Spengler, T. and Bronner, M.** (2010). Snapshot: neural crest. Cell 143, 486-486 e1.
- Schebesta, M., Serluca F.C.,** (2009). *olig1* Expression identifies developing oligodendrocytes in zebrafish and requires hedgehog and notch signaling. Dev Dyn 238,887-898.
- Scherer, S.S.,** (1997). The biology and pathobiology of Schwann cells. Curr Op Neurol 10, 386-397.
- Scherer, S.S., Salzer, J.L.,** (2001). Axon-Schwann cell interactions during peripheral nerve degeneration and regeneration. In Glial Cell Development 299-330.
- Scherer, S.S., Wrabetz, L.,** (2008). Molecular mechanisms of inherited demyelinating neuropathies. Glia 56, 1578-1589.
- Schneider, C.A., Rasband, W.S., Eliceiri, K.W.,** (2012). NIH Image to ImageJ: 25 years of image analysis. Nat Methods 9, 671-675.
- Shoji, W., Yee, C.S., Kuwada, J.Y.,** (1998). Zebrafish semaphorin Z1a collapses specific growth cones and alters their pathways in vivo. Development 125,1275-1283.
- Schuster, K., Dambly-Chaudière, C., Ghysen, A.,** (2010). Glial cell line-derived neurotrophic factor defines the path of developing and regenerating axons in the lateral line system of zebrafish. Proc Natl Acad Sci USA 107, 19531-19536.
- Schwab, M., Strittmatter, S.M.,** (2014) Nogo limits neural plasticity and recovery from injury. Curr Opin Neurobiol 27, 53-60.
- Shah, A.N., Davey, C.F., Whitebirch, A.C., Miller, A.C., Moens, C.B.,** (2015). Rapid reverse genetic screening using CRISPR in zebrafish. Nat Methods 12, 535-540.
- Shamash, S., Reichert, F., Rotshenker, S.,** (2002). The cytokine network of Wallerian degeneration: tumor necrosis factor- α , interleukin-1 α , and interleukin-1 β . J Neurosci 22, 3052-3060.
- Sharghi-Namini, S., Turmaine, M., Meier, C., Sahni, V., Umehara, F., Jessen, K.R., Mirsky, R.,** (2006). The structural and functional integrity of peripheral nerves depends on the glial-derived signal desert hedgehog. J Neurosci 26, 6364-6376.

- Sheppard, C.J., Wilson, T.,** (1981). The theory of the direct-view confocal microscope. J Microsc 124, 107-117.
- Shin, J., Park, H.C., Topczewska, J.M., Mawdsley, D.J., Appel, B.,**(2003). Neural cell fate analysis in zebrafish using olig2 BAC transgenics. Methods Cell Sci 25, 7-14.
- Shy, M.E.,** (2009). Biology of peripheral inherited neuropathies: Schwann cell axonal interactions. Advances in experimental medicine and biology 652, 171-181.
- Silver, J., Schwab, M.E., Popovich, P.G.,** (2014). Central nervous system regenerative failure: role of oligodendrocytes, astrocytes, and microglia. Cold Spring Harb Perspect Biol 7, p. a020602
- Small, S.L., Buccino, G., Solodkin, A.,** (2014). Brain repair after stroke--a novel neurological model. Nat Rev Neurology 9, 698-707.
- Smith, K.J., Hall, S.M.,** (1988). Peripheral demyelination and remyelination initiated by the calcium-selective ionophore ionomycin: *In vivo* observations. J Neurol Sci 83, 37-53.
- Smith, S.J.,** (2006). Neuronal cytomotility: the actin-based motility of growth cones. Science 242, 708-715.
- Soares, L., Parisi, M., Bonini, N.M.,** (2014). Axon injury and regeneration in the adult *Drosophila*. Scientific Rep 4, 6199.
- Solnica-Krezel, L., Schier, A.F., Driever, W.,** (1994). Efficient recovery of ENU-induced mutations from the zebrafish germline. Genetics 136, 1401-1420.
- Spencer, T., Filbin, M.T.,** (2004). A role for cAMP in regeneration of the adult mammalian CNS. J Anat 204, 49-55.
- Spira, M.E., Benbassat, D., Dormann, A.,** (1993). Resealing of the proximal and distal cut ends of transected axons: electrophysiological and ultrastructural analysis. J Neurobiol 24, 300-316.
- Stankovic, K., Rio, C., Xia, A., Sugawara, M., Adams, J.C., Liberman, M.C., Corfas, G.,** (2004). Survival of adult spiral ganglion neurons requires erbB receptor signaling in the inner ear. J Neurosci 24, 8651-61.
- Stierl, M., Stumpf, P., Udvari, D.,** (2011) Light modulation of cellular cAMP by a small bacterial photoactivated adenylyl cyclase, bPAC, of the soil bacterium *Beggiatoa*. J Biol Chem 286, 1181-1188.
- Sulaiman, O.A., Gordon, T.,** (2009). Role of chronic Schwann cell denervation in poor functional recovery after nerve injuries and experimental strategies to combat it. Neurosurgery 65, A105-114.

- Sulaiman, O.A., Midha, R., Munro, C.A., Matsuyama, T., Al-Majed, A., Gordon, T.,** (2002). Chronic Schwann cell denervation and the presence of a sensory nerve reduce motor axonal regeneration. Exp Neurol 176, 342-354.
- Svahn, A.J., Graeber, M.B., Ellett, F., Lieschke, G.J., Rinkwitz, S., Bennett, M.R., Becker, T.S.,** (2013). Development of ramified microglia from early macrophages in the zebrafish optic tectum. Dev Neurobiol 73, 60-71.
- Svennigsen, A.F., Dahlin L.B.,** (2013). Repair of the peripheral nerve-remyelination that works. Brain Sci 3, 1182-1197.
- Takeoka, A., Vollenweider, I., Courtine, G., Arber, S.,** (2014). Muscle spindle feedback directs locomotor recovery and circuit reorganization after spinal cord injury. Cell 159, 1626-1639.
- Taniuchi, M., Clark, H.B., Johnson, E.M., Jr.** (1986). Induction of nerve growth factor receptor in Schwann cells after axotomy. Proc Natl Acad Sci USA 83, 4094-4098.
- Tawk, M., Tuil, D., Torrente, Y., Vriza, S., Paulin, D.,** (2002). High-efficiency gene transfer into adult fish: a new tool to study fin regeneration. Genesis 32, 27-31.
- Taylor, K.S., Anastakis, D.J., Davis, K.D.,** (2009). Cutting your nerve changes your brain. Brain 132, 3122-3133.
- Torii ,T., Miyamoto, Y., Takada, S., Tsumura, H., Arai, M., Nakamura, K., Ohbuchi, K., Yamamoto, M., Tanoue, A., Yamauchi, J.,** (2014) In vivo knockdown of ErbB3 in mice inhibits Schwann cell precursor migration. Biochem Biophys Res Commun 452:782-8.
- Touma, E., Kato, S., Fukui, K., Koike, T.,** (2007). Calpain-mediated cleavage of collapsin response mediator protein(CRMP)-2 during neurite degeneration in mice. Eur J Neurosci 26, 3368-3381.
- Toy, D., Namgung, U.,** (2013). Role of glial cells in axonal regeneration. Exp Neurobiol 22, 68-76.
- Toyama, B.H., Savas, J.N., Park, S.K., Harris, M.S., Ingolia, N.T., Yates, J.R., Hetzer, M.W.,** (2013). Identification of long-lived proteins reveals exceptional stability of essential cellular structures. Cell 154, 971-982.
- Trapp, B.D., Hauer, P., Lemke, G.,** (1988). Axonal regulation of myelin protein mRNA levels in actively myelinating Schwann cells. J Neurosci 8, 3515-3521.
- Tryon, R.C., Pisat, N., Johnson, S.L., Dougherty, J.D.,** (2013). Development of translating ribosome affinity purification for Zebrafish. Genesis 51, 187-192.

- Vajn, K., Plunkett, J.A., Tapanes-Castillo, A., Oudega, M.,** (2013). Axonal regeneration after spinal cord injury in zebrafish and mammals: differences, similarities, translation. Neurosci Bull 29, 402-410.
- Vargas, M.E., Yamagishi, Y., Tessier-Lavigne, M., Sagasti, A.,** (2015). Live imaging of calcium dynamics during axon degeneration reveals two functionally distinct phases of calcium influx. J Neurosci 11, 15026-15038.
- Viader, A., Golden, J., Baloh, R., Schmidt, R., Hunter, D., Milbrandt, J.,** (2011). Schwann cell mitochondrial metabolism supports long-term axonal survival and peripheral nerve function. J Neurosci 31, 10128-10140.
- Villegas, R., Martin, S.M., O'Donnell, K.C., Carrillo, S.A., Sagasti, A., Allende, M.L.,** (2012). Dynamics of degeneration and regeneration in developing zebrafish peripheral axons reveals a requirement for extrinsic cell types. Neural development 7, 19.
- Villegas, R., Martinez, N.W., Lillo, J., Pihan, P., Hernandez, D., Twiss, J.L., Court, F.A.,** (2014). Calcium release from intra-axonal endoplasmic reticulum leads to axon degeneration through mitochondrial dysfunction. J Neurosci 34, 7179-7189.
- Voz, M.L., Coppieters, W., Manfroid, I., Baudhuin, A., Berg, V.V., Carole Charlier, C., Dirk Meyer, D., Driever, W., Martial, J.A., Peers, B.,** (2012). Fast homozygosity mapping and identification of a zebrafish ENU-induced mutation by whole-genome sequencing. PloS one 7, p. e34671.
- Wada, N., Javidan, Y., Nelson, S., Carney, T.J., Kelsh, R.N., Schilling, T.F.,** (2005). Hedgehog signaling is required for cranial neural crest morphogenesis and chondrogenesis at the midline in the zebrafish skull. Development 132, 3977-3988.
- Weinberg, H.J., Spencer, P.S.,** (1978). The fate of Schwann cells isolated from axonal contact. J Neurocytol 7, 555-569.
- White, F.V., Toews, A.D., Goodrum, J.F., Novicki, D.L., Bouldin, T.W., Morell, P.,** (1989). Lipid metabolism during early stages of Wallerian degeneration in the rat sciatic nerve. J Neurochem 52,1085-1092.
- Wills, A.A., Kidd A.R., Lepilina A., Poss K.D.,** (2008). Fgfs control homeostatic regeneration in adult zebrafish fins. Development 135,3063-70.
- Wilson-Sanders S.E.,** (2011). Models for biomedical research, testing and education. ILAR J

52,126-52.

Woldeyesus, M.T., Britsch, S., Riethmacher, D., Xu, L., Sonnenberg-Riethmacher, E., Abou-Rebyeh, F., Harvey, R., Caroni, P., Birchmeier, C., (1999). Peripheral nervous system defects in erbB2 mutants following genetic rescue of heart development. *Genes Dev* 13, 2538-2548.

Xiao, T., Roeser, T., Staub, W., Baier, H., (2005). A GFP-based genetic screen reveals mutations that disrupt the architecture of the zebrafish retinotectal projection. *Development* 132, 2955-2967.

Xiao, T., Shoji, W., Zhou, W., Su, F., Kuwada J.Y., (2003). Transmembrane sema4E guides branchiomotor axons to their targets in zebrafish. *J Neurosci* 23, 4190-4198.

Xiao, T., Wendy, S., Estuardo R., Nathan J.G., Gregory J.C., Baier, H., (2011). Assembly of lamina-specific neuronal connections by Slit bound to type IV Collagen. *Cell* 146, 164-176.

Xu Q., Stemple D., Joubin K., (2008). Microinjection and cell transplantation in zebrafish embryos. *Methods Mol Biol* 461, 513-520.

Yang, D.P., Kim, J., Syed, N., Tung, Y.J., Bhaskaran, A., Mindos, T., Mirsky, R., Jessen, K.R., Maurel, P., Parkinson, D.B., Kim, H.A., (2012). P38 MAPK activation promotes denervated Schwann cell phenotype and functions as a negative regulator of Schwann cell differentiation and myelination. *J Neurosci* 32, 7158-7168.

Yanik M.F., Rohde C.B., Pardo-Martin C., (2011). Technologies for micromanipulating, imaging, and phenotyping small invertebrates and vertebrates. *Annu Rev Biomed Eng* 13,185-217.

Yoshida, M., Macklin, W.B., (2005). Oligodendrocyte development and myelination in GFP-transgenic zebrafish. *J Neurosci Res* 81, 1-8.

Zecca, A., Dyballa, S., Voltes, A., Bradley, R., Pujades, C., (2015). The order and place of neuronal differentiation establish the topography of sensory projections and the entry points within the hindbrain. *J Neurosci* 35, 7475-7486.

Zhang, C.W., Gao, J.X., Zhang, H.F., Sun, L., Peng G., (2012). Robo2–Slit and Dcc–Netrin1 coordinate neuron axonal pathfinding within the embryonic axon tracts. *J Neurosci* 32,12589-12602.

Zhang, Y., Chen, K., Sloan, S.A., Bennett, M.L., Scholze, A.R., O’Keeffe, S., Phatnani, H.P., Guarnieri, P., Caneda, C., Ruderisch, N., (2014). An RNA-sequencing transcriptome and splicing database of glia, neurons, and vascular cells of the cerebral cortex. *J Neurosci* 34, 11929-11947.

Zou, S., Tian, C., Ge, S., Hu, B., (2005). Neurogenesis of retinal ganglion cells is not essential to visual functional recovery after optic nerve injury in adult zebrafish. *PLoS One* 8:e57280.

Acknowledgements

First and foremost, I would like to thank my supervisor Dr. Hernán López-Schier for providing me the opportunity to study and work in his lab, and for his excellent supervision and advice to work on projects that I really love. His continuous encouragement, scientific enthusiasm and persistence have given me with a solid research base on which I could build my future career in science.

I would like to effusively thank my co-supervisor Prof. Dr. Wolfgang Wurst for his valuable guidance and always asking why I do an experiment to make me think carefully and learn to be a better scientist during thesis advisory committee. I am also grateful to the member of my thesis advisory committee PD Dr. Lars Kunz, for his advice and willingness to mentor my work. I would also like to thank Prof. Dr. Martin Hrabě de Angelis for taking the chair and Prof. Dr. Ilona Grunwald Kadow for being the examiner of my thesis evaluation.

I am extremely grateful for the past member of this lab, Dr. Jesús Pujol-Martí for answering all of my questions and his patient discussing at the first year of my PhD studies. And I have benefited enormously from his expertise. I would like to express my gratitude to Laura Pola-Morell for her technical assistance and taking care of my fish for conducting the experiments. Furthermore, I would particularly like to acknowledge Dr. Prisca Chapouton for the guidance and discussion for cell transplantation in zebrafish embryos, also to Petra Hammerl for her kindly non-academic help. I would also like to extend my sincere thanks to all the other SBO colleagues: Oriol Viader-Llargués, Elen Torres-Mejía, Amir Asgharsharghi, Marta Lozano-Ortega, Gema Valera, Weili Tian, Javier Carbajo-Lozoya, for providing me with a friendly cheerful, and pleasant environment and necessary academic assistance throughout my PhD life. I am also grateful to Dr. Tim Czopka for his valuable suggestions on thesis presentation, Dr. Laura Jane Hoodless for the English proofreading and Dr. Franziska Auer for German translation of thesis summary. It has definitely been mad years full of memorized and unforgettable experiences, and I will remember all you guys forever.

Last but not least, a very big thank you to my parents and parents in law, aunts and uncles, cousins and all the friends in China for their love and constant support. I am immensely and deeply grateful to my husband for his love, understanding, advice, encouragement and unconditional support during these challenging years. Without him, I would not have capability to overcome all the difficult times.

Affirmation

Ich erkläre hiermit an Eides statt, dass ich die vorliegende Arbeit selbstständig, ohne unzulässige fremde Hilfe und ausschließlich mit den angegebenen Quellen und Hilfsmitteln angefertigt habe.

Die verwendeten Literaturquellen sind im Literaturverzeichnis (References) vollständig zitiert.

Diese Arbeit hat in dieser oder ähnlicher Form noch keiner anderen Prüfungsbehörde vorgelegen.

München, am

(Yan Xiao)

Publications based on this thesis

Yan Xiao, Adèle Faucherre, Laura Pola-Morell, John M. Heddleston, Tsung-Li Liu, Teng-Leong Chew, Fuminori Sato, Atsuko Sehara-Fujisawa, Koichi Kawakami, Hernán López-Schier. **High-resolution live imaging reveals axon-glia interactions during peripheral nerve injury and repair in zebrafish.** *Dis Model Mech.* 2015, 8(6):553-564.

Yan Xiao, Weili Tian, Hernán López-Schier. **Optogenetic stimulation of neuronal repair.** *Current Biology.* 2015, 25 (22):1068-1069.

CURRICULUM VITAE

Name: Yan Xiao
Geburtsdatum: 14/10/1986
Staatsangehörigkeit: China
Familienstand: Verheiratet
E-Mail: yan.xiao@tum.de

Promotion

- 02/2013-10/2017** Helmholtz Zentrum München (TU München)
Abschluss: Dr. rer. nat. (Doctor rerum naturalium)
Dissertationstitel: Development and regeneration of the peripheral and central axons in the zebrafish lateral-line afferent neurons
- 09/2008-07/2011** Ostchina Universität für Wissenschaft und Technologie, Shanghai, China
Abschluss: Master-Biologie (Dipl.-Biol.)
- 09/2004-07/2008** Diplomstudiengang Biologie an der Southwest Jiaotong Universität, Chengdu, China
- 09/2001-06/2004** Abitur, Yichun, China

Veröffentlichungen

Marta Lozano-Ortega, Gema Valer, **Yan Xiao**, Adèle Faucherre, Hernán López-Schier. Hair cell identity establishes labeled lines of directional mechanosensation. **PLoS Biology**. 2018, 16:e2004404.

Yan Xiao, Hernán López-Schier. Studying axonal regeneration by laser microsurgery and high-resolution videomicroscopy. **Methods in Molecular Biology**. 2016, 1451:271-280.

Yan Xiao, Weili Tian, Hernán López-Schier. Optogenetic stimulation of neuronal repair. **Current Biology**. 2015, 25 (22):1068-1069.

Yan Xiao, Adèle Faucherre, Laura Pola-Morell, John M. Heddleston, Tsung-Li Liu, Teng-Leong Chew, Fuminori Sato, Atsuko Sehara-Fujisawa, Koichi Kawakami, and Hernán López-Schier. High-resolution live imaging reveals axon-glia interactions during peripheral nerve injury and repair in zebrafish. **Disease Models and Mechanisms**. 2015, 8(6): 553-564.

Yan Zheng, Qin Liu, **Yan Xiao**, Haizhen Wu, Qiyao Wang, Jingfan Xiao, Yuanxing Zhang. Different approaches to expressing *Edwardsiella tarda* antigen GAPDH in attenuated *Vibrio anguillarum* for multivalent fish vaccines. **Journal of Fish Diseases**. 2012, 35(8):569-577.

Yan Xiao, Qin Liu, Hao Chen, Yuanxing Zhang. A stable plasmid system for heterologous antigen expression in attenuated *Vibrio anguillarum*. **Vaccine**. 2011, 29(40): 6986-6993.